

Effects of High Temperature Treatment on Curl And Microstructure of Heavily Boron Doped Silicon

by

Denise M. Bruce, Capt, USAF

Degree Awarded: Master of Science (Materials Science and Engineering)

Institution: Massachusetts Institute of Technology, Cambridge, MA

Year of Degree Award: 1997

Number of Pages: 110

ABSTRACT

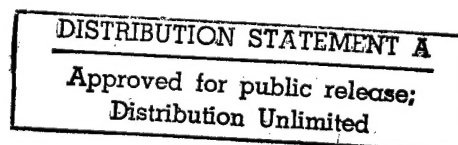
An experimental study was performed to investigate the effects of high temperature treatment on the microstructure and curling behavior of heavily boron-doped silicon structures. Cantilever structures were created from p++ boron diffused silicon wafers. The post-diffusion high temperature "anneal" treatment temperature was varied while the anneal time remained constant. The micromechanical cantilevers were analyzed for curl as a function of the anneal temperature using an optical profiler. Bulk sections from the wafers were analyzed to obtain boron concentration using secondary ion mass spectroscopy (SIMS) and to obtain the distribution of lattice constant using x-ray diffraction. Microstructure of plan-view and cross-section samples was investigated with the transmission electron microscope (TEM).

Results of the curl measurements revealed that all non-annealed cantilever structures were curled in one direction, and those annealed for 90 minutes above 1100°C were all curled in the other direction, with an apparent transition temperature of about 1050°C.

SIMS analysis confirmed that boron concentration becomes more uniform through the wafer thickness with increasing anneal temperature. X-ray diffraction revealed that the magnitude of the smallest lattice constant present in a wafer increases with increasing anneal temperature. TEM observations showed that dislocation and precipitate density do not change with anneal temperature.

19970424 026

DTIC QUALITY INSPECTED 3



REPORT DOCUMENTATION PAGE			Form Approved OMB No. 0704-0188	
Public reporting burden for this collection of information is estimated to average 1 hour per response, including the time for reviewing instructions, searching existing data sources, gathering and maintaining the data needed, and completing and reviewing the collection of information. Send comments regarding this burden estimate or any other aspect of this collection of information, including suggestions for reducing this burden, to Washington Headquarters Services, Directorate for Information Operations and Reports, 1215 Jefferson Davis Highway, Suite 1204, Arlington, VA 22202-4302, and to the Office of Management and Budget, Paperwork Reduction Project (0704-0188), Washington, DC 20503.				
1. AGENCY USE ONLY (Leave blank)		2. REPORT DATE 17 Apr 97		3. REPORT TYPE AND DATES COVERED
4. TITLE AND SUBTITLE Effects of High Temperature on Curl and Microstructure of Heavily Boron Doped Silicon			5. FUNDING NUMBERS	
6. AUTHOR(S) Denise M. Bruce				
7. PERFORMING ORGANIZATION NAME(S) AND ADDRESS(ES) Massachusetts Institute of Technology, Cambridge MA			8. PERFORMING ORGANIZATION REPORT NUMBER 97-015	
9. SPONSORING/MONITORING AGENCY NAME(S) AND ADDRESS(ES) DEPARTMENT OF THE AIR FORCE AFIT/CI 2950 P STRRET WRIGHT-PATTERSON AFB OH 45433-7765			10. SPONSORING/MONITORING AGENCY REPORT NUMBER	
11. SUPPLEMENTARY NOTES				
12a. DISTRIBUTION AVAILABILITY STATEMENT			12b. DISTRIBUTION CODE	
13. ABSTRACT (Maximum 200 words)				
14. SUBJECT TERMS			15. NUMBER OF PAGES 110	
			16. PRICE CODE	
17. SECURITY CLASSIFICATION OF REPORT	18. SECURITY CLASSIFICATION OF THIS PAGE	19. SECURITY CLASSIFICATION OF ABSTRACT	20. LIMITATION OF ABSTRACT	

CSDL-T-1279

**EFFECTS OF HIGH TEMPERATURE TREATMENT
ON CURL AND MICROSTRUCTURE
OF HEAVILY BORON DOPED SILICON**

by

Denise M. Bruce

February 1997

**Master of Science Thesis
Massachusetts Institute of Technology**



The Charles Stark Draper Laboratory, Inc.
555 Technology Square, Cambridge, Massachusetts 02139-3563

Effects of High Temperature Treatment on
Curl and Microstructure of Heavily Boron Doped Silicon

by

Denise M. Bruce


B.S. Mechanical Engineering
The Ohio State University, 1992

Submitted to the Department of Materials Science and Engineering
in Partial Fulfillment of the Requirements for the Degree of
Master of Materials Science and Engineering

at the
Massachusetts Institute of Technology
February 1997

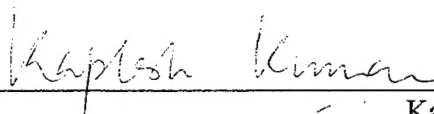
©1997 Denise M. Bruce
All rights reserved

Signature of Author



Department of Materials Science and Engineering
January 17, 1997

Approved by



Kaplesh Kumar

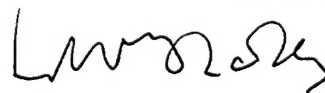
Technical Supervisor, Draper Laboratory

Certified by



Eugene A. Fitzgerald
Thesis Advisor

Accepted by



Linn W. Hobbs

John F. Elliott Professor of Materials
Chairman, Department Committee on Graduate Students

Effects of High Temperature Treatment on Curl And Microstructure of Heavily Boron Doped Silicon

by

Denise M. Bruce

Submitted to the Department of Materials Science and Engineering
on January 17, 1997 in Partial Fulfillment of the Requirements for
the Degree of Master of Materials Science and Engineering

ABSTRACT

An experimental study was performed to investigate the effects of high temperature treatment on the microstructure and curling behavior of heavily boron-doped silicon structures. Cantilever structures were created from p++ boron diffused silicon wafers. The post-diffusion high temperature "anneal" treatment temperature was varied while the anneal time remained constant. The micromechanical cantilevers were analyzed for curl as a function of the anneal temperature using an optical profiler. Bulk sections from the wafers were analyzed to obtain boron concentration using secondary ion mass spectroscopy (SIMS) and to obtain the distribution of lattice constant using x-ray diffraction. Microstructure of plan-view and cross-section samples was investigated with the transmission electron microscope (TEM).

Results of the curl measurements revealed that all non-annealed cantilever structures were curled in one direction, and those annealed for 90 minutes above 1100°C were all curled in the other direction, with an apparent transition temperature of about 1050°C.

SIMS analysis confirmed that boron concentration becomes more uniform through the wafer thickness with increasing anneal temperature. X-ray diffraction revealed that the magnitude of the smallest lattice constant present in a wafer increases with increasing anneal temperature. TEM observations showed that dislocation and precipitate density do not change with anneal temperature.

Thesis Advisor: Eugene A. Fitzgerald

Title: Associate Professor of Materials Science and Engineering

TABLE OF CONTENTS

	<u>Page</u>
ABSTRACT	2
TABLE OF CONTENTS	3
LIST OF FIGURES	5
LIST OF TABLES	6
ACKNOWLEDGMENTS	7
1. INTRODUCTION	8
2. BACKGROUND THEORY AND LITERATURE REVIEW	10
2.1 Diffusion Theory and Studies	10
2.2 Microstructural Theory and Studies	12
2.2.1 Dislocation Theory	12
2.2.2 X-Ray Theory	14
2.3 Annealing Theory and Studies	15
3. EXPERIMENTAL PROCEDURE	19
3.1 General Approach	19
3.2 Wafer Layout	19
3.3 Tablet Tracking	20
3.4 WYKO Tablet (Cantilever Structures) Design	21
3.5 Wafer Fabrication Process	22
3.6 Test Methods and Equipment	27
3.6.1 WYKO Tablet Cantilever Deflection	27
3.6.2 X-ray Diffraction	28
3.6.3 Transmission Electron Microscopy (TEM)	28
3.6.4 Secondary Ion Mass Spectroscopy (SIMS)	30

TABLE OF CONTENTS (Continued)

	<u>Page</u>
4. RESULTS AND DISCUSSION	32
4.1 Cantilever Structures	32
4.1.1 CS01 Results	33
4.1.2 CS02 Results	35
4.1.3 Comparison of CS01 and CS02	36
4.2 X-ray Diffraction	38
4.3 TEM Observations	41
4.4 SIMS Analysis	42
5. CONCLUSIONS	44
5.1 Cantilever Structures	44
5.2 X-Ray Diffraction	45
5.3 TEM Observations	45
5.4 SIMS Analysis	46
5.5 Correlation Between Microstructural Observations and Curl Reversal	46
6. RECOMMENDATIONS FOR FUTURE WORK	48
APPENDIX A: DERIVATION OF EQUATIONS	49
APPENDIX B: WYKO DATA	52
APPENDIX C: X-RAY DATA	71
APPENDIX D: TEM PHOTOGRAPHS	86
APPENDIX E: SIMS DATA	91
REFERENCES	109

LIST OF FIGURES

	<u>Page</u>
Figure 1: Diamond Cubic Slip System	13
Figure 2: Wafer Tablet Layout	20
Figure 3: WYKO Tablet Layout	22
Figure 4: Pictorial Representation of Wafer Processing	25
Figure 5: Comparison of Beam Tip Deflections for CS01 Wafers	33
Figure 6: Linear Trendlines for Beam Tip Deflections for CS01 Wafers	34
Figure 7: Prediction of Curl Reversal Anneal Temperature	35
Figure 8: Comparison of Beam Tip Deflections for CS02 Wafers	36
Figure 9: Comparison of Tip Deflections for CS01 and CS02 1100°C Annealed Wafers	37
Figure 10: Comparison of Control Wafer Tip Deflections with Theory	38
Figure 11: Normalized θ - 2θ Scan Plots	39
Figure 12: Comparison of Boron Profiles for CS02 Control and 1100°C Wafers	43
Figure 13: CS02-A Cross-Section Sample Dislocations	86
Figure 14: CS02-F Cross-Section Sample Dislocations	87
Figure 15: CS02-A Plan-View Sample Kikuchi Pattern	88
Figure 16: CS02-A Plan-View Sample Dislocations and Precipitates	88
Figure 17: Plan-View Sample Precipitate-Free Region (CS01-1175°C Test Wafer)	89
Figure 18: Plan-View Sample Dislocations and Precipitates (CS01-1175°C Test Wafer)	89
Figure 19: Plan-View Sample Precipitates -- Boxed Region of Figure 18 (CS01-1175°C Test Wafer)	90

LIST OF TABLES

	<u>Page</u>
Table 1: Primary Lattice Constants	40
Table 2: Cross-Section TEM Sample First Dislocation Depth	41

ACKNOWLEDGMENTS

Special thanks to my Draper Laboratory advisor, Kaplesh Kumar, for convincing me that this project was a worthwhile endeavor and to my MIT advisor, Gene Fitzgerald, for spending so much time getting me up to speed on the previous work, and for teaching me how to get something useful from the TEM! I would also like to thank Connie Cardoso of Draper Laboratory for her endless patience and help with getting my experimental wafers fabricated, Ken Wu of MIT for teaching me TEM sample preparation, Mayank Bulsara of MIT for running my x-ray diffraction samples, Bill Lampert and Jim Solomon of Wright Laboratory for running my SIMS samples, and the Air Force for making me a reasonably well-paid graduate student. Last, but far from least, many thanks to my husband, Jeff, for inspiring me to get started on the writing and supporting me through long hours of homework, ion milling, TEM work, and more writing.

This thesis was prepared at The Charles Stark Draper Laboratory, Inc. with funding provided by a Draper Independent Research and Development project.

Publication of this thesis does not constitute approval by Draper of the findings or conclusions contained herein. It is published for the exchange and stimulation of ideas.

I hereby assign my copyright of this thesis to The Charles Stark Draper Laboratory, Inc., Cambridge, Massachusetts.


January 17, 1997

Permission is hereby granted by The Charles Stark Draper Laboratory, Inc., to the Massachusetts Institute of Technology to reproduce any or all of this thesis.

Chapter 1: INTRODUCTION

Heavy boron doping is routinely used in the fabrication of silicon structures for micromechanical applications. Boron increases the resistance of silicon to some etchants, thus allowing fabrication of thin structures, such as cantilevers and membranes [1]. The high boron concentration ($\sim 10^{20} \text{ cm}^{-3}$) has the unfortunate side effect of contracting the pure silicon lattice [2]. Non-uniform concentrations of boron through the thickness of a micromechanical structure lead to unwanted curl due to the stresses associated with the compositional variations.

A typical process for creating micromechanical structures involves creating mesas (elevated regions) on the front (shiny) surface of a silicon wafer by masking the areas to become mesas and etching away a few microns from the rest of the front surface. Next, boron is diffused into the wafer from the front surface. Then, the wafer is subjected to a high temperature “anneal” treatment to achieve greater uniformity in boron concentration. Structures are formed by masking the wafer with the structure pattern and performing a deep etch of the front surface. A glass wafer can then be bonded to the silicon wafer using the mesas as bond points. The final step releases the structures by etching away all silicon that does not contain enough boron to stop the etchant. Since the highest boron concentrations will be near the front surface, this final step will etch away silicon from the back surface until the etch-stop boron concentration is reached.

Since the anneal step is performed to reduce the curl of the final micromechanical structures, it would be best to anneal after the structure has been released. However, this

is not always practically possible, due to other processing temperature limitations. For example, the silicon-to-glass bond cannot withstand the high temperatures required for annealing. In this case, the anneal is performed before structure release, which makes optimizing the anneal process very difficult. An additional difficulty is the possibility of causing a structure initially curled in one direction to curl in the opposite direction with the annealing process.

It is the goal of this thesis to postulate an ideal anneal treatment and to understand the different effects that may contribute to the curl-reversal behavior. Three parameters are investigated under several different anneal conditions, namely: 1) change in lattice constant, 2) dislocation movement, and 3) actual boron distribution. These effects are correlated with anneal temperature and observations of physical curling in cantilever structures.

Chapter 2: BACKGROUND THEORY AND LITERATURE REVIEW

The literature revealed substantial interest in curling of micromechanical silicon structures, since it is a significant problem in many applications. However, no experimental work was found which carried out a complete study of the effects of different high temperature treatments on microstructure and correlated those results with measurements of physical structural curling. To conduct this study, it was important to understand several key concepts. Diffusion, microstructure, and annealing are reviewed below along with discussions of applicable literature.

2.1 Diffusion Theory and Studies

Boron is diffused into silicon wafers from the front surface during processing in order to create an etch-stop to define structure thickness. The boron concentration required for an ethylenediamine-pyrazene-catechol (EDP) etch-stop in silicon is about $7 \times 10^{19} \text{ cm}^{-3}$, which results in even higher front surface concentrations.

Normal diffusion follows Fick's Second Law, which is:

$$\frac{\partial C(x, t)}{\partial t} = \frac{\partial}{\partial x} \left(D \frac{\partial C}{\partial x} \right). \quad (1)$$

In the above equation, D is the diffusion coefficient which changes according to substrate and diffused elements, and diffusion conditions. The variables C , t , and x stand for diffused species concentration, diffusion time, and diffusion depth respectively. Solving this equation for a solid source diffusion into a semi-infinite slab gives equation (2) [3].

$$C(x, t) = C_s \operatorname{erfc} \left(\frac{x}{2\sqrt{Dt}} \right) \quad (2)$$

In equation (2), C_s is surface concentration and erfc is the complementary error function. Unfortunately, for high concentration ($>10^{19} \text{ cm}^{-3}$) diffusions of boron in silicon, this simple model does not correctly predict the actual diffusion.

At high doping densities, the diffusion coefficient is not constant, but exhibits a dependence on local boron concentration [4, 5]. In 1969, Thai [4] proposed a theoretical model for diffusion of boron in silicon that incorporated a concentration dependent diffusion coefficient. He postulated that dislocation multiplication and movement caused an increase in local vacancy concentration. In 1975, Fair [5] described the concentration dependence of boron diffusivity in silicon, and created theoretical high concentration boron diffusion profiles in silicon for diffusions performed in non-oxidizing ambients. An oxidizing environment also affects boron atom mobility [6], and further complicates a prediction of boron concentration profile.

Secondary ion mass spectroscopy (SIMS) data of deep boron diffusion profiles with no anneal show that variation in boron concentration from about $1 \mu\text{m}$ depth to the etch-stop ($7 \times 10^{19} \text{ cm}^{-3}$ in EDP) is reasonably linear [7]. To obtain a simple model for the curling expected in an as-diffused cantilever structure, a linear gradient of boron will be assumed. Furthermore, it will be assumed that no relaxation of the lattice has occurred. Equation (3) gives vertical deflection, v , for a linear boron gradient through the thickness of a rectangular cantilever structure. See Appendix A for the derivation of equation (3).

$$v = \frac{\alpha_T - \alpha_B}{2 h \alpha_{Si}} y^2 \quad (3)$$

In the above equation, α_T is the lattice constant at the top surface, α_B is the lattice constant at the bottom surface, α_{Si} is the lattice constant of pure silicon, h is the cantilever beam height, and y is the distance along the length of the cantilever beam. Positive values of v indicate downward deflections.

2.2 Microstructural Theory and Studies

Dislocation and x-ray theory are discussed in this section.

2.2.1 Dislocation Theory

When boron diffuses into silicon, it primarily enters substitutional sites in the silicon structure. Since the boron atom is smaller than the silicon atom, its presence will shrink the region it occupies, resulting in a tensile stress within the material. When the strain energy present exceeds the energy required to form a dislocation (dislocation energy) a dislocation will form to introduce plastic relaxation of the material [8]. These dislocations are called misfit dislocations. With higher boron concentration, strain energy becomes higher, and more dislocations are created.

Pure silicon has a diamond cubic crystal structure, which has a primary slip system (slip plane / slip direction) of $\{111\} / \langle 110 \rangle$, as shown in Figure 1. Misfit dislocations of 60° type would be expected with this slip system. However, 60° dislocations may combine to form edge dislocations.

In 1964, Washburn, Thomas, and Queisser [9] examined misfit dislocations caused by phosphorus diffusion in silicon. They used the transmission electron microscope (TEM) to observe dislocations, and found primarily edge dislocations. They also observed that dislocation lines were often decorated by precipitates.

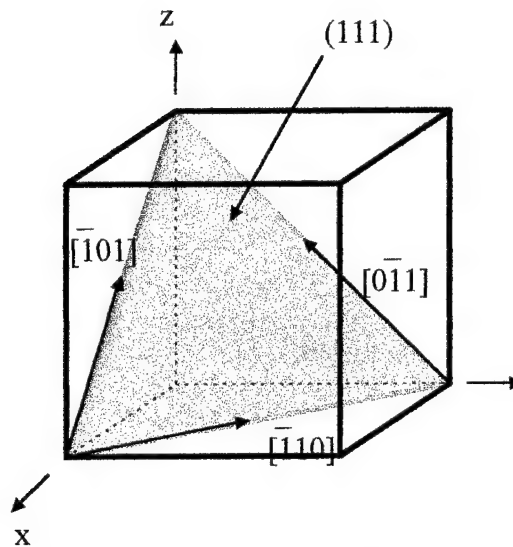


Figure 1: Diamond Cubic slip system.

A plan-view and cross-sectional TEM study of dislocations in heavily boron-doped silicon was done by Ning and Pirouz in 1991 [10]. They showed a dislocation free zone near the surface, with a layer containing dislocations beneath. Thicknesses of the dislocation-free zone and the layer of dislocations were found to be functions of diffusion time. Dislocations were found to be mostly of 60° type with some screw. The Burgers vector was determined to be $\frac{1}{2}\langle 110 \rangle$. Another TEM study was done by Ning, Pirouz, Mehregany, and Chu in 1991 [11] which compared the microstructures of heavily boron-doped silicon subjected to thermal oxidation or having a surface layer of borosilicate glass. Their cross-sectional TEM work did not reveal significant differences.

After dislocation glide has removed the lattice mismatch stress, the dislocations will not move without some sort of external stress. The stress required to cause dislocation motion decreases with increasing temperature. Presence of obstructions, such as precipitates, will increase the required stress.

When the temperature of a wafer is raised in the anneal process, boron diffusion occurs. Changing the boron concentration in a relaxed lattice will introduce a stress. If the stress and temperature combination is high enough, dislocations may move by glide or climb.

In 1970, Erofeev and Nikitenko [12] studied mobility of dislocations in silicon containing impurities, and observed that the activation energy for dislocation motion decreases with increasing electrically active impurity concentration. The effect for donor impurities was stronger than for acceptor.

2.2.2 X-Ray Theory

A relaxed boron-silicon lattice will have a lattice constant smaller than that of pure silicon. In 1991, Baribeau and Rolfe [13] determined variation of the lattice constant of boron-doped silicon as a function of dopant concentration using SIMS and x-ray diffraction. They found a linear relationship between boron concentration and lattice constant. In 1992, Holloway and McCarthy [2] did a thorough review of previous work in determination of lattice contraction of boron-doped silicon.

X-ray diffraction is often used to determine lattice constants associated with a crystalline material using Bragg's law, given in equation (4).

$$n \lambda = 2 d \sin(\theta_B) \quad (4)$$

In the Bragg equation, n is an integer, λ is the x-ray beam wavelength, d is the interplanar spacing and θ_B is the Bragg angle. The lattice constant, α , is related to the interplanar spacing, d , of the (hkl) plane by equation (5).

$$\alpha = d \sqrt{h^2 + k^2 + l^2} \quad (5)$$

A “triple axis $\theta - 2\theta$ ” scan is often used to determine lattice constants with x-ray diffraction. When the x-ray beam leaves the emitter, it passes through a “first crystal” and a narrow slit to minimize $\Delta\lambda$ and to collimate the beam. It then reflects from the sample and passes through another collimator before entering the detector. The term “triple axis” comes from the fact that the beam is redirected at three points: the first crystal, the sample, and the final collimator.

In x-ray diffraction, the Bragg angle, θ_B , is the angle between the incident x-ray beam and the sample surface normal. The diffracted beam will leave the sample at twice the Bragg angle from the incident beam, or $2\theta_B$. While scanning the sample, the x-ray emitter is stationary while the sample rotates to change θ_B . For the detector to receive the diffracted beam, it must rotate by 2θ for every θ rotation of the sample. This procedure explains the term “ $\theta - 2\theta$ scan.”

A triple axis $\theta - 2\theta$ scan will show a narrow peak for the silicon lattice, and other peaks for other lattice constants. The plot of this scan uses seconds ($1/3600$ of a degree) for the abscissa. The Bragg angle associated with a given reflection in pure silicon is known, and the difference in seconds from the silicon peak to other peaks can be measured. Therefore, the Bragg angles for the other peaks can be computed, and thus the lattice constants determined.

2.3 Annealing Theory and Studies

A high temperature anneal treatment is often used to reduce curl in micromechanical structures by creating a more uniform boron distribution through the structure thickness.

In 1990, Ding, Ko, and Mansour [14] created cantilever beams from boron-diffused silicon. They presented optimum anneal conditions for beam flatness with annealing before and after beam release. They did not observe any curl reversal after annealing, but that may have been due to the short beam lengths (600 μm) or limitations of the measurement method used. The method used to measure curl was not discussed.

In 1993, Chu and Mehregany [15] investigated the effect of thermal oxidation (an oxidizing anneal) on the residual stress distribution through the thickness of heavily boron-doped silicon films. They looked at as-diffused and thermally oxidized cantilever beam structures, and observed a curl reversal after thermal oxidation at 1100°C for 50 minutes. Also in 1993, Holloway [16] proposed a theoretical solution for curvature of a structure strained by substitutional doping with an arbitrary concentration profile. He postulated that there would be a tendency for curvature with the opposite sense if conditions occurred where diffusion of the dopant was not accompanied by migration of misfit dislocations.

In 1994, Wang, Xu, Lu, Sun, and Wang [17, 18] reported on the effects of rapid thermal annealing of heavily boron-doped silicon. Rapid anneals were done with ten second durations and $\sim 200^\circ\text{C}/\text{second}$ heating and cooling rates. They observed that boron atoms can be present in interstitial sites and boron-rich silicon precipitates if the boron concentration exceeds the solid solubility limit in bulk silicon material, which affects lattice distortion. They found that lattice mismatch was proportional to substitutional boron concentration rather than total doping concentration in the range $7.5 \times 10^{19} \text{ cm}^{-3}$ to $3.1 \times 10^{20} \text{ cm}^{-3}$. Randomly distributed precipitates cause inhomogeneous strain which results in broadening of the x-ray Bragg reflection peak. They also observed

that boron-rich precipitates dissociate at anneal temperatures above 1100°C and further contract the lattice parameter.

Most recently, in 1995, Cabuz, Fukatsu, Kurabayashi, Minami, and Esashi [19] investigated characteristics of heavily boron-doped silicon mechanical structures. They observed a curl reversal in annealed structures. They explained this behavior by proposing that during the post-diffusion anneal process, low-doped regions experience increasing boron concentration and thus develop tensile stress, while highly-doped regions experience decreasing boron concentration and thus develop compressive stress. They also suggested that a potential solution would be to eliminate formation of dislocations during initial boron diffusion. However, this solution is impractical since it is not possible to prevent dislocations from forming with high concentration boron doping.

The theory presented by Cabuz, et. al. could be tested by investigating boron concentration profiles, lattice constants and dislocations in both as-diffused (curled in one direction) and annealed (curled in the opposite direction) structures. The following results would support the theory.

1) Boron concentration profile becomes more flat after annealing. - The boron gradient through the thickness of an as-diffused wafer causes diffusion of boron when the wafer temperature is elevated during the anneal process. This diffusion will cause the boron distribution to become more uniform.

2) Smallest lattice constants disappear after annealing. - The areas of highest boron concentration before annealing exhibit the smallest lattice constants. During the anneal

treatment, these areas will experience a decrease in boron concentration due to diffusion.

A decrease in boron concentration will cause an increase in lattice constant.

3) Dislocations do not move during annealing. - If the dislocations cannot move, areas of increasing boron concentration will develop a tensile stress, while areas of decreasing boron concentration will develop a compressive stress. These stresses would be relaxed if dislocation motion were to occur.

Chapter 3: EXPERIMENTAL PROCEDURE

3.1 General Approach

Several different methods were used to gain information about the effects of different anneal (high temperature treatment) temperatures on micromechanical structures fabricated from heavily boron-doped silicon. Eleven wafers were fabricated by identical processing except for anneal temperature. Two wafers did not undergo the anneal step at all. The other nine wafers were annealed: one at 900°C, one at 950°C, one at 1000°C, one at 1050°C, two at 1100°C, two at 1150°C, and one at 1175°C.

3.2 Wafer Layout

Each 3-inch diameter wafer was designed to contain 44 tablets. Each tablet was 9mm square and contained a specimen for one of five test methods. The five test methods used were optical measurement (WYKO) of cantilever structure deflections, X-ray diffraction, cross-section TEM, plan-view TEM, and Secondary Ion Mass Spectroscopy (SIMS). The corresponding five types of tablets were called WYKO (W), X-ray (X), cross (C), plan (P) and SIMS (S) respectively. The particular placement shown in Figure 2 was chosen to accomplish maximum number of specimens from each wafer, and allow an automated wafer sawing procedure to efficiently produce the specimens.

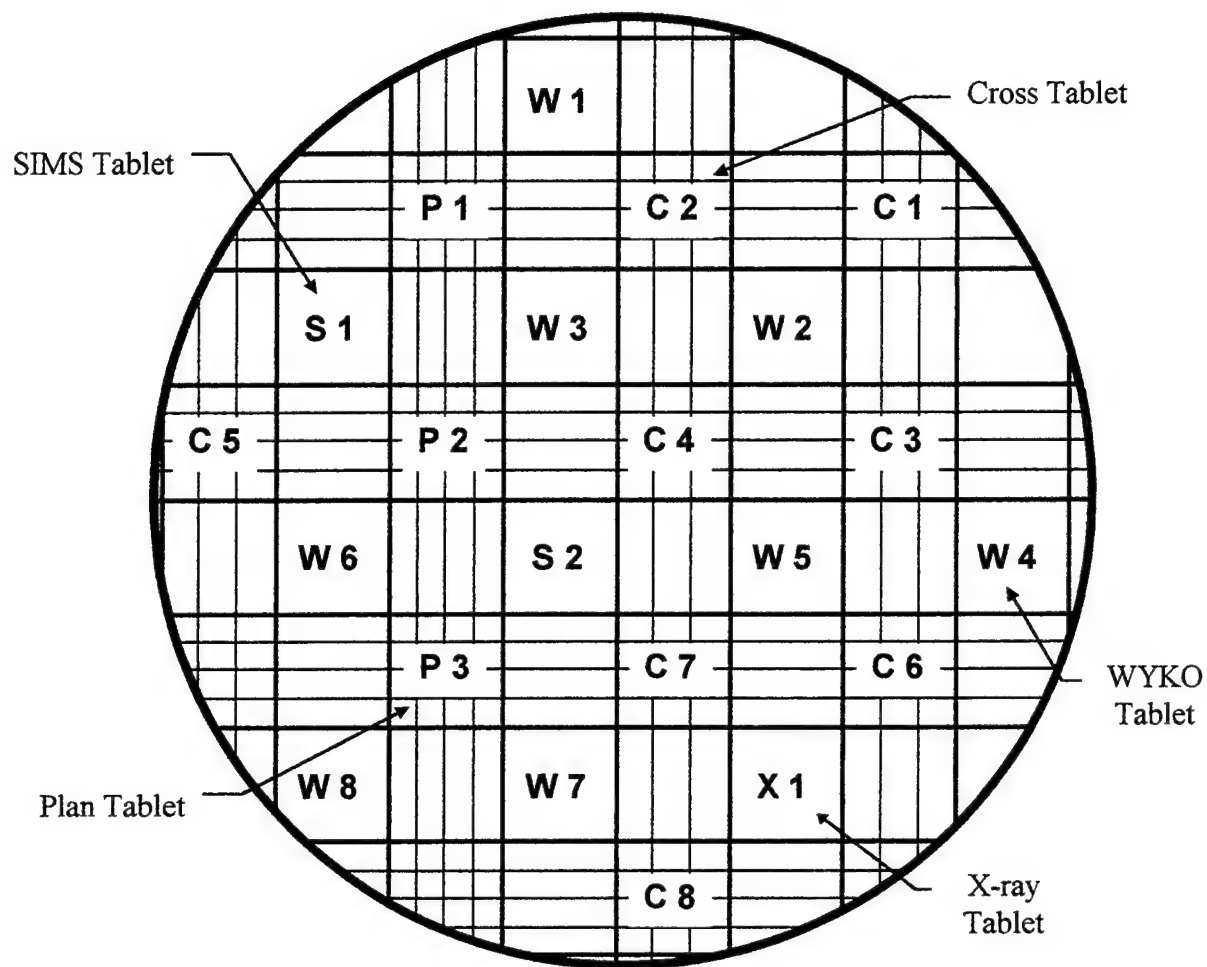


Figure 2: Wafer tablet layout.

3.3 Tablet Tracking

It was important to keep track of the original tablet position on the wafer because previous experimental data had shown that within-wafer variation of properties can be significant. Wafer position designations are included in Figure 2. Each WYKO tablet (cantilever structures) was fabricated with a number on it. X-ray and SIMS tablets were scribed on the back with appropriate numbers before placing them in containers. Tablets

of plan-view and cross-section specimens were placed in separate boxes, which were labeled with appropriate wafer designation and position. WYKO, plan-view and cross-section TEM, and SIMS tablet data from different wafers were only compared when the tablets came from the same wafer positions.

3.4 WYKO Tablet (Cantilever Structures) Design

The WYKO tablets were fabricated with four sets of cantilever beams and two reference structures on each tablet. Each of the four sets of beams had different widths, in particular 30 μ m, 60 μ m, 150 μ m, and 400 μ m. Several beams of each width were fabricated with various lengths from about 30 μ m up to about 3700 μ m. The longest beam length was chosen based on the imaging capability of the WYKO instrument. Each individual beam was attached to glass in the anodic bond processing step by a bond pad. The bond pads were placed such that the beam tips were aligned at a distance of 20 μ m from a reference structure. The reference structures were fabricated as very short (30 μ m) ledges protruding from a rectangular bond pad. These ledges were constructed to be too short to allow any measurable curl, and therefore could be used as a common reference point for beam tip measurements. Figure 3 shows the WYKO tablet layout.

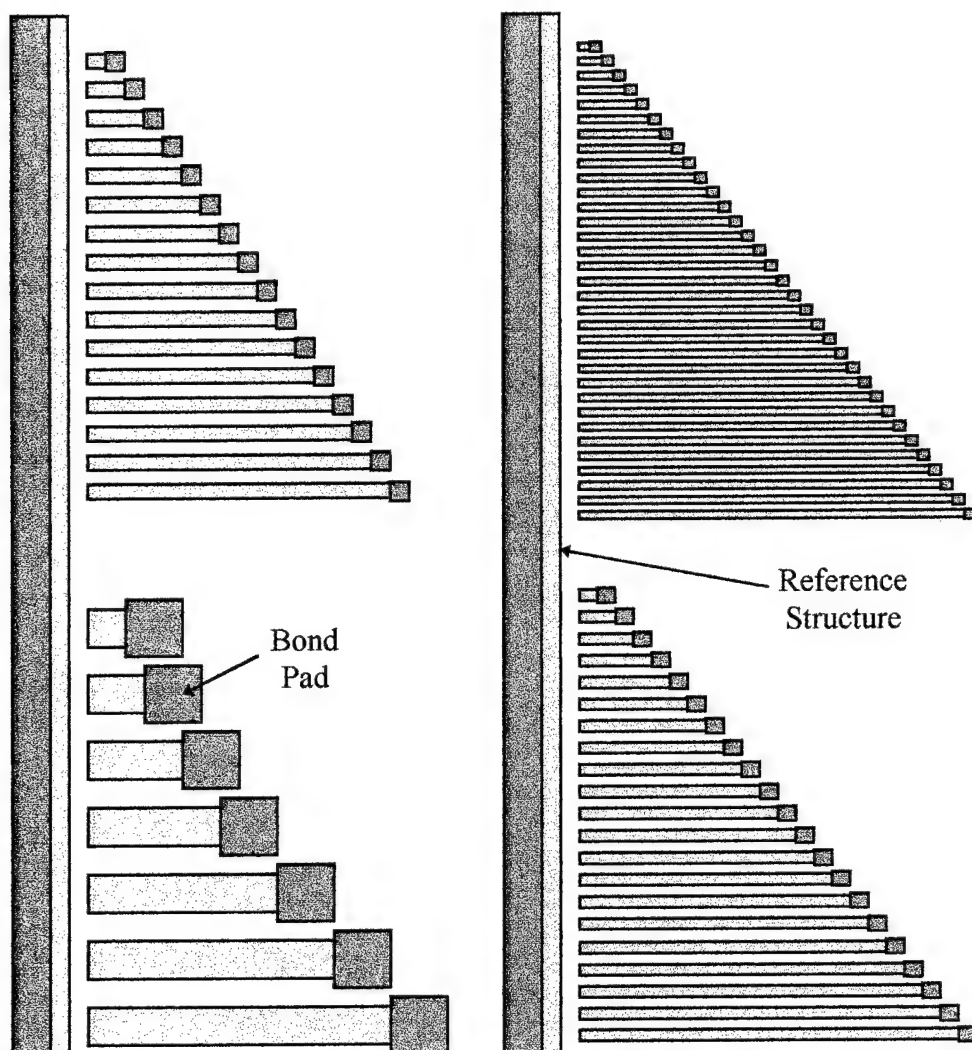


Figure 3: WYKO Tablet Layout

3.5 Wafer Fabrication Process

Before processing was begun, each wafer was scribed on the back with the lot number and a letter designation corresponding to a particular anneal condition. One test wafer was also processed with each experiment wafer. The test wafers did not contain any structures, and were designated by lot number and anneal temperature used. The lot

numbers used were “CS01” and “CS02” which stand for “Curl Study - run #01” and “Curl Study - run #02,” respectively.

The wafer processing procedure described below was used to fabricate the wafers. See Figure 4 for an overall pictorial representation of the fabrication process.

KOH Etch - A pattern was created on the front (shiny) side of the wafer using photoresist as a mask. The unmasked portions of the wafer were etched to a depth of about $2.5\mu\text{m}$ to create “mesas.” After etching, the photoresist was stripped off the wafer.

Boron Diffusion - Boron was diffused on the front side from a solid source. Diffusion temperature, duration, and environment were chosen based on experimental data and recommendations from the boron solid source manufacturer. Since many current micromechanical applications require structure thicknesses greater than $10\mu\text{m}$, diffusion times are quite long. For this experiment, boron diffusion was done for 20 hours at 1150°C in a 4% oxygen environment to achieve the etch-stop concentration of $7 \times 10^{19} \text{cm}^{-3}$ at a depth of about $11\mu\text{m}$.

Dilution Oxidation - This step deposited an oxide on the wafer surface to more easily remove the boron-silicide coating (a remnant of boron diffusion) from the wafer front surface.

Oxide Etch - The oxide deposited in the previous step was removed along with the boron-silicide coating.

Plate Anneal - A high temperature treatment was conducted to help distribute the boron more uniformly through the thickness of interest. The term “anneal” is a

bit of a misnomer, but it is used in practice to refer to the post-diffusion high temperature treatment. As mentioned above, two wafers skipped this step. All other wafers were annealed for 90 minutes in a nitrogen and 6% oxygen ambient. Different wafers were subjected to different anneal temperatures, ranging from 900°C to 1175°C.

Reactive Ion Etch (RIE) - This process “digs trenches” straight down into the wafer to define structure edges. As in the KOH etch step, photoresist was used as a mask. All unmasked parts of the wafer were etched. Trench depth was about 25 μm .

Wafer Saw - The wafer was sawed into tablets.

Anodic Bond - The WYKO tablets were anodically bonded to glass substrate tablets. The bond points were the mesas created during the KOH etch step.

Ethylenediamine pyrazene catechol (EDP) Etch - The excess silicon was etched away from the back surface to release the cantilever structures on the WYKO tablets. Pure silicon etched away quickly. The etch rate slowed with increasing boron concentration up to a concentration of about 7×10^{19} atoms/cm³ which provided a nearly complete etch stop.

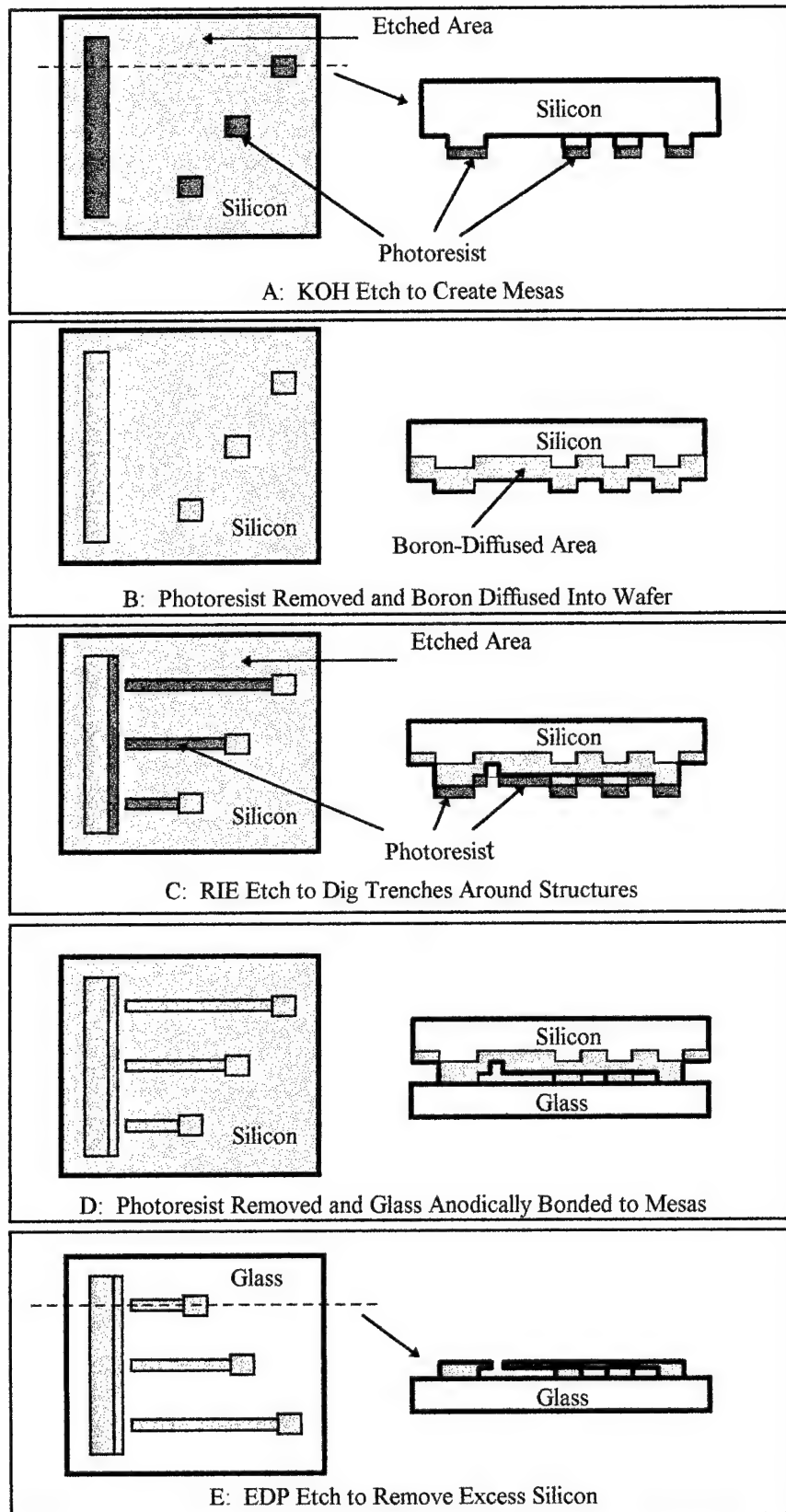


Figure 4: Pictorial Representation of Wafer Processing

CS01 wafer letter "A" was annealed at 1150°C, wafer "B" was annealed at 1100°C, wafer "C" was annealed at 1175°C, and wafer "D" did not undergo the anneal step. Since wafer CS01-D was not annealed it is called the CS01 control wafer.

Initial analysis of the CS01 WYKO tablets revealed that the cantilever structures from wafers A, B and C were all significantly curled up, while the CS01-D structures were all curled down. An RIE mask error was discovered which rendered all the CS01 tablets other than the WYKO tablets unusable. The bulk sections of the wafer had not been properly masked with photoresist prior to the RIE processing step. The RIE mask was repaired to correct the problem, and a second fabrication run, CS02, was done. The CS02 run also included a wider range of anneal temperatures to obtain continuous data from "curled down" beams to "curled up" beams.

CS02 wafer letter "A" was not annealed, wafer "B" was annealed at 900°C, wafer "C" was annealed at 950°C, wafer "D" was annealed at 1000°C, wafer "E" was annealed at 1050°C, wafer "F" was annealed at 1100°C, and wafer "G" was annealed at 1150°C.

After the "wafer saw" step, the various tablets from each wafer were separated into appropriate containers. Only the WYKO tablets completed the last two steps, "anodic bond" and "EDP etch". SIMS tablets were sent out for analysis. TEM specimens were made from both the plan-view and cross-section tablets.

3.6 Test Methods and Equipment

Several different tests were performed on the fabricated wafers to obtain meaningful results. Theories of operation for various types of test equipment used and sample preparation techniques are discussed below.

3.6.1 WYKO Tablet Cantilever Deflection

The WYKO surface profiler was used to measure deflections of the cantilever structures. Data acquired for the “W3” and “W5” tablets for each of the wafers are included in Appendix B.

“WYKO” is a trade name, as opposed to an acronym. The WYKO system is a non-contact optical profiler that can measure a range of surface heights up to 500 μ m. The vertical resolution of the particular instrument used was limited to about 0.08 μ m by its second floor location which experiences building vibration.

The WYKO uses a technique called vertical-scanning interferometry (VSI) to measure rough surfaces and steps. The following explanation of operation is taken directly from the WYKO Users Manual [20]: “In VSI, a white-light beam passes through a microscope objective to the sample surface. A beam splitter reflects half of the incident beam to the reference surface. The beams reflected from the sample and the reference surface recombine at the beam splitter to form interference fringes. During the measurement, a reference arm containing the interferometric objective moves vertically to scan the surface at varying heights. Fringe contrast reaches a peak as the sample becomes completely focused, then falls again. The system scans through focus, and the interference signal for each point is recorded. Finally, the vertical position corresponding

to the peak of the interference signal for each point on the surface is extracted, and a computer image of the surface height profile is displayed.”

3.6.2 X-ray Diffraction

X-ray measurements were made with the Bede D³ diffractometer using a silicon first crystal and copper K α radiation, which gives a characteristic x-ray wavelength, λ , of 1.541Å. The X1 X-ray tablets from the CS01-1175°C test wafer and CS02-A, C, E, and F wafers were analyzed using the triple axis θ - 2θ scan technique to determine lattice constants in the wafers. Data acquired are contained in Appendix C.

For pure silicon with surface normal [001], the first Bragg reflection occurs from the (004) plane with Bragg angle, θ_B , of 34.571°. Using equations (4) and (5) from the Background Theory and Literature Review section and $n=1$, the interplanar spacing, d , is found to be 1.35788Å, and the lattice constant, a , computed as 5.43154Å.

3.6.3 Transmission Electron Microscopy (TEM)

The JEOL JEM-200CX TEM was used to examine dislocations and precipitates in test samples created under different anneal conditions. Selected photographs taken with the TEM are included in Appendix D.

Plan view TEM samples were prepared to look at the density of dislocations near the wafer surface and to look at the topology of the surface itself. Cross-section TEM samples were used to inspect dislocations throughout the wafer thickness.

The TEM used was capable of tilting the sample about two axes, thus allowing orientation of the sample along a particular crystallographic direction of interest. The

double-tilting capability of the TEM was used to view dislocations. The Kikuchi pattern of a single crystal can be observed when the microscope is in "SA Diffraction" mode. In general, higher index directions produce wider Kikuchi lines. The specimen is tilted until the transmitted beam is placed on one side of the Kikuchi line corresponding to the desired direction. At the correct location, another bright spot will light up on the opposite side of the Kikuchi line, producing a "2-beam" condition. Next, an objective aperture is inserted and centered around the transmitted beam. When the TEM is placed back into "MAG" (regular magnification) mode, the dislocations corresponding to the direction selected will appear as dark lines against a bright background. For more information on Kikuchi patterns and TEM theory and operation, see reference [21].

Plan-View Samples - Plan-view TEM specimens were made from the 2.25mm x 2.25mm specimens of the "P2" plan tablets. Each specimen was mechanically thinned from the back surface of the wafer using a South Bay Technologies Model 145 Lapping and Polishing Fixture. Bulk thinning was accomplished with 320 grit paper and final thinning with 600 grit paper. Polishing was then done with 3 μ m paper followed by 1 μ m paper to a mirror finish. Final specimens had an average thickness of about 45 μ m after mechanical thinning.

After each specimen was thinned and polished, a standard 3mm copper grid was cemented to it. Then the specimen was ion milled from the back side until a hole developed in it, so that the thinned area surrounding the hole could be used for TEM analysis. The final specimen had a normal direction of [001]. After inspecting the specimen surface under TEM, the top side of the specimen was milled to reveal

specimen surface at a depth of approximately $5\mu\text{m}$, since dislocations were expected at this depth.

Cross-Section Samples - Cross-section TEM specimens were made from the $2.25\text{mm} \times 3.00\text{mm}$ samples of the "C4" cross tablets. Four cross-section samples were bonded together to make a specimen "sandwich". The sandwich was then mechanically thinned from the 3.00mm edge to about half the original 2.25mm thickness using the same thinning and polishing method as described above for the plan-view TEM samples. The specimen was then turned over and the procedure repeated until a final polished thickness of about $45\mu\text{m}$ was accomplished. This procedure produced a viewing normal direction of $[011]$. After the specimen was thinned and polished, a standard 3mm copper grid was cemented to it. Then the specimen was ion milled from both sides until a hole developed in the center of the specimen, so that the thinned area surrounding the hole could be used for TEM analysis.

3.6.4 Secondary Ion Mass Spectroscopy (SIMS)

SIMS analysis was accomplished at Wright Laboratory, Wright-Patterson Air Force Base, Ohio, using a quadrupole-based SIMS with a mass-filtered 12kV oxygen beam at 70° incidence angle. SIMS depth profiling is a technique used to determine elemental concentrations of dopant and impurity atoms within a material as a function of depth. To generate a depth profile, a primary ion beam is scanned over the sample surface. Atoms are ejected from the surface, with some being positive or negative ions. These ions are collected, mass filtered, and ions with the desired mass are counted using

a mass spectrometer. The material surface is continuously eroded, and thus chemical information is determined as a function of depth.

The S2 SIMS tablets from two wafers were sent to Wright Laboratory at Wright-Patterson Air Force Base, Ohio, for SIMS analysis. SIMS depth profile data for boron content was acquired for the CS02-A wafer (control - no anneal) and the CS02-F wafer (1100°C anneal). Data received are contained in Appendix E.

Chapter 4: RESULTS AND DISCUSSIONS

High temperature treatment and its effects on curl and microstructure of heavily boron-doped silicon were investigated. The results of these investigations are included below, beginning with the direct optical measurement of curl of cantilever structures and followed by results of x-ray diffraction, TEM observations, and SIMS analysis.

4.1 Cantilever Structures

Data taken from the WYKO tablets are included in Appendix B. On most of the WYKO tablets, several beams were missing or broken after completing the EDP etch processing step. Beams that were missing or broken were reported as such in the data recorded in Appendix B.

The WYKO instrument was used to measure cantilever beam deflections. All measurements on the beams that were curled up were taken at the beam tip. These measurements were taken relative to the reference structures. For beams that were curled down, the tips of beams with sufficient length would contact the glass, causing the middle part of the beam to get pushed up. Therefore, for beams that were curled down far enough to touch the glass, a measurement was taken of the highest point on the beam. Since this point was often too far from the reference structure to include in the same measurement, measurements of highest points were taken relative to the glass. This measurement was then converted to a predicted tip deflection (as if the glass was not present) using equation (6), where v_t is the tip deflection, C is a constant, L is the beam

length, and h is the beam thickness. The derivation of equation (6) is included in Appendix A.

$$v_t = \frac{CL^2}{2h} \quad (6)$$

4.1.1 CS01 Results

The tip deflection data taken from the 150 μm width beams of WYKO tablets number 5 from each wafer is shown graphically in Figure 5.

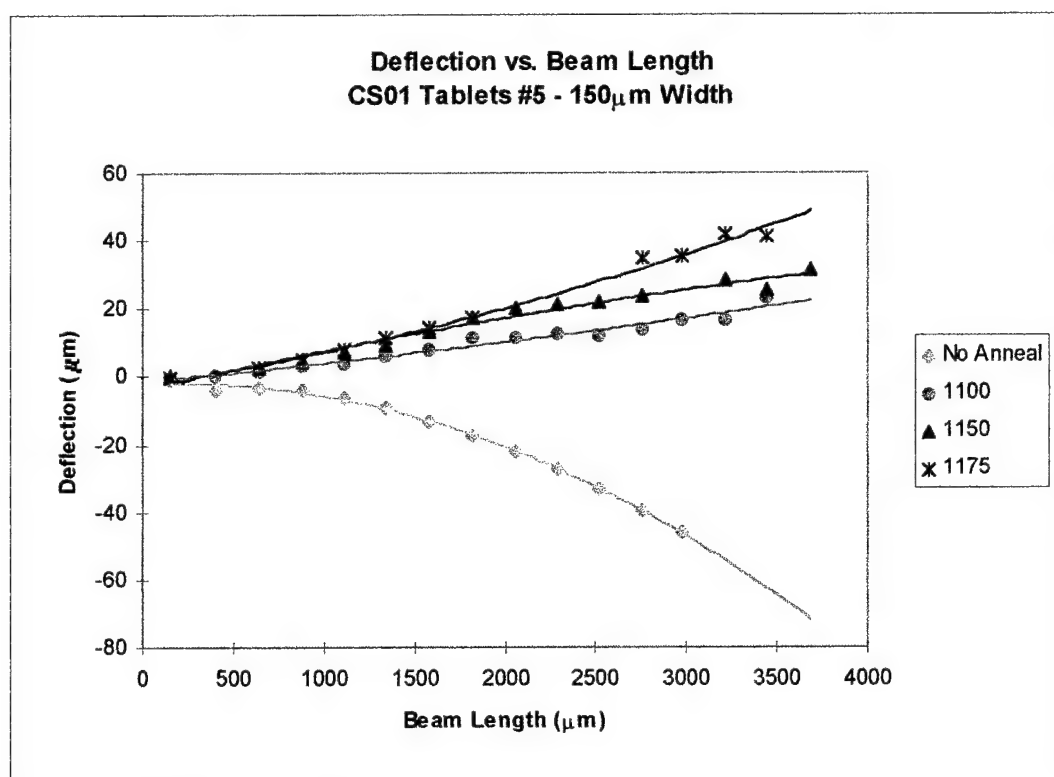


Figure 5: Comparison of Beam Tip Deflections for CS01 Wafers

Figure 5 clearly shows that all cantilever beams are curled down when no anneal is used (wafer CS01-D), and that all beams are curled up when annealed at temperatures of

1100°C and above (wafers CS01-A, B and C). Furthermore, Figure 5 shows that the upward curl becomes greater with increasing anneal temperature.

Unfortunately, none of the anneal temperatures used was low enough to allow the beams to remain curled down. Data from Figure 5 was used to predict the transition point from curled down cantilevers to curled up. First the data points for the 1100°C, 1150°C, and 1175°C wafers were plotted again and each data set was fit with a linear trendline. These data points, along with the trendline formulae are shown in Figure 6.

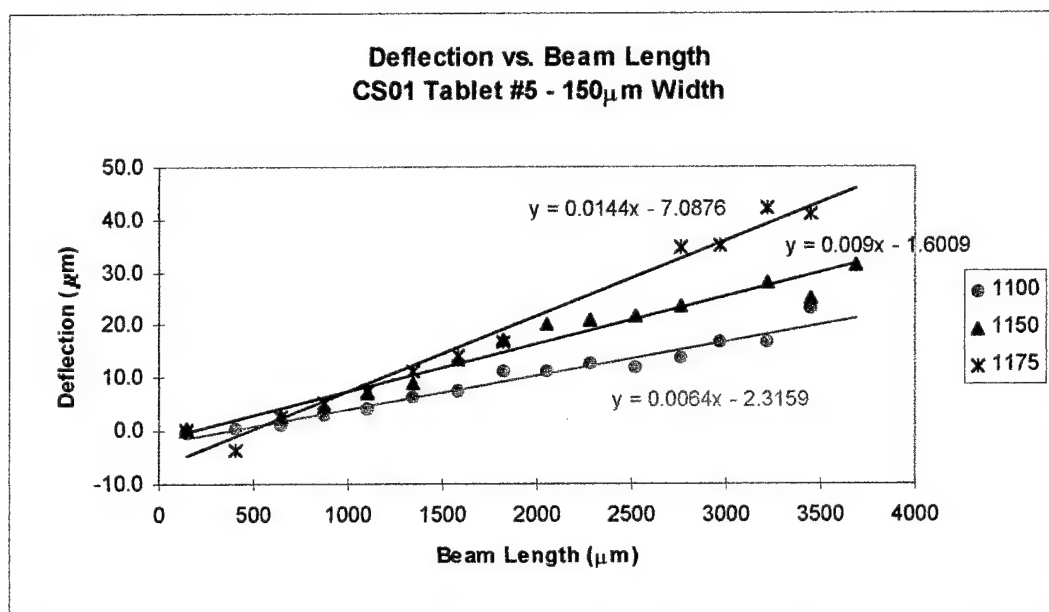


Figure 6: Linear Trendlines for Beam Tip Deflections for CS01 Wafers

Next, using the slopes calculated for the trendlines shown in Figure 6, another plot was created for anneal temperature vs. slope. This plot is shown in Figure 7. A linear trendline was fitted to this data, and the y-intercept (point of zero slope) was taken as the predicted curl reversal temperature. As seen in the trendline formula in Figure 7, the y-intercept was about 1050°C; this value is, therefore, a rough estimate of where curl reversal would be expected for a 90 minute anneal.

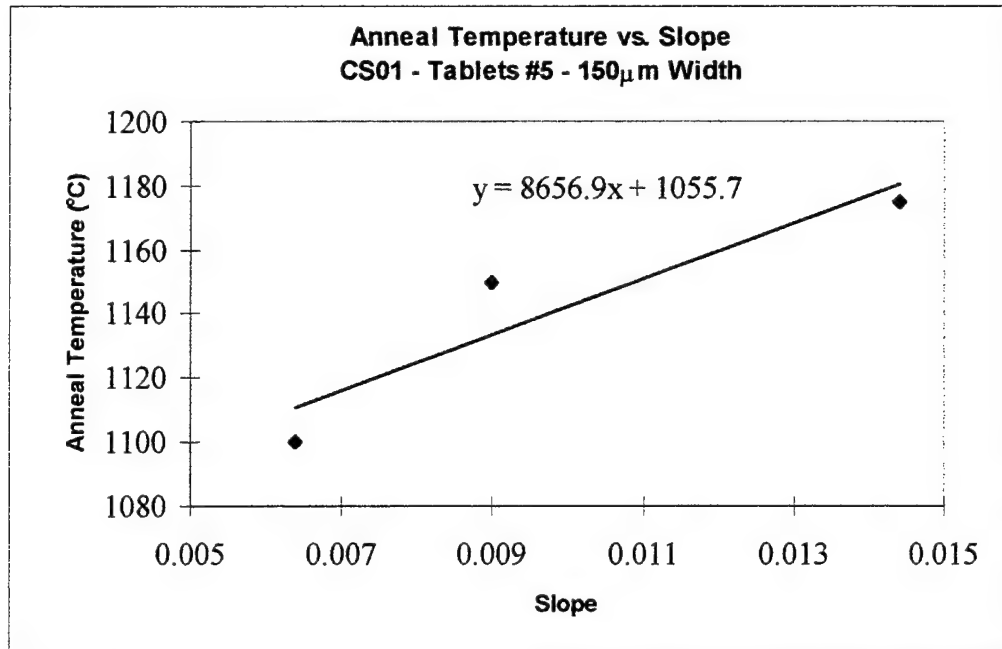


Figure 7: Prediction of Curl Reversal Anneal Temperature

4.1.2 CS02 Results

Based on data acquired from CS01, CS02 was processed to include several lower anneal temperatures. The tip deflection data taken from the 150µm width beams of WYKO tablets number 5 from each wafer is shown graphically in Figure 8. Wafer CS02-G (1150°C anneal) was not included because this wafer was destroyed during processing. Figure 8 clearly shows that all cantilever beams are curled down when no anneal is used (wafer CS02-A) or if the anneal temperatures are at or below 1000°C (wafers CS02-B, C and D), and that all beams are curled up for the 1100°C anneal temperature (wafer CS02-F). This data suggests that there is a transition from curled down to curled up somewhere between 1000°C and 1100°C.

Cantilever structures from the wafer annealed at 1050°C (CS02-E) exhibited interesting behavior. Narrow width cantilevers (30µm and 60µm) were primarily curled

up, while wider cantilevers ($150\mu\text{m}$ and $400\mu\text{m}$) were predominantly curled down. The reasons for this behavior are unknown. The wide cantilevers may be responding to curl stresses as plates instead of beams. This transitional behavior does support the prediction from CS01 data of a transition point near 1050°C .

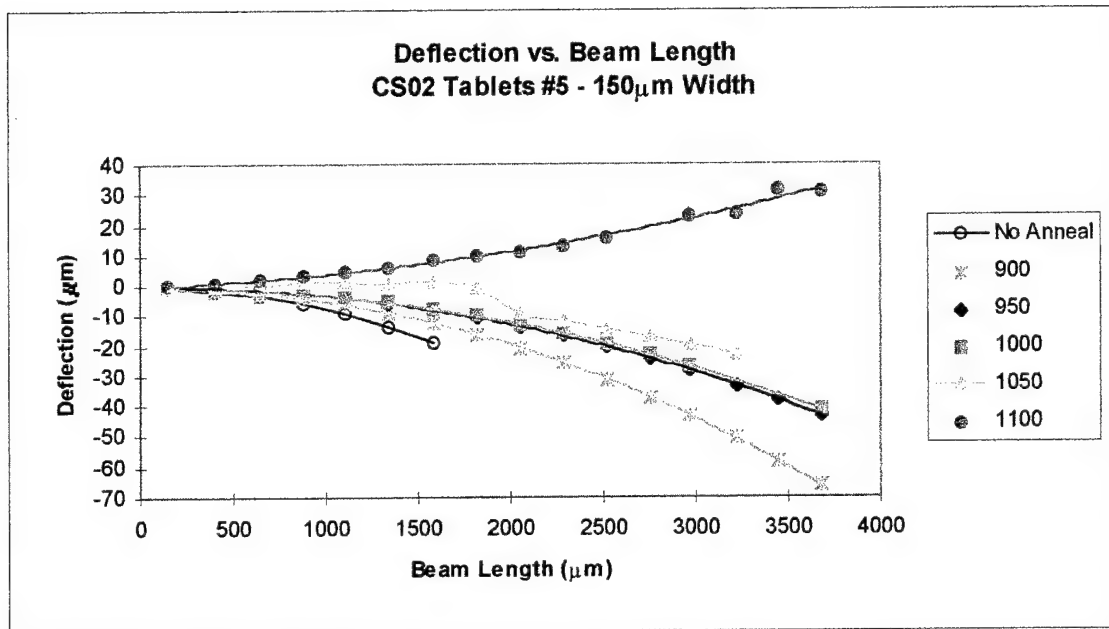


Figure 8: Comparison of Beam Tip Deflections for CS02 Wafers

4.1.3 Comparison of CS01 and CS02

A control wafer and a wafer with an 1100°C anneal were successfully fabricated in both processing runs. The cantilever beam tip deflection data was compared for these wafers to show run variations. All beams for both control wafers were curled down, all beams for the 1100°C wafers were curled up, and there was good agreement between the magnitudes of the deflections. Data for the $150\mu\text{m}$ width beams on tablets number 5 of the 1100°C annealed wafers are compared in Figure 9.

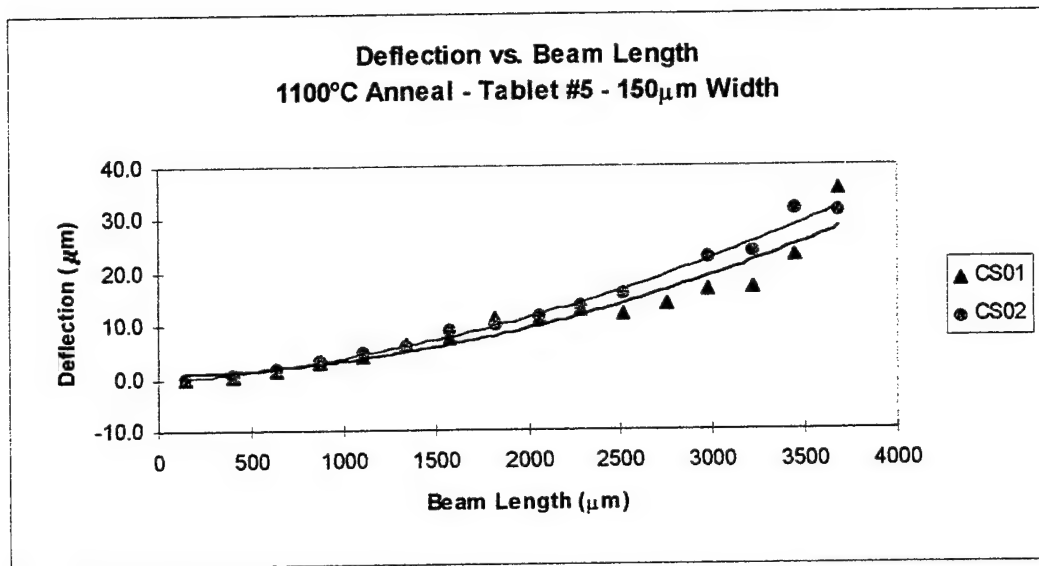


Figure 9: Comparison of Tip Deflections for CS01 and CS02
1100°C Annealed Wafers

Figure 10 shows a comparison of data for the 150μm width beams on tablets number 5 of the control wafers to the theoretical deflection expected using equation (3) from the Background Theory and Literature Review section.

In equation (3), the following values were used: $\alpha_T = 5.4274\text{\AA}$, which corresponds to a top surface boron concentration of $7 \times 10^{19} \text{cm}^{-3}$ (etch-stop concentration), $\alpha_B = 5.4240\text{\AA}$, which corresponds to a bottom surface boron concentration of $2 \times 10^{20} \text{cm}^{-3}$, $\alpha_{Si} = 5.4315\text{\AA}$, and $h = 11\text{\AA}$. The boron concentrations were converted to lattice constants using data compiled by Baribeau and Rolfe [13]. Note that the bottom surface of the cantilever beam was originally the front (diffused) surface of the wafer, and the top surface of the beam was formed from the EDP etch processing step (see Figure 1 in Background Theory and Literature Review section). Equation (3) gives an expected cantilever deflection of $28.45 \text{ y}^2/\text{m}$ along the length y .

From Figure 10, it is clear that the theoretical solution is not accurate for the cantilever beams fabricated in this experiment. This is true because equation (3) holds for a completely strained lattice. The presence of dislocations would significantly reduce the expected deflection.

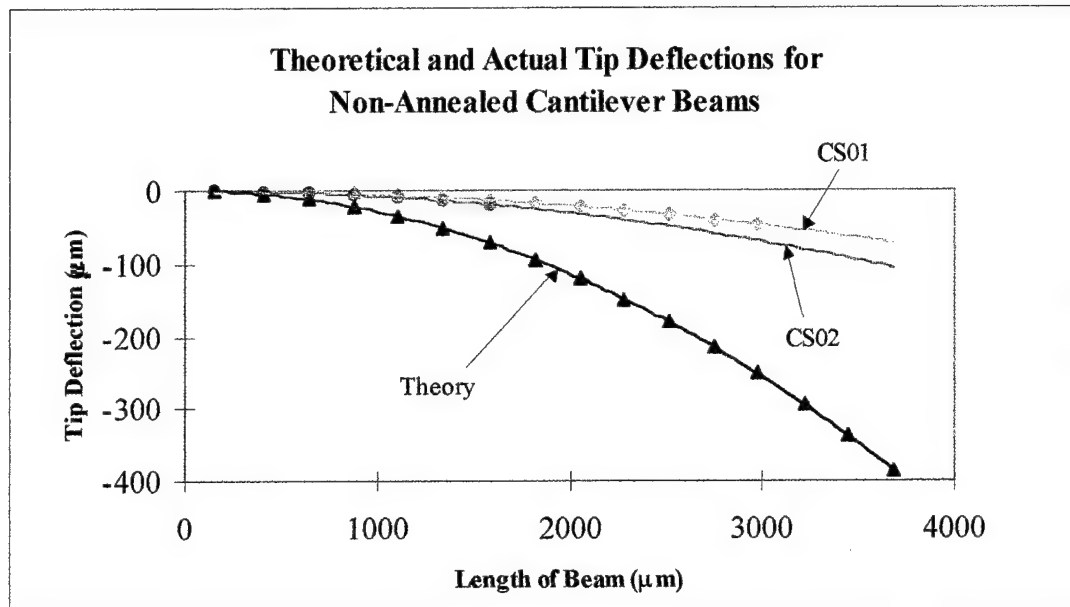


Figure 10: Comparison of Control Wafer Tip Deflections with Theory

4.2 X-ray Diffraction

Triple axis $\theta - 2\theta$ scans were done on samples taken from the CS01-1175°C test wafer, and from the CS02-A, C, E, and F wafers (control, 950°C, 1050°C, and 1100°C, respectively). X-ray diffractometer data are included in Appendix C. It is known that the first narrow peak of the $\theta - 2\theta$ scans corresponds to silicon for all the wafers tested. Therefore, all plots were normalized to each other by giving the silicon peak an amplitude of 1000 counts at an angle of zero. Figure 11 shows this normalized plot.

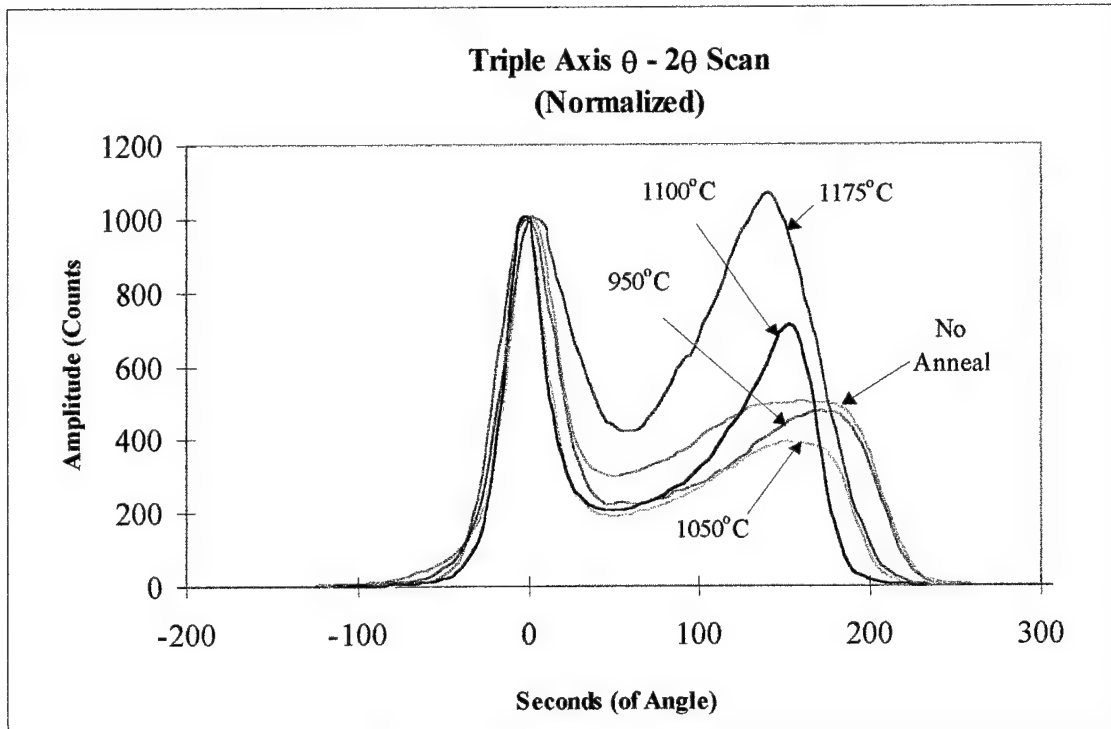


Figure 11: Normalized $\theta - 2\theta$ Scan Plots

The second peaks showing other lattice constants in the wafers are all to the right of the silicon peak. This shows that the Bragg angles are larger and, therefore, the lattice constants smaller than that of pure silicon. This result was expected since the substitutional boron in the silicon lattice will decrease the lattice size. Previous SIMS work [7] has shown boron concentrations as high as $2 \times 10^{20} \text{ cm}^{-3}$ near the surface of as-diffused wafers. Using information recorded by Baribeau and Rolfe [13], boron concentrations from the $7 \times 10^{19} \text{ cm}^{-3}$ to $2 \times 10^{20} \text{ cm}^{-3}$ would give an expected range of lattice constants from 5.4240 \AA to 5.4274 \AA .

The second peaks are broad compared to the silicon peak, which indicates a range of lattice constants. The second peaks become more narrow with increasing anneal temperature and show increasing amplitude with increasing anneal temperature above 1100°C .

To determine the primary lattice constants present, a peak was considered to cover the range of angles corresponding to amplitudes at least 95% of the greatest amplitude in that particular peak. The angles were converted to lattice constants using equations (4) and (5) in the Background Theory and Literature Review section, with $\lambda = 1.541\text{\AA}$ and $\theta_B = 34.571 + \theta_d$, where θ_d is the angle difference between the silicon peak and the second peak of interest. For comparison, the lattice constant of pure silicon is 5.43154\AA . These results are contained in Table 1.

Wafer Identification	95% Peak Angles (seconds)	Primary Lattice Constants (\AA)	Difference From Silicon Lattice Constant (\AA)
CS02 - None	130 to 185	5.42657 to 5.42448	-0.00496 to -0.00706
CS02 - 950	155 to 185	5.42562 to 5.42448	-0.00592 to -0.00706
CS02 - 1050	140 to 170	5.42619 to 5.42505	-0.00534 to -0.00649
CS02 - 1100	150 to 155	5.42581 to 5.42562	-0.00572 to -0.00592
CS01 - 1175	135 to 145	5.42638 to 5.42600	-0.00515 to -0.00553

Table 1: Primary Lattice Constants

The range of primary lattice constants listed in Table 1 are all within the expected range of 5.4240\AA to 5.4274\AA . The boldface data in Table 1 show that the smallest primary lattice constant present in a wafer becomes larger with increasing anneal temperature. This result supports the theory presented by Cabuz et. al. [19], which suggests that the most highly boron-doped regions (which have the smallest lattice constants) experience a decrease in boron content during post-diffusion annealing, which increases their lattice constants.

4.3 TEM Observations

Several cross-section and plan-view TEM samples were made and inspected. For the cross-section samples, the distance from the wafer surface to the first and last dislocations, and the dislocation density were of interest. Visual inspection of photographs taken from each sample indicated that dislocation density remains roughly constant for all wafers. Measuring the distance of first dislocations from the wafer surface was fairly simple since all samples showed a clear dislocation-free zone near the surface. However, measuring the distance to the last dislocation was subjective, since small dislocations could still be found quite deep (i.e., $>20\mu\text{m}$) into the wafers. There was a slight trend of decreasing distance to first dislocations with increasing anneal temperature, as shown in Table 2. This motion is driven by the boron diffusion during the anneal process, and the mechanism may be dislocation climb. Representative photographs of cross-section TEM specimens are included in Appendix D.

Wafer Identification	Range of First Dislocation Depth (μm)	Average First Dislocation Depth (μm)
CS02 - No Anneal	3.7 to 6.2	4.93
CS02 - 950	3.5 to 5.0	4.00
CS02 - 1100	2.5 to 4.3	3.40
CS01 - 1175	2.5 to 4.3	3.65

Table 2: Cross-Section TEM Sample First Dislocation Depth

For the plan-view samples, dislocation density and precipitate density were of interest. As with the cross-section samples, visual inspection of photographs taken from each plan-view sample did not show any noticeable variation in dislocation density. Many precipitates were found, but there did not appear to be any change in precipitate density with different anneal processes. Close examination of precipitates revealed that

some dislocations nucleate at precipitate sites. TEM photographs are included in Appendix D.

4.4 SIMS Analysis

SIMS analysis was conducted on the CS02-A (control) wafer and the CS02-F (1100°C anneal) wafer. Data are included in Appendix E. The data provided by Wright Laboratory gives the amplitude ratio of boron to silicon signals versus sputter time. The B/Si signal amplitude ratio corresponds to boron concentration. Sputter time was converted to sputter depth using the sputter rate of 1.91 nm/sec provided by Wright Laboratory. Exact boron concentration information could not be determined from the data available, but concentration profiles of the two wafers were compared. The profile amplitudes were adjusted to reflect the assumption that total boron content remains constant during annealing. This comparison is shown in Figure 12.

Figure 12 indicates that the boron concentration profile for non-annealed wafers is fairly linear from 1 μ m to 11 μ m in depth. Since the expected etch-stop depth in this wafer was 11 μ m, this result shows that the boron distribution through the thickness of a non-annealed structure was reasonably linear. Figure 12 also reveals that the profile flattens out considerably after annealing at 1100°C. This result is expected since the boron gradient in a non-annealed wafer will cause further boron diffusion upon heating to a sufficiently high temperature.

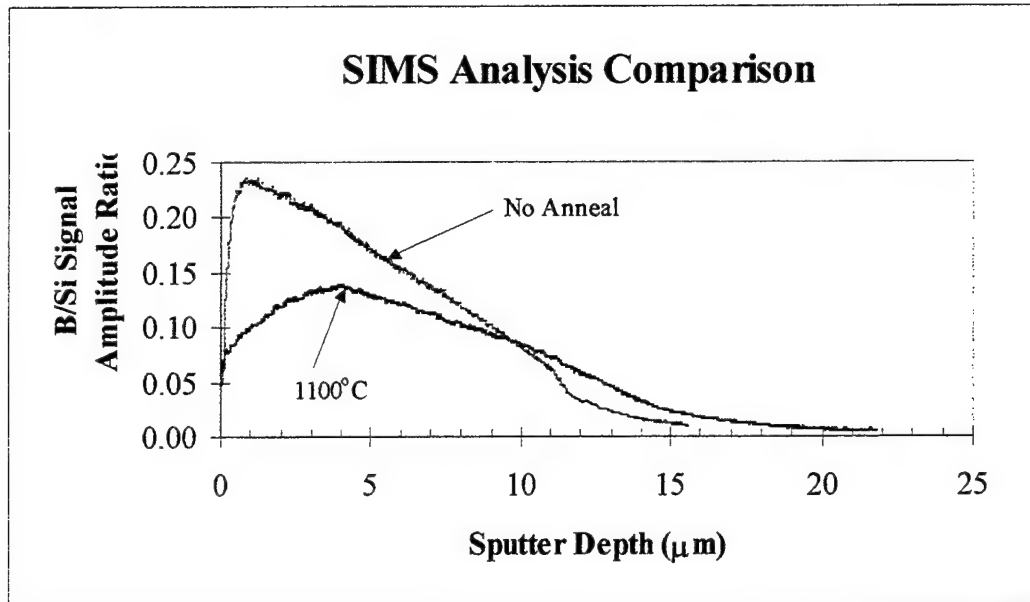


Figure 12: Comparison of Boron Profiles for CS02 Control and 1100°C Wafers

Chapter 5: CONCLUSIONS

Several conclusions have been reached from the data acquired in this work and review of previous work.

5.1 Cantilever Structures

Data from cantilever structure tip deflections has shown that curl is a strong function of anneal temperature. Downward curl decreases with increasing anneal temperature until some transition temperature at which the curl reverses; upward curl increases with further increase in anneal temperature. The transition temperature is difficult to predict exactly, but is between 1000°C and 1100°C, and most probably near 1050°C. Near the transition temperature, narrow and wide cantilevers tend to curl in opposite directions.

The optimum anneal temperature must not be too close to the actual transition point since structure curl may be unstable at the transition temperature. Further work must be done to pinpoint an optimum stable temperature.

The control wafers and 1100°C annealed wafers showed good agreement in tip deflections from CS01 to CS02.

The tip deflections of the control wafers were much smaller in magnitude than the theoretical deflections calculated from equation (3). This is primarily due to the presence of dislocations, which relax the lattice. The presence of boron-rich silicon precipitates also creates a deviation from the model. Also, since the etch-stop ($7 \times 10^{19} \text{ cm}^{-3}$) is reached inside the graded boron-silicon region, the lattice constant change through the thickness of actual cantilever beams will not be linear. Thus, the

assumptions of a completely strained (i.e., unrelaxed) lattice and linear change in lattice constant were not correct in the derivation of equation (3).

5.2 X-Ray Diffraction

Magnitudes of lattice constants obtained through triple axis $\theta - 2\theta$ scans were in the range expected using data compiled by Baribeau and Rolfe [13] for lattice constant as a function of boron concentration in silicon. Amplitude of the second (contracted lattice) peaks increased with increasing anneal temperature above 1100°C, which is expected to occur with a flattening of the boron concentration profile, since a greater area would be obtaining the same lattice constant. Magnitude of the smallest lattice constant present in a wafer increased with increasing anneal temperature. This increase in lattice constant results from areas of highest boron concentration losing boron during the anneal process.

5.3 TEM Observations

A dislocation-free zone is present near the surface of all annealed and non-annealed wafers. The large spread in this data may be due to within-wafer variations during boron diffusion and subsequent annealing. The size of the dislocation-free zone appears to decrease slightly with increasing anneal temperature.

The decrease in the size of the dislocation-free zone may be due to diffusion of boron during annealing. During the anneal process, boron moves to cause a more uniform distribution through the wafer. The areas of high boron concentration (near the front surface of the wafer) lose boron, which should be accompanied by the removal of

dislocations. Thus, dislocations would be observed moving toward the surface of the boron-silicon layer, which is the front surface of the wafer.

Dislocation and precipitate density did not visually change with anneal temperature. Some precipitates served as dislocation nucleation sites. Boron-rich precipitates did not dissociate with high temperature anneals, in contrast to results reported by Wang et. al. [17] for rapid thermal anneals above 1100°C.

5.4 SIMS Analysis

The boron concentration profile for non-annealed wafers is fairly linear from 1 μm to 11 μm in depth. The profile becomes much more flat, indicating a more uniform boron distribution, to a depth of about 11 μm after annealing at 1100°C. This results from boron diffusion that occurs during the anneal treatment.

If the boron diffusion takes place more quickly than the dislocations in the wafer can move, the areas of decreasing boron concentration would develop a compressive stress, and the areas of increasing boron concentration would develop a tensile stress.

5.5 Correlation Between Microstructural Observations and Curl Reversal

The data acquired in this work partially supports the theory presented by Cabuz et. al. [19] as discussed in the Background Theory and Literature Review section. For the theory to hold, the following must be observed after anneal at sufficiently high temperature: 1) the boron concentration profile should become more flat, 2) the smallest lattice constants should disappear, and 3) dislocations should not move.

This work has shown that the boron concentration profile does flatten, and that the smallest lattice constants do disappear after annealing. However, dislocations do not remain stationary.

Although dislocation motion does occur, this motion may not be great enough to fully relax the lattice. In this case, stresses may still remain which explain the curl reversal behavior found in annealed cantilevers.

Chapter 6: RECOMMENDATIONS FOR FUTURE WORK

There is still much useful work yet to be done in the investigations of microstructure and curling behavior of heavily boron-doped silicon. Repeatability of experiments done in this work should first be thoroughly tested. In particular, more fabrication runs should be done using the same environments to verify repeatability of the process used.

There are several areas where more extensive research could be done to continue the work presented in this thesis. The curl reversal anneal temperature should be investigated more thoroughly by focusing on anneal temperatures between 1000°C and 1100°C, particularly in the region around 1050°C. The apparent width dependence of curl direction seen in cantilever structures annealed at 1050°C should also be verified.

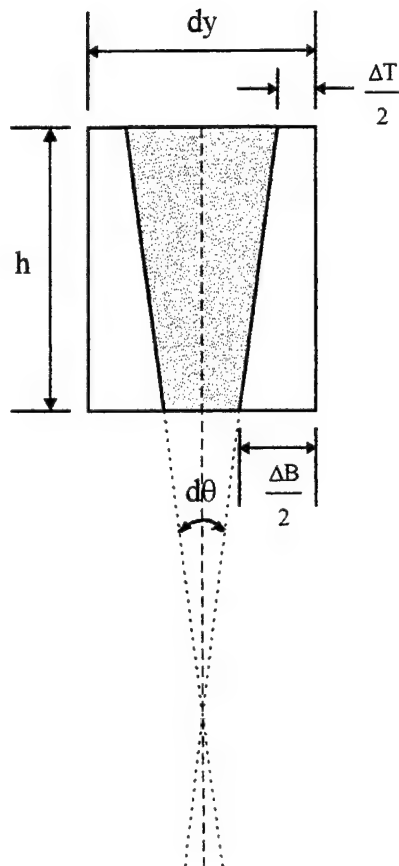
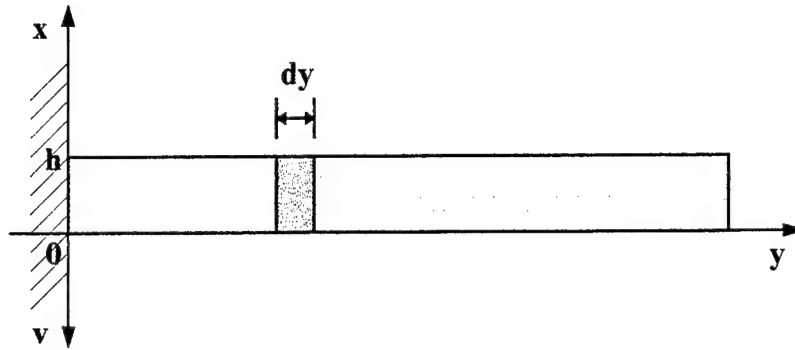
More extensive TEM analysis should be done. Actual dislocation and precipitate densities should be determined. Dislocation types should be determined for different anneal conditions, and studies done to describe dislocation motion during annealing.

Since temperature was the only variable in this experiment, other annealing variables should also be analyzed, such as time and environment.

A related issue is variation of properties at different locations on a single wafer. A study of this problem might begin by comparing cantilever beam deflections from different areas on a single wafer.

APPENDIX A: DERIVATION OF EQUATIONS

Derivation of Equation (3): Theoretical Curl in Non-Annealed Cantilever Structures



Definition of Terms

v = vertical deflection of beam (positive down)

h = height of beam

ΔT = shrinkage of top surface of beam

ΔB = shrinkage of bottom surface of beam

θ = angle of rotation of beam

α_{Si} = lattice constant of pure silicon

α_T = lattice constant of top surface of beam

α_B = lattice constant of bottom surface of beam

$$\Delta T = dy \left(1 - \frac{\alpha_T}{\alpha_{Si}} \right) \quad \Delta B = dy \left(1 - \frac{\alpha_B}{\alpha_{Si}} \right)$$

$$\frac{dy}{\alpha_{Si}} = \frac{dy - \Delta T}{\alpha_T} = \frac{dy - \Delta B}{\alpha_B}$$

$$\tan\left(\frac{d\theta}{2}\right) = \frac{\Delta B - \Delta T}{h}$$

$$\text{For small } d\theta, \tan(d\theta/2) \approx d\theta/2 \Rightarrow d\theta = \frac{\Delta B - \Delta T}{h} = \frac{dy}{h} \left[\frac{\alpha_T - \alpha_B}{\alpha_{Si}} \right]$$

$$\boxed{\frac{d\theta}{dy} = \frac{\alpha_T - \alpha_B}{h \alpha_{Si}}} \quad \text{For curl, } \frac{d\theta}{dy} = \frac{d^2 v}{dy^2}$$

$$\frac{d^2 v}{dy^2} = \frac{\alpha_T - \alpha_B}{h \alpha_{Si}} = \frac{d}{dy} \left(\frac{dv}{dy} \right)$$

$$\frac{dv}{dy} = \int \frac{\alpha_T - \alpha_B}{h \alpha_{Si}} dy = \frac{\alpha_T - \alpha_B}{h \alpha_{Si}} y + K1$$

$$v = \int \left(\frac{\alpha_T - \alpha_B}{h \alpha_{Si}} y + K1 \right) dy = \frac{\alpha_T - \alpha_B}{2 h \alpha_{Si}} y^2 + K1 y + K2 \quad (A)$$

Boundary Conditions:

$$\text{At } y = 0, dv/dy = 0 \Rightarrow K1 = 0$$

$$\text{At } y = 0, v = 0 \Rightarrow K2 = 0$$

$$\boxed{v = \frac{\alpha_T - \alpha_B}{2 h \alpha_{Si}} y^2} \quad (3)$$

Derivation of Equation (6): Predicted Tip Deflection of Beams Curled Down

Beginning with Equation (A) from above:

$$v = \frac{\alpha_T - \alpha_B}{2 h \alpha_{Si}} y^2 + K1 y + K2 \quad (A)$$

To simplify the nomenclature, let $\frac{\alpha_T - \alpha_B}{\alpha_{Si}} = C$.

For beams that are curled down far enough for the tip to contact the glass (giving measured tip deflection of G , which is about $3.5\mu\text{m}$), we have the following boundary conditions:

$$\text{At } y=0, v=0 \Rightarrow K2=0$$

$$\text{At } y=L, v=G \Rightarrow K1 = \frac{G}{L} - \frac{CL}{2h}, \text{ where } L = \text{length of the beam.}$$

$$\text{This gives: } v = C \frac{y^2 - Ly}{2h} + \frac{Gy}{L}$$

We can measure experimentally the highest beam deflection, v_h , and the length along the beam at which that deflection occurs, y_h . C can be found by substituting these values, and rearranging the above equation to give:

$$C = \frac{2h}{y_h^2 - Ly_h} \left(v_h - \frac{Gy_h}{L} \right) \text{ which is a unitless constant.}$$

Now, the predicted tip deflection, v_t (as if the glass was not there) can be found by substituting C and $y=L$ into Equation (3) from above, to give Equation (6):

$$\boxed{v_t = \frac{CL^2}{2h}} \quad (6)$$

APPENDIX B: WYKO DATA

Wafer **CS01 - A**

Tablet # **3**

Width = 30μm			Width = 60μm			Width = 150μm			Width = 400μm		
	Beam Length (μm)	Tip Deflection (μm)		Beam Length (μm)	Tip Deflection (μm)		Beam Length (μm)	Tip Deflection (μm)		Beam Length (μm)	Tip Deflection (μm)
1	28	-0.75	1	49	-1.07	1	148	-0.06	1	393	1.27
2	67	-0.98	2	70	-0.82	2	408	0.91	2	872	4.20
3	108	-0.96	3	107	-0.96	3	644	2.36	3	1343	2.46
4	147	-0.93	4	188	-0.73	4	878	4.35	4	1823	5.65
5	188	-0.77	5	230	-0.75	5	1106	6.81	5	2287	missing
6	228	-0.88	6	360	-0.16	6	1345	9.00	6	2751	26.65
7	258	-0.68	7	459	0.38	7	1581	12.06	7	3211	51.49
8	357	-4.25	8	658	1.78	8	1819	13.46			
9	457	0.06	9	759	2.43	9	2056	15.06			
10	557	1.02	10	959	4.37	10	2284	17.32			
11	657	1.70	11	1056	5.55	11	2520	19.95			
12	759	1.79	12	1256	8.13	12	2756	20.31			
13	857	3.66	13	1356	10.74	13	2973	22.08			
14	958	3.92	14	1558	12.07	14	3218	23.46			
15	1054	4.58	15	1697	missing	15	3449	22.15			
16	1153	6.07	16	1987	16.74	16	3684	23.53			
17	1254	6.43	17	2289	24.26						
18	1356	8.36	18	2588	32.07						
19	1451	10.33	19	2895	41.17						
20	1556	11.76	20	3197	48.22						
21	1653	11.63	21	3498	66.18						
22	1762	16.75									
23	1861	17.38									
24	1955	16.67									
25	2050	24.05									
26	2153	20.88									
27	2253	22.80									
28	2352	25.82									
29	2451	31.12									
30	2550	29.67									
31	2691	43.67									
32	2892	38.84									
33	3184	missing									

Wafer **CS01 - B**

Tablet # **3**

Width = 30μm			Width = 60μm			Width = 150μm			Width = 400μm		
	Beam Length (μm)	Tip Deflection (μm)		Beam Length (μm)	Tip Deflection (μm)		Beam Length (μm)	Tip Deflection (μm)		Beam Length (μm)	Tip Deflection (μm)
1	28	-1.23	1	49	-0.80	1	148	-0.44	1	393	0.77
2	67	-1.10	2	70	-1.02	2	408	0.29	2	872	1.06
3	108	-1.09	3	107	-0.85	3	644	1.26	3	1343	0.92
4	147	-1.31	4	188	-0.82	4	878	2.55	4	1823	broken
5	188	-1.00	5	230	-0.61	5	1106	3.16	5	2287	broken
6	228	-0.76	6	360	broken	6	1345	4.73	6	2751	broken
7	258	-0.71	7	459	broken	7	1581	6.60	7	3211	20.85
8	357	broken	8	658	0.80	8	1819	6.31			
9	457	broken	9	759	1.50	9	2056	6.04			
10	557	0.63	10	959	3.31	10	2284	8.64			
11	657	0.92	11	1056	3.85	11	2520	10.40			
12	759	1.27	12	1256	5.44	12	2756	8.05			
13	857	1.89	13	1356	6.20	13	2973	broken			
14	958	4.09	14	1558	broken	14	3218	7.65			
15	1054	4.08	15	1697	broken	15	3449	broken			
16	1153	5.12	16	1987	broken	16	3684	13.01			
17	1254	5.08	17	2289	broken						
18	1356	5.11	18	2588	broken						
19	1451	7.80	19	2895	broken						
20	1556	8.07	20	3197	broken						
21	1653	10.56	21	3498	broken						
22	1762	8.99									
23	1861	broken									
24	1955	12.34									
25	2050	15.31									
26	2153	19.62									
27	2253	21.03									
28	2352	13.86									
29	2451	16.42									
30	2550	21.01									
31	2691	19.78									
32	2892	missing									
33	3184	missing									

Wafer **CS01 - C**

Tablet # **3**

Width= 30μm			Width= 60μm			Width= 150μm			Width= 400μm		
	Beam Length (μm)	Tip Deflection (μm)		Beam Length (μm)	Tip Deflection (μm)		Beam Length (μm)	Tip Deflection (μm)		Beam Length (μm)	Tip Deflection (μm)
1	28	-1.00	1	49	-1.22	1	148	0.27	1	393	1.55
2	67	-1.04	2	70	-0.98	2	408	0.96	2	872	3.94
3	108	-0.99	3	107	-0.93	3	644	2.68	3	1343	5.95
4	147	-1.04	4	188	-0.79	4	878	5.01	4	1823	9.54
5	188	-0.89	5	230	-0.60	5	1106	7.81	5	2287	17.90
6	228	-0.66	6	360	0.07	6	1345	10.92	6	2751	33.07
7	258	-0.37	7	459	-4.06	7	1581	13.87	7	3211	54.42
8	357	-0.25	8	658	2.52	8	1819	16.79			
9	457	0.60	9	759	3.19	9	2056	19.11			
10	557	1.25	10	959	4.71	10	2284	24.64			
11	657	1.91	11	1056	7.22	11	2520	25.74			
12	759	2.91	12	1256	9.79	12	2756	34.01			
13	857	4.36	13	1356	12.55	13	2973	38.45			
14	958	5.21	14	1558	14.39	14	3218	36.56			
15	1054	6.35	15	1697	16.76	15	3449	38.38			
16	1153	7.02	16	1987	-3.65	16	3684	45.61			
17	1254	9.69	17	2289	missing						
18	1356	11.85	18	2588	missing						
19	1451	12.39	19	2895	missing						
20	1556	15.31	20	3197	missing						
21	1653	16.20	21	3498	missing						
22	1762	17.73									
23	1861	21.56									
24	1955	22.89									
25	2050	24.65									
26	2153	25.56									
27	2253	28.58									
28	2352	32.34									
29	2451	32.59									
30	2550	37.85									
31	2691	44.78									
32	2892	47.19									
33	3184	46.57									

Wafer **CS01 - D**

Tablet # **3**

Width= 30μm		Width= 60μm		Width= 150μm		Width= 400μm	
Beam Length (μm)	Tip Deflection (μm)	Beam Length (μm)	Tip Deflection (μm)	Beam Length (μm)	Tip Deflection (μm)	Beam Length (μm)	Tip Deflection (μm)
1 28	-1.63	1 49	-1.68	1 148	-0.72	1 393	-0.65
2 67	-1.92	2 70	-1.73	2 408	-2.15	2 872	-1.53
3 108	-1.82	3 107	-1.77	3 644	-3.33	3 1343	-1.29
4 147	-1.93	4 188	-1.94	4 878	-3.15	4 1823	-1.38
5 188	-1.96	5 230	-1.93	5 1106	-3.00	5 2287	missing
6 228	-2.13	6 360	-2.45	6 1345	-2.82	6 2751	-1.50
7 258	-2.41	7 459	-2.76	7 1581	-2.77	7 3211	-2.12
8 357	-4.64	8 658	-4.04	8 1819	-2.62		
9 457	-4.65	9 759	-3.98	9 2056	-2.59		
10 557	-4.78	10 959	-4.02	10 2284	-2.12		
11 657	-4.59	11 1056	-3.85	11 2520	-2.41		
12 759	-4.54	12 1256	-3.75	12 2756	-2.32		
13 857	-4.46	13 1356	-3.68	13 2973	-1.54		
14 958	-4.27	14 1558	-3.59	14 3218	-1.55		
15 1054	-4.14	15 1697	-3.59	15 3449	-1.28		
16 1153	-4.02	16 1987	-3.32	16 3684	-1.36		
17 1254	-3.66	17 2289	-2.97				
18 1356	-3.79	18 2588	missing				
19 1451	-3.78	19 2895	-3.29				
20 1556	-3.83	20 3197	missing				
21 1653	-3.68	21 3498	missing				
22 1762	-3.76						
23 1861	-3.63						
24 1955	-3.50						
25 2050	-3.55						
26 2153	-3.71						
27 2253	-3.49						
28 2352	-3.10						
29 2451	-3.53						
30 2550	missing						
31 2691	missing						
32 2892	missing						
33 3184	missing						

Wafer **CS01 - A**

Tablet # **5**

Width= 30μm		Width= 60μm		Width= 150μm		Width= 400μm	
Beam Length (μm)	Tip Deflection (μm)	Beam Length (μm)	Tip Deflection (μm)	Beam Length (μm)	Tip Deflection (μm)	Beam Length (μm)	Tip Deflection (μm)
1 28	-0.96	1 49	-1.29	1 148	0.30	1 393	1.43
2 67	-1.03	2 70	-1.15	2 408	-3.01	2 872	3.07
3 108	-1.14	3 107	-1.20	3 644	2.69	3 1343	3.25
4 147	-1.16	4 188	-0.91	4 878	4.42	4 1823	4.02
5 188	-0.98	5 230	-0.80	5 1106	7.23	5 2287	6.23
6 228	-0.79	6 360	-0.33	6 1345	9.15	6 2751	25.75
7 258	-0.87	7 459	broken	7 1581	13.36	7 3211	broken
8 357	-0.42	8 658	1.77	8 1819	17.26		
9 457	broken	9 759	2.54	9 2056	20.06		
10 557	broken	10 959	4.61	10 2284	21.08		
11 657	1.19	11 1056	5.59	11 2520	21.64		
12 759	2.42	12 1256	7.44	12 2756	23.57		
13 857	2.74	13 1356	9.74	13 2973	18.80		
14 958	broken	14 1558	10.94	14 3218	28.11		
15 1054	broken	15 1697	14.51	15 3449	25.20		
16 1153	broken	16 1987	22.47	16 3684	31.54		
17 1254	broken	17 2289	missing				
18 1356	broken	18 2588	9.64				
19 1451	broken	19 2895	missing				
20 1556	broken	20 3197	missing				
21 1653	broken	21 3498	41.28				
22 1762	broken						
23 1861	broken						
24 1955	broken						
25 2050	broken						
26 2153	broken						
27 2253	broken						
28 2352	3.92						
29 2451	broken						
30 2550	26.35						
31 2691	25.28						
32 2892	missing						
33 3184	missing						

Wafer **CS01 - B**Tablet # **5**

Width= 30μm			Width= 60μm			Width= 150μm			Width= 400μm		
	Beam Length (μm)	Tip Deflection (μm)		Beam Length (μm)	Tip Deflection (μm)		Beam Length (μm)	Tip Deflection (μm)		Beam Length (μm)	Tip Deflection (μm)
1	28	-0.99	1	49	-1.09	1	148	-0.21	1	393	0.61
2	67	-1.15	2	70	-1.02	2	408	0.31	2	872	1.88
3	108	-0.91	3	107	-0.87	3	644	1.28	3	1343	2.29
4	147	-0.90	4	188	-0.77	4	878	3.02	4	1823	3.90
5	188	-0.84	5	230	-0.64	5	1106	4.00	5	2287	missing
6	228	-1.02	6	360	-0.09	6	1345	6.33	6	2751	14.13
7	258	-0.86	7	459	0.42	7	1581	7.61	7	3211	31.20
8	357	-0.55	8	658	1.74	8	1819	11.35			
9	457	-0.04	9	759	2.37	9	2056	11.25			
10	557	0.51	10	959	3.46	10	2284	12.77			
11	657	1.02	11	1056	4.44	11	2520	12.12			
12	759	1.01	12	1256	5.68	12	2756	13.68			
13	857	2.44	13	1356	6.87	13	2973	16.66			
14	958	2.84	14	1558	8.79	14	3218	16.84			
15	1054	4.98	15	1697	11.84	15	3449	23.12			
16	1153	4.89	16	1987	missing	16	3684	35.37			
17	1254	7.58	17	2289	missing						
18	1356	7.71	18	2588	27.82						
19	1451	broken	19	2895	missing						
20	1556	8.33	20	3197	missing						
21	1653	10.86	21	3498	missing						
22	1762	12.86									
23	1861	13.35									
24	1955	17.49									
25	2050	18.84									
26	2153	21.20									
27	2253	20.88									
28	2352	22.69									
29	2451	25.59									
30	2550	23.35									
31	2691	35.94									
32	2892	31.64									
33	3184	missing									

Wafer **CS01 - C**

Tablet # **5**

Width= 30μm		Width= 60μm		Width= 150μm		Width= 400μm					
Beam Length (μm)	Tip Deflection (μm)	Beam Length (μm)	Tip Deflection (μm)	Beam Length (μm)	Tip Deflection (μm)	Beam Length (μm)	Tip Deflection (μm)				
1	28	-0.93	1	49	-1.03	1	148	-0.07	1	393	1.62
2	67	-1.17	2	70	-0.94	2	408	-3.70	2	872	3.91
3	108	-1.21	3	107	-1.07	3	644	2.62	3	1343	6.88
4	147	-1.17	4	188	-0.63	4	878	5.15	4	1823	8.75
5	188	-0.71	5	230	-0.39	5	1106	7.68	5	2287	missing
6	228	-0.84	6	360	-0.08	6	1345	11.30	6	2751	33.38
7	258	-0.69	7	459	0.43	7	1581	14.07	7	3211	59.93
8	357	broken	8	658	1.73	8	1819	17.01			
9	457	broken	9	759	2.53	9	2056	broken			
10	557	1.24	10	959	4.84	10	2284	broken			
11	657	1.73	11	1056	5.23	11	2520	broken			
12	759	3.00	12	1256	7.60	12	2756	34.56			
13	857	3.65	13	1356	10.03	13	2973	35.24			
14	958	5.83	14	1558	12.81	14	3218	42.08			
15	1054	6.74	15	1697	15.05	15	3449	41.04			
16	1153	8.15	16	1987	missing	16	3684	11.77			
17	1254	8.72	17	2289	missing						
18	1356	11.30	18	2588	29.41						
19	1451	13.22	19	2895	missing						
20	1556	15.70	20	3197	missing						
21	1653	15.44	21	3498	missing						
22	1762	18.52									
23	1861	19.39									
24	1955	20.54									
25	2050	22.96									
26	2153	25.24									
27	2253	25.93									
28	2352	26.55									
29	2451	30.32									
30	2550	broken									
31	2691	broken									
32	2892	44.32									
33	3184	missing									

Wafer **CS01 - D**

Tablet # **5**

Width= 30μm		Width= 60μm		Width= 150μm		Width= 400μm	
Beam Length (μm)	Tip Deflection (μm)	Beam Length (μm)	Tip Deflection (μm)	Beam Length (μm)	Tip Deflection (μm)	Beam Length (μm)	Tip Deflection (μm)
1 28	-1.44	1 49	-1.66	1 148	-1.00	1 393	-0.54
2 67	-2.01	2 70	-1.80	2 408	-3.91	2 872	-1.57
3 108	-1.87	3 107	-1.88	3 644	-3.42	3 1343	-1.28
4 147	-2.16	4 188	-1.82	4 878	-3.19	4 1823	-1.83
5 188	-2.17	5 230	-1.70	5 1106	-2.82	5 2287	missing
6 228	-2.34	6 360	-2.46	6 1345	-2.67	6 2751	-2.42
7 258	-2.34	7 459	-2.97	7 1581	-2.86	7 3211	-2.10
8 357	-4.60	8 658	-4.02	8 1819	-2.42		
9 457	-5.03	9 759	-4.51	9 2056	-2.58		
10 557	-4.55	10 959	-3.90	10 2284	-2.59		
11 657	-4.35	11 1056	-3.57	11 2520	-2.17		
12 759	-4.72	12 1256	-3.66	12 2756	-2.05		
13 857	-4.24	13 1356	-4.03	13 2973	-1.53		
14 958	-4.48	14 1558	-3.71	14 3218	-1.30		
15 1054	-4.47	15 1697	-3.78	15 3449	-1.25		
16 1153	-4.31	16 1987	-3.74	16 3684	-1.41		
17 1254	-3.06	17 2289	-3.36				
18 1356	-3.84	18 2588	-3.66				
19 1451	-4.17	19 2895	missing				
20 1556	-3.66	20 3197	missing				
21 1653	-3.95	21 3498	-3.59				
22 1762	-3.82						
23 1861	-3.97						
24 1955	-3.93						
25 2050	-3.92						
26 2153	-3.61						
27 2253	-3.89						
28 2352	missing						
29 2451	missing						
30 2550	missing						
31 2691	missing						
32 2892	missing						
33 3184	missing						

Wafer **CS02 - A**

Tablet # **3**

Width= 30μm			Width= 60μm			Width= 150μm			Width= 400μm		
	Beam Length (μm)	Tip Deflection (μm)		Beam Length (μm)	Tip Deflection (μm)		Beam Length (μm)	Tip Deflection (μm)		Beam Length (μm)	Tip Deflection (μm)
1	28	-1.26	1	49	-1.15	1	148	-0.56	1	393	-0.98
2	67	-1.38	2	70	-1.11	2	408	-3.43	2	872	-2.34
3	108	-1.21	3	107	-1.01	3	644	-3.52	3	1343	-1.01
4	147	-1.37	4	188	-1.43	4	878	-3.34	4	1823	-2.17
5	188	-1.52	5	230	-1.81	5	1106	-3.19	5	2287	-2.23
6	228	-1.72	6	360	-2.10	6	1345	-2.99	6	2751	-2.46
7	258	-1.83	7	459	-2.69	7	1581	-2.81	7	3211	-2.68
8	357	-4.26	8	658	-4.10	8	1819	-2.78			
9	457	-2.81	9	759	-3.94	9	2056	-2.79			
10	557	-4.18	10	959	-4.01	10	2284	-2.65			
11	657	-4.32	11	1056	-3.92	11	2520	-2.54			
12	759	missing	12	1256	-3.74	12	2756	-2.56			
13	857	missing	13	1356	-3.57	13	2973	-2.21			
14	958	-4.25	14	1558	-3.53	14	3218	-2.14			
15	1054	-4.18	15	1697	-3.59	15	3449	-2.32			
16	1153	missing	16	1987	-3.53	16	3684	-2.49			
17	1254	missing	17	2289	-3.51						
18	1356	missing	18	2588	-3.54						
19	1451	missing	19	2895	missing						
20	1556	missing	20	3197	-3.48						
21	1653	missing	21	3498	missing						
22	1762	missing									
23	1861	missing									
24	1955	missing									
25	2050	missing									
26	2153	missing									
27	2253	missing									
28	2352	missing									
29	2451	missing									
30	2550	missing									
31	2691	missing									
32	2892	missing									
33	3184	missing									

Wafer **CS02 - C**

Tablet # **3**

Width= 30μm		Width= 60μm		Width= 150μm		Width= 400μm						
Beam Length (μm)	Tip Deflection (μm)	Beam Length (μm)	Tip Deflection (μm)	Beam Length (μm)	Tip Deflection (μm)	Beam Length (μm)	Tip Deflection (μm)					
1	28	-0.91	1	49	-0.78	1	148	-0.27	1	393	-0.53	
2	67	-0.95	2	70	-0.88	2	408	-1.13	2	872	-2.41	
3	108	-1.01	3	107	-0.75	3	644	-2.12	3	1343	-2.56	
4	147	-0.94	4	188	-1.00	4	878	-3.13	4	1823	broke off	
5	188	-1.13	5	230	-0.54	5	1106	-3.08	5	2287	missing	
6	228	-1.25	6	360	-0.77	6	1345	-3.03	6	2751	-1.90	
7	258	-1.30	7	459	-0.97	7	1581	-2.99	7	3211	-2.92	
8	357	-1.45	8	658	-1.72	8	1819	-2.86				
9	457	-1.79	9	759	-0.84	9	2056	-2.78				
10	557	-1.82	10	959	-1.98	10	2284	-2.95				
11	657	-2.76	11	1056	-2.29	11	2520	-2.78				
12	759	-3.89	12	1256	-2.26	12	2756	-2.85				
13	857	-3.97	13	1356	-3.56	13	2973	-2.84				
14	958	-3.97	14	1558	-3.51	14	3218	-2.46				
15	1054	-3.89	15	1697	-3.46	15	3449	-2.36				
16	1153	-3.60	16	1987	-3.41	16	3684	-2.39				
17	1254	-3.58	17	2289	-1.67							
18	1356	-3.66	18	2588	missing							
19	1451	-3.82	19	2895	missing							
20	1556	-2.57	20	3197	missing							
21	1653	-2.47	21	3498	missing							
22	1762	-2.50										
23	1861	-2.55										
24	1955	-2.83										
25	2050	-3.96										
26	2153	missing										
27	2253	missing										
28	2352	missing										
29	2451	missing										
30	2550	missing										
31	2691	missing										
32	2892	missing										
33	3184	missing										

Wafer **CS02 - D**

Tablet # **3**

Width= 30μm			Width= 60μm			Width= 150μm			Width= 400μm		
	Beam Length (μm)	Tip Deflection (μm)		Beam Length (μm)	Tip Deflection (μm)		Beam Length (μm)	Tip Deflection (μm)		Beam Length (μm)	Tip Deflection (μm)
1	28	-1.44	1	49	-1.39	1	148	-0.19	1	393	-0.13
2	67	-1.53	2	70	-1.43	2	408	-0.61	2	872	-1.74
3	108	-1.44	3	107	-1.36	3	644	-3.14	3	1343	-1.08
4	147	-1.64	4	188	-1.39	4	878	-3.08	4	1823	-1.92
5	188	-1.65	5	230	-1.42	5	1106	-2.88	5	2287	missing
6	228	-1.71	6	360	-1.44	6	1345	-2.91	6	2751	-2.39
7	258	-1.75	7	459	-1.63	7	1581	-2.72	7	3211	-2.48
8	357	-4.73	8	658	-2.27	8	1819	-2.81			
9	457	-4.63	9	759	-2.46	9	2056	-2.80			
10	557	-0.33	10	959	-3.19	10	2284	-2.84			
11	657	-4.44	11	1056	-3.31	11	2520	-2.44			
12	759	-4.31	12	1256	-3.52	12	2756	-2.63			
13	857	-4.31	13	1356	-3.70	13	2973	-2.63			
14	958	-4.33	14	1558	-2.35	14	3218	-2.35			
15	1054	missing	15	1697	-3.53	15	3449	-2.05			
16	1153	missing	16	1987	-3.39	16	3684	-2.01			
17	1254	missing	17	2289	-3.54						
18	1356	missing	18	2588	missing						
19	1451	missing	19	2895	missing						
20	1556	missing	20	3197	-3.52						
21	1653	missing	21	3498	missing						
22	1762	missing									
23	1861	missing									
24	1955	missing									
25	2050	missing									
26	2153	missing									
27	2253	missing									
28	2352	missing									
29	2451	missing									
30	2550	missing									
31	2691	missing									
32	2892	missing									
33	3184	missing									

Wafer **CS02 - E**

Tablet # **3**

Width= 30μm		Width= 60μm		Width= 150μm		Width= 400μm	
Beam Length (μm)	Tip Deflection (μm)	Beam Length (μm)	Tip Deflection (μm)	Beam Length (μm)	Tip Deflection (μm)	Beam Length (μm)	Tip Deflection (μm)
1 28	-1.04	1 49	-1.41	1 148	-0.04	1 393	0.50
2 67	-1.31	2 70	-1.60	2 408	0.20	2 872	-0.89
3 108	-1.20	3 107	-1.36	3 644	0.81	3 1343	-2.03
4 147	-1.17	4 188	-1.19	4 878	1.20	4 1823	-1.17
5 188	-1.08	5 230	-0.98	5 1106	0.85	5 2287	missing
6 228	-1.14	6 360	-1.22	6 1345	1.16	6 2751	-2.93
7 258	-1.13	7 459	-1.04	7 1581	-0.94	7 3211	9.12
8 357	-1.18	8 658	0.18	8 1819	-2.64		
9 457	-0.82	9 759	0.70	9 2056	-2.46		
10 557	-0.39	10 959	1.10	10 2284	-2.15		
11 657	-0.34	11 1056	3.28	11 2520	-2.46		
12 759	0.59	12 1256	1.43	12 2756	-2.38		
13 857	0.64	13 1356	2.24	13 2973	-2.48		
14 958	0.72	14 1558	2.78	14 3218	-2.27		
15 1054	3.51	15 1697	missing	15 3449	-2.34		
16 1153	2.69	16 1987	missing	16 3684	-2.30		
17 1254	4.28	17 2289	missing				
18 1356	4.75	18 2588	missing				
19 1451	4.52	19 2895	missing				
20 1556	6.16	20 3197	1.26				
21 1653	5.54	21 3498	missing				
22 1762	5.91						
23 1861	7.73						
24 1955	8.86						
25 2050	8.98						
26 2153	11.92						
27 2253	11.74						
28 2352	11.57						
29 2451	16.08						
30 2550	16.42						
31 2691	missing						
32 2892	missing						
33 3184	missing						

Wafer **CS02 - F**

Tablet # **3**

Width= 30μm		Width= 60μm		Width= 150μm		Width= 400μm	
Beam Length (μm)	Tip Deflection (μm)	Beam Length (μm)	Tip Deflection (μm)	Beam Length (μm)	Tip Deflection (μm)	Beam Length (μm)	Tip Deflection (μm)
1 28	-0.41	1 49	-0.83	1 148	-0.08	1 393	0.94
2 67	-0.60	2 70	-0.93	2 408	0.78	2 872	2.25
3 108	-0.62	3 107	-0.82	3 644	1.84	3 1343	1.65
4 147	-0.63	4 188	-0.78	4 878	3.74	4 1823	broken
5 188	-0.54	5 230	-0.47	5 1106	5.51	5 2287	missing
6 228	-0.64	6 360	broken	6 1345	7.32	6 2751	15.82
7 258	-0.41	7 459	0.60	7 1581	10.33	7 3211	38.86
8 357	-0.18	8 658	1.42	8 1819	10.05		
9 457	broken	9 759	1.91	9 2056	11.55		
10 557	1.25	10 959	4.14	10 2284	13.36		
11 657	1.79	11 1056	broken	11 2520	16.73		
12 759	2.83	12 1256	broken	12 2756	18.13		
13 857	broken	13 1356	7.84	13 2973	21.86		
14 958	3.13	14 1558	broken	14 3218	27.72		
15 1054	5.61	15 1697	broken	15 3449	23.63		
16 1153	6.42	16 1987	broken	16 3684	34.47		
17 1254	8.39	17 2289	21.47				
18 1356	10.16	18 2588	missing				
19 1451	9.71	19 2895	missing				
20 1556	12.42	20 3197	missing				
21 1653	14.85	21 3498	missing				
22 1762	15.40						
23 1861	15.08						
24 1955	broken						
25 2050	missing						
26 2153	missing						
27 2253	missing						
28 2352	missing						
29 2451	missing						
30 2550	missing						
31 2691	missing						
32 2892	missing						
33 3184	missing						

Wafer **CS02 - A**

Tablet # **5**

Width= 30μm			Width= 60μm			Width= 150μm			Width= 400μm		
	Beam Length (μm)	Tip Deflection (μm)		Beam Length (μm)	Tip Deflection (μm)		Beam Length (μm)	Tip Deflection (μm)		Beam Length (μm)	Tip Deflection (μm)
1	28	-1.10	1	49	-1.25	1	148	-0.60	1	393	-0.95
2	67	-1.10	2	70	-1.18	2	408	-1.75	2	872	-5.18
3	108	-1.30	3	107	-1.08	3	644	-3.24	3	1343	broke off
4	147	-1.35	4	188	-1.22	4	878	-3.06	4	1823	broke off
5	188	-1.61	5	230	-1.46	5	1106	-2.76	5	2287	missing
6	228	-1.47	6	360	-1.87	6	1345	-0.67	6	2751	missing
7	258	-1.89	7	459	-2.47	7	1581	-2.44	7	3211	-13.89
8	357	-2.11	8	658	-3.79	8	1819	-2.22			
9	457	-2.86	9	759	-3.75	9	2056	-2.13			
10	557	-4.06	10	959	-3.91	10	2284	-1.97			
11	657	-4.35	11	1056	-3.82	11	2520	-2.37			
12	759	-4.31	12	1256	-3.69	12	2756	-2.22			
13	857	-4.14	13	1356	-3.03	13	2973	-2.05			
14	958	-4.34	14	1558	-3.08	14	3218	-2.22			
15	1054	-4.22	15	1697	-3.51	15	3449	-2.39			
16	1153	-3.42	16	1987	-3.60	16	3684	-2.49			
17	1254	-3.79	17	2289	-3.51						
18	1356	-3.82	18	2588	missing						
19	1451	-3.72	19	2895	missing						
20	1556	-3.77	20	3197	missing						
21	1653	-4.00	21	3498	missing						
22	1762	-4.08									
23	1861	-3.94									
24	1955	-4.02									
25	2050	-3.92									
26	2153	-4.12									
27	2253	-4.14									
28	2352	-4.25									
29	2451	-4.23									
30	2550	-4.20									
31	2691	-4.12									
32	2892	missing									
33	3184	-4.27									

Wafer **CS02 - C**

Tablet # **5**

Width= 30μm		Width= 60μm		Width= 150μm		Width= 400μm					
Beam Length (μm)	Tip Deflection (μm)	Beam Length (μm)	Tip Deflection (μm)	Beam Length (μm)	Tip Deflection (μm)	Beam Length (μm)	Tip Deflection (μm)				
1	28	-0.85	1	49	-1.20	1	148	-0.38	1	393	-0.36
2	67	-0.97	2	70	-1.12	2	408	-0.70	2	872	-2.15
3	108	-0.88	3	107	-1.18	3	644	-2.00	3	1343	-2.61
4	147	-1.08	4	188	-1.15	4	878	-3.05	4	1823	-2.26
5	188	-1.31	5	230	-1.00	5	1106	-3.08	5	2287	missing
6	228	-1.10	6	360	-1.35	6	1345	-3.02	6	2751	-2.69
7	258	-1.14	7	459	-1.35	7	1581	-2.71	7	3211	-2.80
8	357	-3.97	8	658	-2.63	8	1819	-2.78			
9	457	-4.03	9	759	-3.11	9	2056	-2.14			
10	557	-2.20	10	959	-3.53	10	2284	-2.87			
11	657	-4.34	11	1056	-3.38	11	2520	-2.83			
12	759	-4.21	12	1256	-3.32	12	2756	-2.68			
13	857	-4.02	13	1356	-3.51	13	2973	-2.78			
14	958	-3.99	14	1558	-3.65	14	3218	-2.44			
15	1054	-4.13	15	1697	-3.59	15	3449	-2.35			
16	1153	-4.36	16	1987	missing	16	3684	-2.31			
17	1254	-4.33	17	2289	missing						
18	1356	-4.30	18	2588	missing						
19	1451	-4.16	19	2895	-3.58						
20	1556	-4.30	20	3197	-3.58						
21	1653	-3.98	21	3498	missing						
22	1762	-3.89									
23	1861	-4.04									
24	1955	-3.96									
25	2050	-3.94									
26	2153	missing									
27	2253	missing									
28	2352	missing									
29	2451	missing									
30	2550	missing									
31	2691	missing									
32	2892	missing									
33	3184	missing									

Wafer **CS02 - D**

Tablet # **5**

Width= 30μm		Width= 60μm		Width= 150μm		Width= 400μm	
Beam Length (μm)	Tip Deflection (μm)	Beam Length (μm)	Tip Deflection (μm)	Beam Length (μm)	Tip Deflection (μm)	Beam Length (μm)	Tip Deflection (μm)
1 28	-1.66	1 49	-1.30	1 148	-0.51	1 393	-0.49
2 67	-1.41	2 70	-1.38	2 408	-1.27	2 872	-2.37
3 108	-1.77	3 107	-1.56	3 644	-2.05	3 1343	-2.61
4 147	-1.76	4 188	-1.40	4 878	-3.39	4 1823	-2.54
5 188	-1.69	5 230	-1.37	5 1106	-3.41	5 2287	broke off
6 228	-1.53	6 360	-1.32	6 1345	-3.30	6 2751	-2.82
7 258	-1.55	7 459	-1.31	7 1581	-2.99	7 3211	-2.91
8 357	-1.61	8 658	-2.11	8 1819	-3.32		
9 457	-2.31	9 759	-2.56	9 2056	-3.22		
10 557	-2.73	10 959	-3.71	10 2284	-3.14		
11 657	-2.77	11 1056	broke off	11 2520	-3.13		
12 759	-3.20	12 1256	-3.67	12 2756	-2.84		
13 857	-4.27	13 1356	-3.69	13 2973	-2.75		
14 958	-4.17	14 1558	-3.63	14 3218	-2.74		
15 1054	-4.29	15 1697	-3.74	15 3449	-2.43		
16 1153	-4.30	16 1987	missing	16 3684	-2.67		
17 1254	-4.09	17 2289	missing				
18 1356	-4.14	18 2588	-3.65				
19 1451	-4.15	19 2895	missing				
20 1556	-4.18	20 3197	-3.83				
21 1653	-4.28	21 3498	missing				
22 1762	-4.02						
23 1861	-4.29						
24 1955	-4.30						
25 2050	-4.35						
26 2153	-4.18						
27 2253	-4.21						
28 2352	-4.03						
29 2451	-4.13						
30 2550	-4.13						
31 2691	missing						
32 2892	missing						
33 3184	missing						

Wafer **CS02 - E**

Tablet # **5**

Width= 30μm			Width= 60μm			Width= 150μm			Width= 400μm		
	Beam Length (μm)	Tip Deflection (μm)		Beam Length (μm)	Tip Deflection (μm)		Beam Length (μm)	Tip Deflection (μm)		Beam Length (μm)	Tip Deflection (μm)
1	28	missing	1	49	-0.95	1	148	-0.33	1	393	0.23
2	67	missing	2	70	-0.96	2	408	0.23	2	872	-0.67
3	108	missing	3	107	-0.93	3	644	0.23	3	1343	-2.35
4	147	missing	4	188	-1.11	4	878	1.12	4	1823	-1.83
5	188	missing	5	230	-1.00	5	1106	1.06	5	2287	broke off
6	228	missing	6	360	-0.77	6	1345	0.95	6	2751	-2.77
7	258	missing	7	459	-0.68	7	1581	1.31	7	3211	-2.87
8	357	missing	8	658	-0.70	8	1819	-0.36			
9	457	missing	9	759	0.05	9	2056	-1.40			
10	557	missing	10	959	0.01	10	2284	-2.66			
11	657	missing	11	1056	0.65	11	2520	-2.46			
12	759	missing	12	1256	1.34	12	2756	-2.52			
13	857	missing	13	1356	0.08	13	2973	-2.17			
14	958	missing	14	1558	1.14	14	3218	-2.30			
15	1054	missing	15	1697	0.09	15	3449	-2.23			
16	1153	missing	16	1987	-0.45	16	3684	-2.24			
17	1254	missing	17	2289	missing						
18	1356	missing	18	2588	missing						
19	1451	missing	19	2895	missing						
20	1556	missing	20	3197	missing						
21	1653	missing	21	3498	missing						
22	1762	missing									
23	1861	missing									
24	1955	missing									
25	2050	missing									
26	2153	missing									
27	2253	missing									
28	2352	missing									
29	2451	missing									
30	2550	missing									
31	2691	missing									
32	2892	missing									
33	3184	missing									

Wafer **CS02 - F**

Tablet # **5**

Width= 30μm		Width= 60μm		Width= 150μm		Width= 400μm	
Beam Length (μm)	Tip Deflection (μm)	Beam Length (μm)	Tip Deflection (μm)	Beam Length (μm)	Tip Deflection (μm)	Beam Length (μm)	Tip Deflection (μm)
1 28	-0.72	1 49	-0.97	1 148	-0.22	1 393	0.98
2 67	-0.68	2 70	-1.14	2 408	0.51	2 872	1.63
3 108	-0.79	3 107	-0.89	3 644	1.93	3 1343	1.47
4 147	-0.75	4 188	-0.76	4 878	3.08	4 1823	1.05
5 188	-0.77	5 230	-0.71	5 1106	4.70	5 2287	broke off
6 228	-0.68	6 360	-0.08	6 1345	5.97	6 2751	13.70
7 258	-0.49	7 459	0.26	7 1581	8.87	7 3211	32.32
8 357	-0.40	8 658	1.52	8 1819	10.13		
9 457	0.24	9 759	2.19	9 2056	11.44		
10 557	0.87	10 959	3.68	10 2284	13.48		
11 657	1.36	11 1056	3.89	11 2520	15.93		
12 759	2.14	12 1256	6.82	12 2756	broken		
13 857	3.09	13 1356	7.34	13 2973	22.66		
14 958	3.90	14 1558	10.47	14 3218	23.65		
15 1054	4.73	15 1697	10.61	15 3449	31.53		
16 1153	6.68	16 1987	missing	16 3684	31.12		
17 1254	7.42	17 2289	missing				
18 1356	8.38	18 2588	missing				
19 1451	9.51	19 2895	missing				
20 1556	12.34	20 3197	missing				
21 1653	15.22	21 3498	missing				
22 1762	15.74						
23 1861	18.98						
24 1955	20.99						
25 2050	23.25						
26 2153	23.47						
27 2253	25.63						
28 2352	29.72						
29 2451	28.65						
30 2550	35.12						
31 2691	37.51						
32 2892	missing						
33 3184	missing						

		Tablets #5		150µm Beam Width			
		CS01-D		CS02-A		CS02-B	
		C = 1.15E-4		C = 1.68E-4		C = 1.08E-4	
	Beam Length (µm)	Highest Deflection (µm)	Predicted Tip Deflection (µm)	Highest Deflection (µm)	Predicted Tip Deflection (µm)	Highest Deflection (µm)	Predicted Tip Deflection (µm)
1	148	Actual	-1.00	Actual	-0.60	Actual	-0.69
2	408	Actual	-3.91	Actual	-1.75	Actual	-1.92
3	644	Actual	-3.42	Actual	-3.24	Actual	-3.17
4	878	12.85	-4.01	14.57	-5.89	14.47	-3.77
5	1106	13.44	-6.37	14.88	-9.35	14.95	-5.99
6	1345	13.98	-9.41	15.8	-13.82	15.12	-8.85
7	1581	14.96	-13.01	16.24	-19.10	15.83	-12.23
8	1819	15.54	-17.23	broken	broken	16.79	-16.19
9	2056	16.75	-22.00	broken	broken	17.43	-20.68
10	2284	18.1	-27.15	broken	broken	18.79	-25.52
11	2520	19.6	-33.05	broken	broken	19.82	-31.07
12	2756	20.26	-39.54	broken	broken	21.06	-37.16
13	2973	22.85	-46.00	broken	broken	22.28	-43.24
14	3218	broken	broken	broken	broken	24.3	-50.67
15	3449	broken	broken	broken	broken	25.98	-58.21
16	3684	broken	broken	broken	broken	28.12	-66.40

		CS02-C		CS02-D		CS02-E	
		C = 7.01E-5		C = 6.69E-5		C = 4.87E-5	
	Beam Length (µm)	Highest Deflection (µm)	Predicted Tip Deflection (µm)	Highest Deflection (µm)	Predicted Tip Deflection (µm)	Highest Deflection (µm)	Predicted Tip Deflection (µm)
1	148	Actual	-0.38	Actual	-0.51	Actual	-0.33
2	408	Actual	-0.70	Actual	-1.27	Actual	0.23
3	644	Actual	-2.00	Actual	-2.05	Actual	0.23
4	878	14.29	-2.46	Actual	-3.39	Actual	1.12
5	1106	14.51	-3.90	14.59	-3.72	Actual	1.06
6	1345	14.85	-5.76	14.93	-5.50	Actual	0.95
7	1581	15.05	-7.97	15.32	-7.61	Actual	1.31
8	1819	15.9	-10.55	15.68	-10.07	Actual	-0.36
9	2056	16.16	-13.47	16.08	-12.86	15.95	-9.36
10	2284	16.73	-16.63	16.85	-15.87	16.26	-11.56
11	2520	broken	-20.24	17.36	-19.32	16.67	-14.07
12	2756	broken	-24.22	18.54	-23.11	16.64	-16.83
13	2973	broken	-28.17	19.85	-26.89	17.24	-19.58
14	3218	20.16	-33.02	broken	broken	17.97	-22.95
15	3449	21.61	-37.93	broken	broken	broken	broken
16	3684	21.84	-43.26	22.54	-41.29	broken	broken

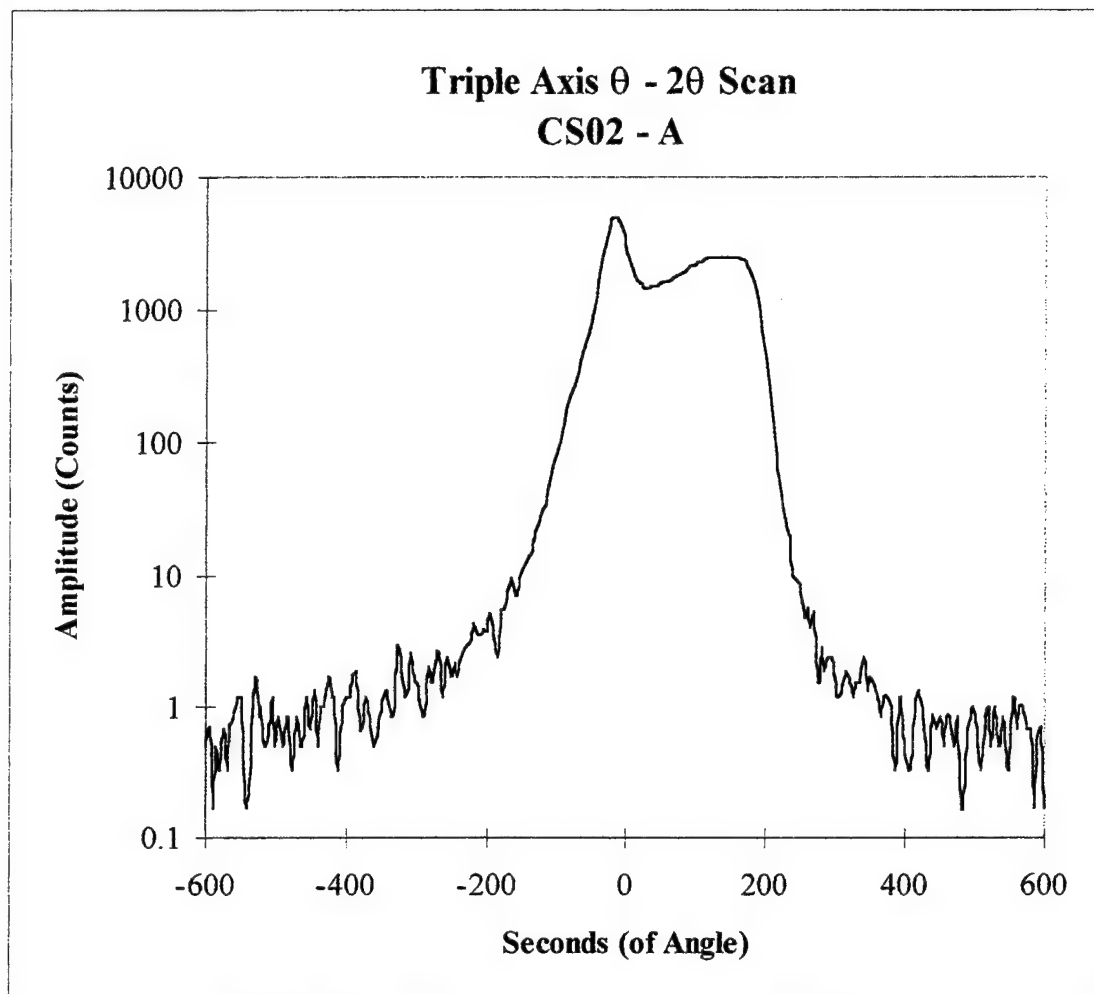
APPENDIX C: X-RAY DIFFRACTION θ - 2θ SCAN DATA

CS02-A, Control Sample, No Anneal

Position	Count	Position	Count	Position	Count	Position	Count
-600.02	0.5	-430.06	1	-260.1	1.17	-90.143	144.5
-595.02	0.67	-425.06	1.67	-255.1	2.33	-85.144	181.83
-590.02	0.17	-420.06	1.17	-250.1	1.67	-80.145	223.83
-585.02	0.5	-415.06	1.17	-245.11	2.17	-75.146	269.33
-580.02	0.33	-410.07	0.33	-240.11	1.67	-70.148	327.5
-575.02	0.67	-405.07	1	-235.11	2.33	-65.149	407.5
-570.03	0.33	-400.07	1.17	-230.11	2.83	-60.15	516.83
-565.03	0.67	-395.07	1.17	-225.11	3	-55.151	651
-560.03	0.83	-390.07	1.67	-220.11	4.33	-50.153	869.67
-555.03	1.17	-385.07	1.83	-215.11	3.83	-45.154	1195.83
-550.03	1.17	-380.07	0.67	-210.11	3.5	-40.155	1709.33
-545.03	0.5	-375.07	0.83	-205.12	3.83	-35.156	2470.17
-540.03	0.17	-370.07	1.17	-200.12	3.67	-30.157	3446.5
-535.03	0.5	-365.08	0.83	-195.12	5.17	-25.159	4422
-530.04	1.67	-360.08	0.5	-190.12	4	-20.16	4971
-525.04	0.83	-355.08	0.67	-185.12	2.33	-15.161	4912.83
-520.04	1	-350.08	1	-180.12	5.33	-10.162	4489.5
-515.04	0.5	-345.08	1.17	-175.12	5.5	-5.164	3601.83
-510.04	0.67	-340.08	1.33	-170.12	6.83	-0.165	2806.17
-505.04	1.17	-335.08	0.83	-165.13	9.5	4.834	2229.67
-500.04	0.5	-330.08	1	-160.13	7	9.833	1836.5
-495.04	0.83	-325.09	2.83	-155.13	8.17	14.832	1640.5
-490.05	0.5	-320.09	2.17	-150.13	10.67	19.83	1566.17
-485.05	0.83	-315.09	1.17	-145.13	12.33	24.829	1498.83
-480.05	0.83	-310.09	1.5	-140.13	14.17	29.828	1480.17
-475.05	0.33	-305.09	2.5	-135.13	15.5	34.827	1521.67
-470.05	0.83	-300.09	1.67	-130.13	21.5	39.825	1536
-465.05	0.5	-295.09	1.33	-125.13	25.17	44.824	1578.67
-460.05	0.67	-290.09	0.83	-120.14	32.33	49.823	1618.17
-455.05	1.17	-285.1	1.17	-115.14	36.33	54.822	1666.33
-450.06	0.67	-280.1	2	-110.14	48	59.821	1700.33
-445.06	1.33	-275.1	1.5	-105.14	66.33	64.819	1766.83
-440.06	0.5	-270.1	2.67	-100.14	82	69.818	1839.67
-435.06	1	-265.1	1.83	-95.142	105.67	74.817	1892.33

CS02-A, Control Sample, No Anneal

Position	Count	Position	Count	Position	Count	Position	Count
79.816	1984	209.784	140.67	339.752	2.33	469.72	0.5
84.814	2097.17	214.783	80.5	344.751	1.33	474.719	0.83
89.813	2152.33	219.781	54.5	349.75	1.67	479.718	0.33
94.812	2200	224.78	33.67	354.749	1.5	484.717	0.17
99.811	2294.17	229.779	23.67	359.747	1.17	489.716	0.67
104.81	2350.17	234.778	17.67	364.746	0.83	494.714	0.83
109.808	2418.5	239.777	10	369.745	1.17	499.713	1
114.807	2455.67	244.775	9.33	374.744	1.17	504.712	0.67
119.806	2444.67	249.774	8.5	379.742	1	509.711	0.33
124.805	2471.33	254.773	4.67	384.741	0.33	514.709	0.83
129.803	2491	259.772	5.67	389.74	1.17	519.708	1
134.802	2473.33	264.771	4	394.739	1.17	524.707	0.5
139.801	2506.17	269.769	5.17	399.738	0.5	529.706	1
144.8	2483.67	274.768	1.5	404.736	0.33	534.705	0.5
149.799	2486	279.767	2.83	409.735	0.5	539.703	0.83
154.797	2480.17	284.766	1.83	414.734	1	544.702	0.67
159.796	2457.83	289.764	2.33	419.733	1.33	549.701	0.33
164.795	2402.17	294.763	2.33	424.731	0.83	554.7	1.17
169.794	2297.67	299.762	1.33	429.73	0.5	559.698	0.67
174.792	2088	304.761	1.17	434.729	0.33	564.697	1
179.791	1797	309.76	1.33	439.728	0.83	569.696	1
184.79	1437.67	314.758	1.83	444.727	0.67	574.695	0.67
189.789	1050.5	319.757	1.5	449.725	0.83	579.694	0.67
194.788	717.5	324.756	1.17	454.724	0.5	584.692	0.17
199.786	449.5	329.755	1.5	459.723	0.83	589.691	0.5
204.785	271.33	334.753	1.5	464.722	0.83	594.69	0.67
						599.689	0.17

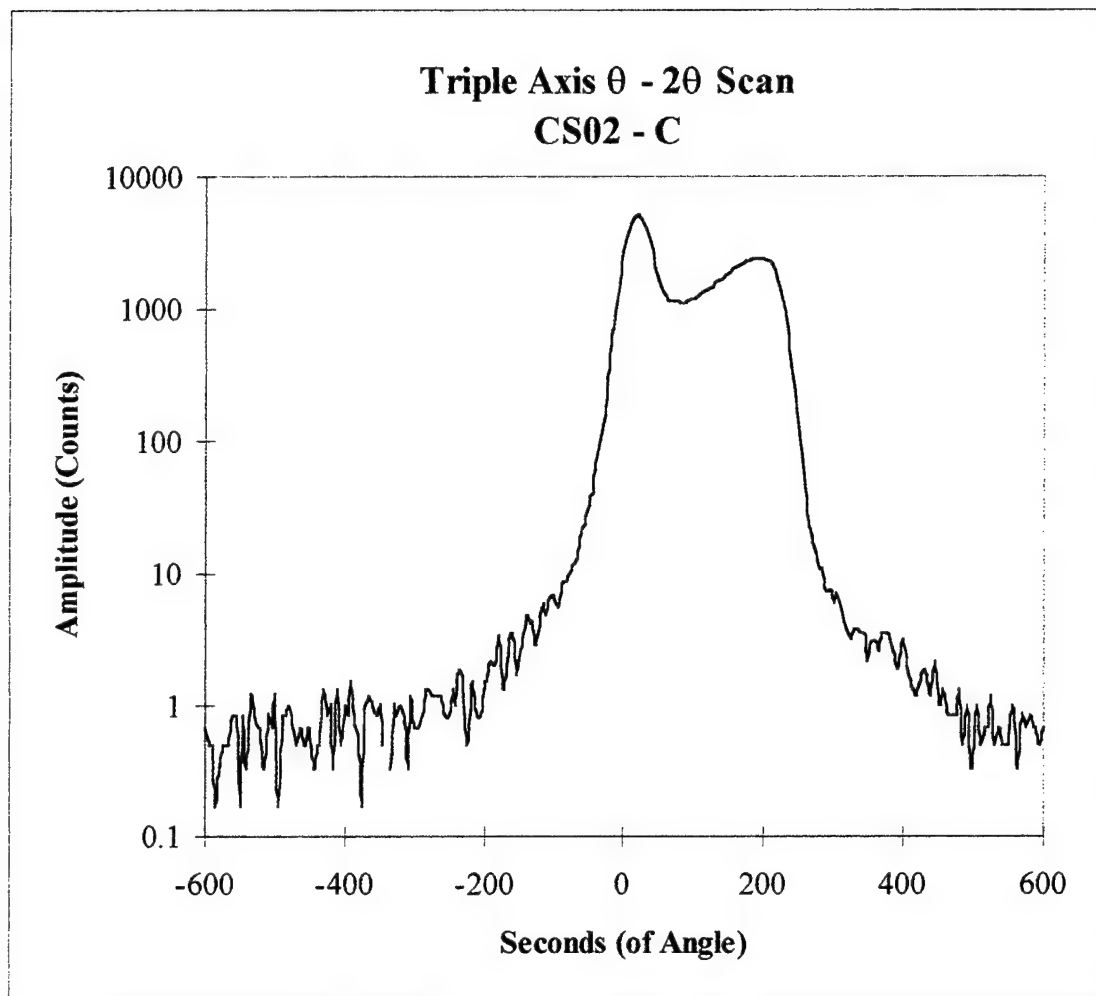


CS02-C, 950°C Anneal Temperature

Position	Count	Position	Count	Position	Count	Position	Count
-600.02	0.67	-430.06	1.33	-260.1	1.17	-90.143	7.83
-595.02	0.5	-425.06	0.83	-255.1	0.83	-85.144	8.5
-590.02	0.5	-420.06	1	-250.1	0.83	-80.145	9
-585.02	0.17	-415.06	0.33	-245.11	1.33	-75.146	11.5
-580.02	0.33	-410.07	1.33	-240.11	1	-70.148	12.33
-575.02	0.5	-405.07	0.5	-235.11	1.83	-65.149	12.83
-570.03	0.5	-400.07	1	-230.11	1.5	-60.15	20.17
-565.03	0.5	-395.07	0.83	-225.11	0.5	-55.151	25.5
-560.03	0.83	-390.07	1.5	-220.11	1.17	-50.153	35.5
-555.03	0.83	-385.07	0.83	-215.11	1.5	-45.154	44.67
-550.03	0.17	-380.07	0.5	-210.11	0.83	-40.155	68.33
-545.03	0.83	-375.07	0.17	-205.12	0.83	-35.156	95.83
-540.03	0.33	-370.07	0.83	-200.12	1.5	-30.157	138.17
-535.03	1.17	-365.08	1.17	-195.12	1.5	-25.159	247.5
-530.04	0.83	-360.08	1	-190.12	2.17	-20.16	400.33
-525.04	0.67	-355.08	0.83	-185.12	2	-15.161	724.83
-520.04	0.67	-350.08	1	-180.12	3.33	-10.162	1199.83
-515.04	0.33	-345.08	0.5	-175.12	2.33	-5.164	1879.83
-510.04	0.83	-340.08	0	-170.12	1.33	-0.165	2735.83
-505.04	0.67	-335.08	0.33	-165.13	3.17	4.834	3650.33
-500.04	1.17	-330.08	1	-160.13	3.5	9.833	4458
-495.04	0.17	-325.09	0.83	-155.13	1.67	14.832	4951.5
-490.05	0.83	-320.09	1	-150.13	2.17	19.83	5087.5
-485.05	0.83	-315.09	0.83	-145.13	2.83	24.829	4858.5
-480.05	1	-310.09	0.33	-140.13	4.83	29.828	4177.83
-475.05	0.83	-305.09	1.17	-135.13	4.17	34.827	3486.17
-470.05	0.5	-300.09	0.67	-130.13	4.33	39.825	2718.5
-465.05	0.67	-295.09	0.67	-125.13	2.83	44.824	2118.17
-460.05	0.5	-290.09	0.83	-120.14	4.67	49.823	1647.5
-455.05	0.5	-285.1	1.33	-115.14	5.83	54.822	1370.17
-450.06	0.67	-280.1	1.33	-110.14	4.67	59.821	1237.33
-445.06	0.33	-275.1	1.17	-105.14	6.5	64.819	1139.83
-440.06	0.5	-270.1	1.17	-100.14	6.67	69.818	1138.5
-435.06	0.5	-265.1	1.17	-95.142	5.5	74.817	1150.67

CS02-C, 950°C Anneal Temperature

Position	Count	Position	Count	Position	Count	Position	Count
79.816	1136.83	209.784	2204.33	339.752	3.5	469.72	0.83
84.814	1124.83	214.783	1955.67	344.751	3.33	474.719	0.83
89.813	1159	219.781	1648	349.75	2.17	479.718	1.33
94.812	1212.33	224.78	1341.33	354.749	3	484.717	0.5
99.811	1206.17	229.779	987.17	359.747	3	489.716	1
104.81	1285.33	234.778	629.83	364.746	2.5	494.714	0.33
109.808	1329	239.777	383.67	369.745	3.5	499.713	0.33
114.807	1369.17	244.775	232.83	374.744	3.5	504.712	1
119.806	1420.5	249.774	126.83	379.742	3.33	509.711	0.5
124.805	1472.33	254.773	66.5	384.741	2.5	514.709	0.67
129.803	1564	259.772	37.33	389.74	1.83	519.708	0.67
134.802	1615.5	264.771	24.33	394.739	2	524.707	1.17
139.801	1726	269.769	19.17	399.738	3.17	529.706	0.5
144.8	1808.33	274.768	12.83	404.736	2	534.705	0.67
149.799	1891.33	279.767	10.67	409.735	1.5	539.703	0.5
154.797	2013.17	284.766	11	414.734	1.33	544.702	0.5
159.796	2062.83	289.764	7.33	419.733	1.17	549.701	0.5
164.795	2167.33	294.763	7.5	424.731	1.67	554.7	1
169.794	2249	299.762	5.83	429.73	1.83	559.698	0.5
174.792	2311.83	304.761	7	434.729	1.67	564.697	0.33
179.791	2340.17	309.76	5.83	439.728	1.17	569.696	0.83
184.79	2396.33	314.758	4.5	444.727	2.17	574.695	0.67
189.789	2427.5	319.757	3.5	449.725	1	579.694	0.83
194.788	2400.83	324.756	3.17	454.724	1.33	584.692	0.67
199.786	2398.83	329.755	3.67	459.723	1.17	589.691	0.67
204.785	2321.83	334.753	3.67	464.722	0.83	594.69	0.5
						599.689	0.67

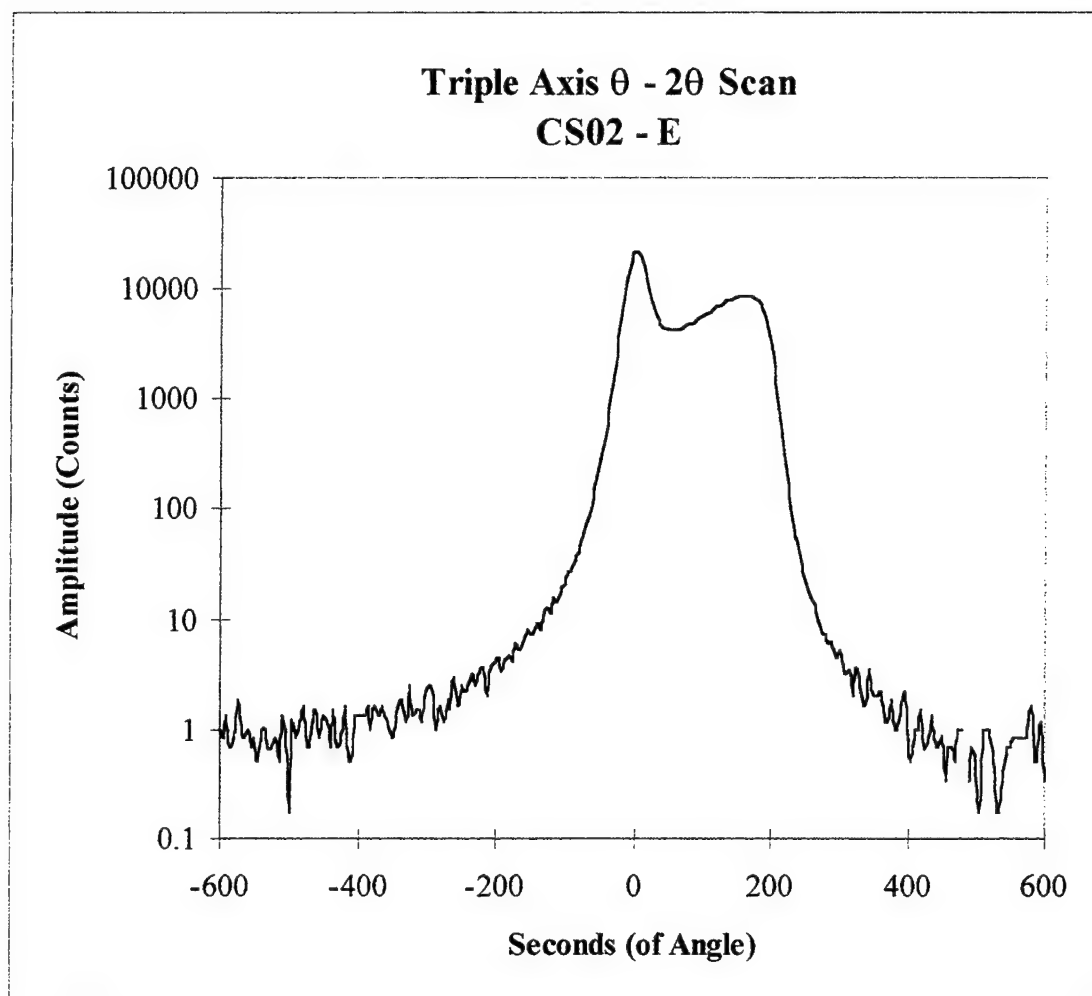


CS02-E, 1050°C Anneal Temperature

Position	Count	Position	Count	Position	Count	Position	Count
-600.02	1	-430.06	0.67	-260.1	3	-90.143	27.83
-595.02	0.83	-425.06	0.83	-255.1	1.67	-85.144	38.17
-590.02	1.33	-420.06	1.67	-250.1	2.5	-80.145	40.5
-585.02	0.67	-415.06	0.83	-245.11	2.17	-75.146	52.33
-580.02	0.83	-410.07	0.5	-240.11	2.33	-70.148	68.83
-575.02	1.83	-405.07	1.33	-235.11	3.17	-65.149	91.67
-570.03	1.5	-400.07	1.33	-230.11	2.5	-60.15	125.5
-565.03	0.83	-395.07	1.33	-225.11	2.83	-55.151	179.17
-560.03	1	-390.07	1.33	-220.11	3.67	-50.153	261.83
-555.03	0.67	-385.07	1.67	-215.11	3	-45.154	368.17
-550.03	0.83	-380.07	1	-210.11	2	-40.155	589.17
-545.03	0.5	-375.07	1.67	-205.12	3.83	-35.156	933
-540.03	1	-370.07	1.33	-200.12	4.17	-30.157	1595.33
-535.03	1	-365.08	1.67	-195.12	4.5	-25.159	2672.33
-530.04	0.67	-360.08	1.33	-190.12	3.33	-20.16	4679.83
-525.04	0.67	-355.08	1.17	-185.12	4.33	-15.161	8010.33
-520.04	0.83	-350.08	0.83	-180.12	4.67	-10.162	12741.3
-515.04	0.5	-345.08	1.17	-175.12	4.17	-5.164	18018.3
-510.04	1.33	-340.08	1.67	-170.12	6	-0.165	21509.7
-505.04	0.83	-335.08	1.83	-165.13	5.33	4.834	21589
-500.04	0.17	-330.08	1.17	-160.13	6.17	9.833	18752.8
-495.04	1.17	-325.09	2.5	-155.13	8.17	14.832	14277.3
-490.05	0.83	-320.09	1.33	-150.13	7.67	19.83	10514.8
-485.05	1.17	-315.09	1.5	-145.13	7.33	24.829	7774.5
-480.05	1.67	-310.09	1.5	-140.13	9.17	29.828	6095
-475.05	1	-305.09	1.17	-135.13	8.17	34.827	5145
-470.05	0.67	-300.09	2.17	-130.13	10.83	39.825	4648.17
-465.05	1.5	-295.09	2.5	-125.13	12.5	44.824	4311
-460.05	1.33	-290.09	2	-120.14	11.33	49.823	4206.83
-455.05	0.83	-285.1	1	-115.14	15.5	54.822	4123.5
-450.06	1.33	-280.1	1.67	-110.14	14.17	59.821	4164
-445.06	1.17	-275.1	1.17	-105.14	19.33	64.819	4269.33
-440.06	0.67	-270.1	1.83	-100.14	21.33	69.818	4407.67
-435.06	1.5	-265.1	1.5	-95.142	26.33	74.817	4498.5

CS02-E, 1050°C Anneal Temperature

Position	Count	Position	Count	Position	Count	Position	Count
79.816	4727.67	209.784	1069.17	339.752	2	469.72	0.5
84.814	4800.17	214.783	565.33	344.751	3.5	474.719	1
89.813	5092.83	219.781	306	349.75	2	479.718	1
94.812	5305	224.78	167	354.749	2	484.717	
99.811	5562.5	229.779	102.17	359.747	2.17	489.716	0.33
104.81	5791	234.778	60.67	364.746	1.5	494.714	0.67
109.808	6073.5	239.777	46	369.745	1.17	499.713	0.5
114.807	6471.83	244.775	29.83	374.744	1.83	504.712	0.17
119.806	6777.67	249.774	23.67	379.742	1.33	509.711	1
124.805	7035.5	254.773	18.5	384.741	1	514.709	1
129.803	7392.17	259.772	14.67	389.74	1.67	519.708	1
134.802	7757.67	264.771	13.17	394.739	2.17	524.707	0.5
139.801	8000.5	269.769	9.67	399.738	1.33	529.706	0.17
144.8	8257.67	274.768	7.83	404.736	0.5	534.705	0.17
149.799	8370	279.767	7.5	409.735	1	539.703	0.33
154.797	8532.17	284.766	6	414.734	1	544.702	0.67
159.796	8496	289.764	6.17	419.733	1.5	549.701	0.67
164.795	8441	294.763	4.5	424.731	0.67	554.7	0.83
169.794	8377.67	299.762	5.17	429.73	0.83	559.698	0.83
174.792	8262.33	304.761	4.67	434.729	1.33	564.697	0.83
179.791	7924.17	309.76	3.17	439.728	0.83	569.696	0.83
184.79	7163.17	314.758	3.5	444.727	0.67	574.695	0.83
189.789	6053.67	319.757	2	449.725	0.83	579.694	1.67
194.788	4557.83	324.756	3.67	454.724	0.33	584.692	0.5
199.786	3090	329.755	3	459.723	0.67	589.691	0.5
204.785	1897.17	334.753	1.67	464.722	0.67	594.69	1.17
						599.689	0.33

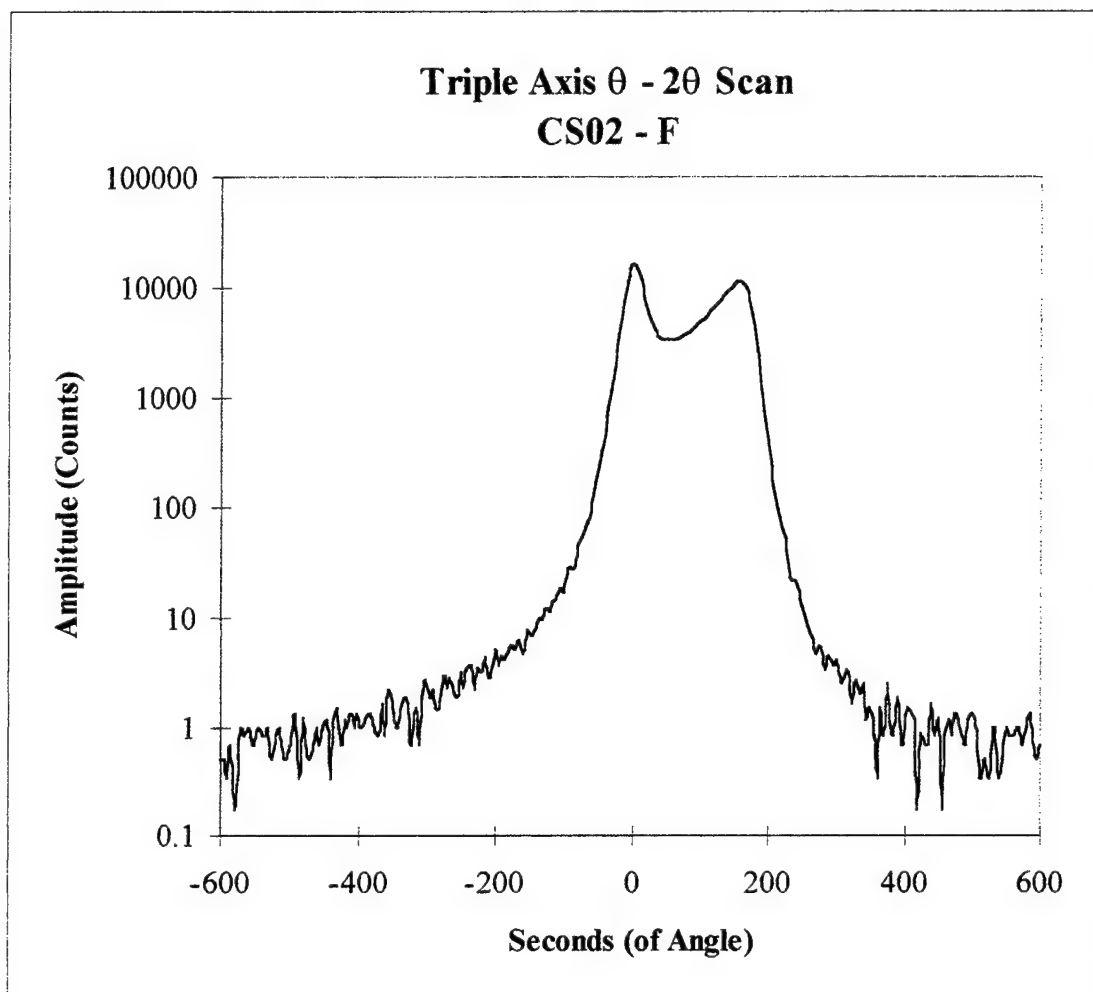


CS02-F, 1100°C Anneal Temperature

Position	Count	Position	Count	Position	Count	Position	Count
-600.02	0.5	-430.06	1.5	-260.1	2.33	-90.143	29.17
-595.02	0.5	-425.06	0.67	-255.1	1.83	-85.144	28.33
-590.02	0.33	-420.06	1.17	-250.1	3.17	-80.145	40.5
-585.02	0.67	-415.06	1	-245.11	2.33	-75.146	50.5
-580.02	0.17	-410.07	1.33	-240.11	3.5	-70.148	60.5
-575.02	0.5	-405.07	1	-235.11	3.67	-65.149	76.5
-570.03	1	-400.07	1.33	-230.11	2.17	-60.15	94.67
-565.03	0.83	-395.07	1	-225.11	3.5	-55.151	134.33
-560.03	1	-390.07	1.17	-220.11	3.17	-50.153	204.83
-555.03	0.67	-385.07	1.33	-215.11	4.33	-45.154	319
-550.03	0.67	-380.07	1.33	-210.11	3.17	-40.155	473.67
-545.03	1	-375.07	1	-205.12	2.83	-35.156	762
-540.03	0.83	-370.07	0.83	-200.12	5	-30.157	1231.5
-535.03	0.83	-365.08	1.67	-195.12	3.67	-25.159	1970.67
-530.04	1	-360.08	0.83	-190.12	4.5	-20.16	3256.33
-525.04	0.5	-355.08	2.17	-185.12	4.17	-15.161	5496.5
-520.04	0.83	-350.08	1.5	-180.12	5.33	-10.162	8804.83
-515.04	1	-345.08	1	-175.12	5.5	-5.164	12916.2
-510.04	0.67	-340.08	1	-170.12	5	-0.165	16038.8
-505.04	0.5	-335.08	1.67	-165.13	6.33	4.834	16224
-500.04	0.67	-330.08	1.83	-160.13	4.67	9.833	13519.5
-495.04	0.67	-325.09	1	-155.13	7.67	14.832	9915.83
-490.05	1.33	-320.09	0.67	-150.13	7.5	19.83	7157.17
-485.05	0.33	-315.09	1.5	-145.13	6.83	24.829	5602
-480.05	1.17	-310.09	0.67	-140.13	8.67	29.828	4579.83
-475.05	0.83	-305.09	1.67	-135.13	9.83	34.827	3988.5
-470.05	0.5	-300.09	2.67	-130.13	9.33	39.825	3610.33
-465.05	0.67	-295.09	1.83	-125.13	12.33	44.824	3396.5
-460.05	1	-290.09	2.17	-120.14	11	49.823	3371.5
-455.05	0.67	-285.1	1.5	-115.14	13.83	54.822	3356.67
-450.06	1	-280.1	1.5	-110.14	15	59.821	3334.83
-445.06	1.17	-275.1	3	-105.14	18.17	64.819	3458.5
-440.06	0.33	-270.1	2.33	-100.14	17	69.818	3587.5
-435.06	1	-265.1	2.83	-95.142	22.5	74.817	3703.67

CS02-F, 1100°C Anneal Temperature

Position	Count	Position	Count	Position	Count	Position	Count
79.816	3834	209.784	143.5	339.752	2.5	469.72	0.83
84.814	4053.17	214.783	92	344.751	1.17	474.719	1.33
89.813	4281.33	219.781	68.17	349.75	1.5	479.718	1.17
94.812	4506.83	224.78	51.33	354.749	1	484.717	0.83
99.811	4886.5	229.779	33.33	359.747	0.33	489.716	0.67
104.81	5219.33	234.778	22.17	364.746	1.5	494.714	1.17
109.808	5561.17	239.777	21.5	369.745	0.83	499.713	1.33
114.807	6106.5	244.775	17	374.744	2.5	504.712	1.17
119.806	6632.5	249.774	12.83	379.742	1.33	509.711	0.33
124.805	7207.33	254.773	9.83	384.741	0.83	514.709	0.33
129.803	7795.17	259.772	7.5	389.74	1.83	519.708	0.5
134.802	8434.17	264.771	6.33	394.739	0.67	524.707	0.33
139.801	9173.83	269.769	4.67	399.738	0.67	529.706	1
144.8	9868.67	274.768	5.5	404.736	1.5	534.705	1
149.799	10728.5	279.767	4.5	409.735	1.33	539.703	0.33
154.797	11441.3	284.766	3.33	414.734	1.17	544.702	0.67
159.796	11410	289.764	4.5	419.733	0.17	549.701	1
164.795	10674.3	294.763	3.67	424.731	0.83	554.7	0.83
169.794	9007.83	299.762	4.17	429.73	0.67	559.698	0.83
174.792	6617.17	304.761	3.5	434.729	0.67	564.697	1
179.791	4292.33	309.76	2.5	439.728	1.67	569.696	1
184.79	2432.17	314.758	3.33	444.727	0.83	574.695	0.67
189.789	1339.83	319.757	2.83	449.725	1.17	579.694	1.17
194.788	741.17	324.756	1.67	454.724	0.17	584.692	1.33
199.786	412.5	329.755	2.67	459.723	0.67	589.691	0.83
204.785	235.67	334.753	2	464.722	1.17	594.69	0.5
						599.689	0.67

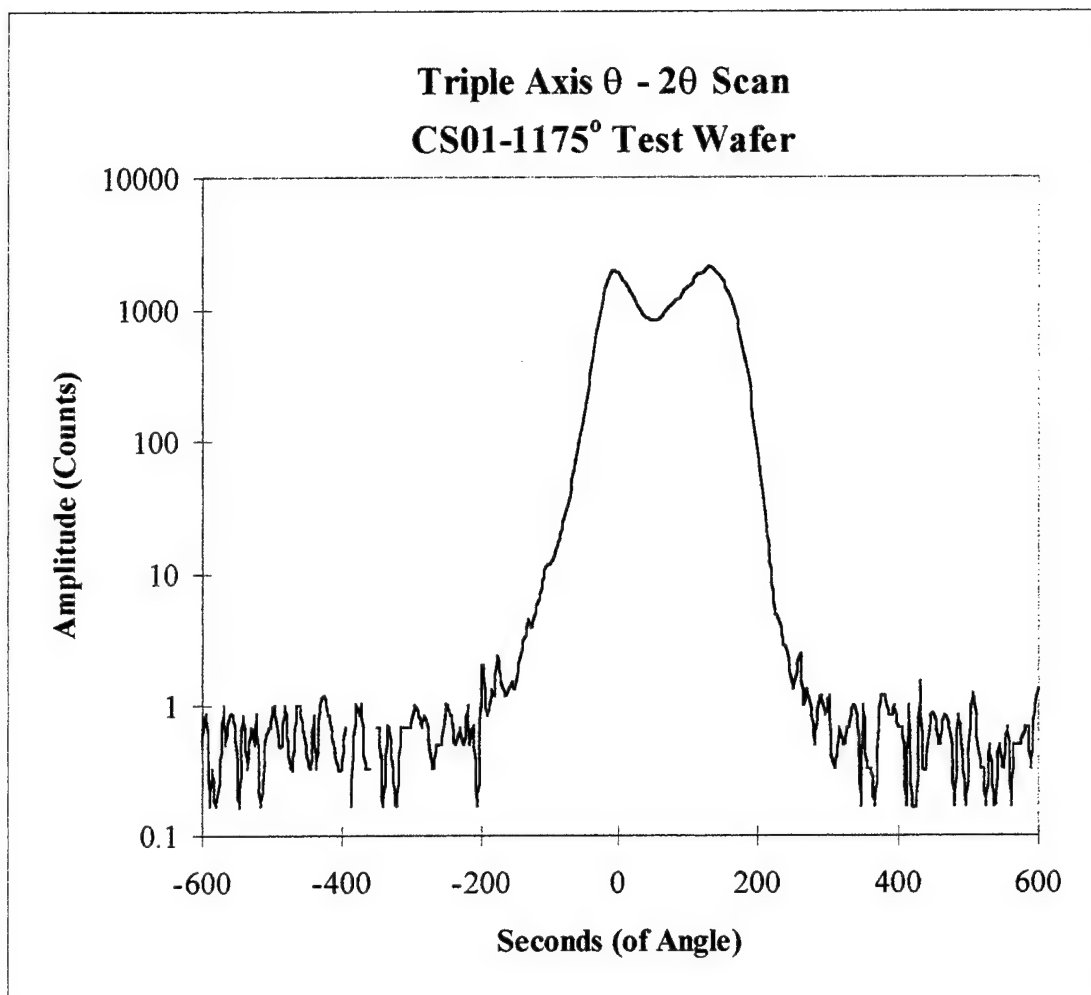


CS01, 1175°C Anneal Temperature Test Wafer

Position	Count	Position	Count	Position	Count	Position	Count
-600.02	0.5	-430.06	1	-260.1	0.5	-90.143	16.67
-595.02	0.83	-425.06	1.17	-255.1	0.5	-85.144	18.33
-590.02	0.17	-420.06	0.83	-250.1	1	-80.145	26.33
-585.02	0.33	-415.06	0.83	-245.11	0.83	-75.146	33.83
-580.02	0.17	-410.07	0.5	-240.11	0.83	-70.148	46.33
-575.02	0.33	-405.07	0.33	-235.11	0.5	-65.149	60.5
-570.03	1	-400.07	0.33	-230.11	0.67	-60.15	91.83
-565.03	0.5	-395.07	0.67	-225.11	0.5	-55.151	125.33
-560.03	0.83	-390.07		-220.11	1	-50.153	183.33
-555.03	0.83	-385.07	0.17	-215.11	0.5	-45.154	273.17
-550.03	0.33	-380.07	1	-210.11	0.67	-40.155	385.5
-545.03	0.17	-375.07	0.83	-205.12	0.17	-35.156	572.83
-540.03	0.83	-370.07	1	-200.12	1.83	-30.157	838.17
-535.03	0.33	-365.08	0.33	-195.12	2	-25.159	1141.5
-530.04	0.67	-360.08	0.33	-190.12	0.83	-20.16	1471.33
-525.04	0.5	-355.08		-185.12	1.33	-15.161	1781.67
-520.04	0.83	-350.08	0.67	-180.12	1.17	-10.162	1985.33
-515.04	0.17	-345.08	0.67	-175.12	2.33	-5.164	1982.17
-510.04	0.5	-340.08	0.17	-170.12	1.67	-0.165	1947.5
-505.04	0.67	-335.08	0.67	-165.13	1.17	4.834	1700.83
-500.04	0.67	-330.08	0.5	-160.13	1.33	9.833	1577.83
-495.04	1	-325.09	0.33	-155.13	1.5	14.832	1388.33
-490.05	0.5	-320.09	0.17	-150.13	1.33	19.83	1238.83
-485.05	0.5	-315.09	0.67	-145.13	1.83	24.829	1111.83
-480.05	1	-310.09	0.67	-140.13	3	29.828	1000.5
-475.05	0.5	-305.09	0.67	-135.13	3.33	34.827	900
-470.05	0.33	-300.09	0.67	-130.13	4.5	39.825	874.5
-465.05	1	-295.09	1	-125.13	3.83	44.824	840.33
-460.05	1	-290.09	0.83	-120.14	5.67	49.823	845.83
-455.05	0.67	-285.1	0.67	-115.14	6.5	54.822	856.5
-450.06	0.5	-280.1	0.83	-110.14	7.83	59.821	907
-445.06	0.33	-275.1	0.67	-105.14	11.5	64.819	966.83
-440.06	0.83	-270.1	0.33	-100.14	11.83	69.818	1044.17
-435.06	0.33	-265.1	0.5	-95.142	13.33	74.817	1121.83

CS01, 1175°C Anneal Temperature Test Wafer

Position	Count	Position	Count	Position	Count	Position	Count
79.816	1213.83	209.784	27.5	339.752	0.83	469.72	0.67
84.814	1254.5	214.783	14.67	344.751	0.17	474.719	0.5
89.813	1351.5	219.781	10	349.75	1	479.718	0.17
94.812	1466.67	224.78	5.33	354.749	0.33	484.717	0.83
99.811	1552.33	229.779	4.33	359.747	0.33	489.716	0.33
104.81	1658	234.778	2.83	364.746	0.17	494.714	0.17
109.808	1821.83	239.777	2.83	369.745	0.33	499.713	0.33
114.807	1914.33	244.775	2.17	374.744	1.17	504.712	1.17
119.806	1978.33	249.774	1.33	379.742	1.17	509.711	0.67
124.805	2076.83	254.773	2	384.741	0.83	514.709	0.33
129.803	2128.67	259.772	2.33	389.74	0.83	519.708	0.33
134.802	2076.67	264.771	1	394.739	1	524.707	0.17
139.801	1964.5	269.769	1.33	399.738	0.67	529.706	0.5
144.8	1808.5	274.768	0.83	404.736	0.67	534.705	0.17
149.799	1655.67	279.767	0.5	409.735	0.17	539.703	0.33
154.797	1429.5	284.766	0.83	414.734	1	544.702	0.5
159.796	1268.83	289.764	1.17	419.733	0.17	549.701	0.33
164.795	1033.17	294.763	0.83	424.731	0.17	554.7	0.67
169.794	845.5	299.762	1.17	429.73	1.5	559.698	0.17
174.792	637.67	304.761	0.5	434.729	0.33	564.697	0.5
179.791	468	309.76	0.33	439.728	0.33	569.696	0.5
184.79	337.5	314.758	0.67	444.727	0.83	574.695	0.5
189.789	231.33	319.757	0.5	449.725	0.83	579.694	0.67
194.788	137.67	324.756	0.67	454.724	0.5	584.692	0.67
199.786	84.67	329.755	0.67	459.723	0.5	589.691	0.33
204.785	49	334.753	1	464.722	0.83	594.69	1
						599.689	1.33



APPENDIX D: TEM PHOTOGRAPHS

Cross-Section TEM Photographs

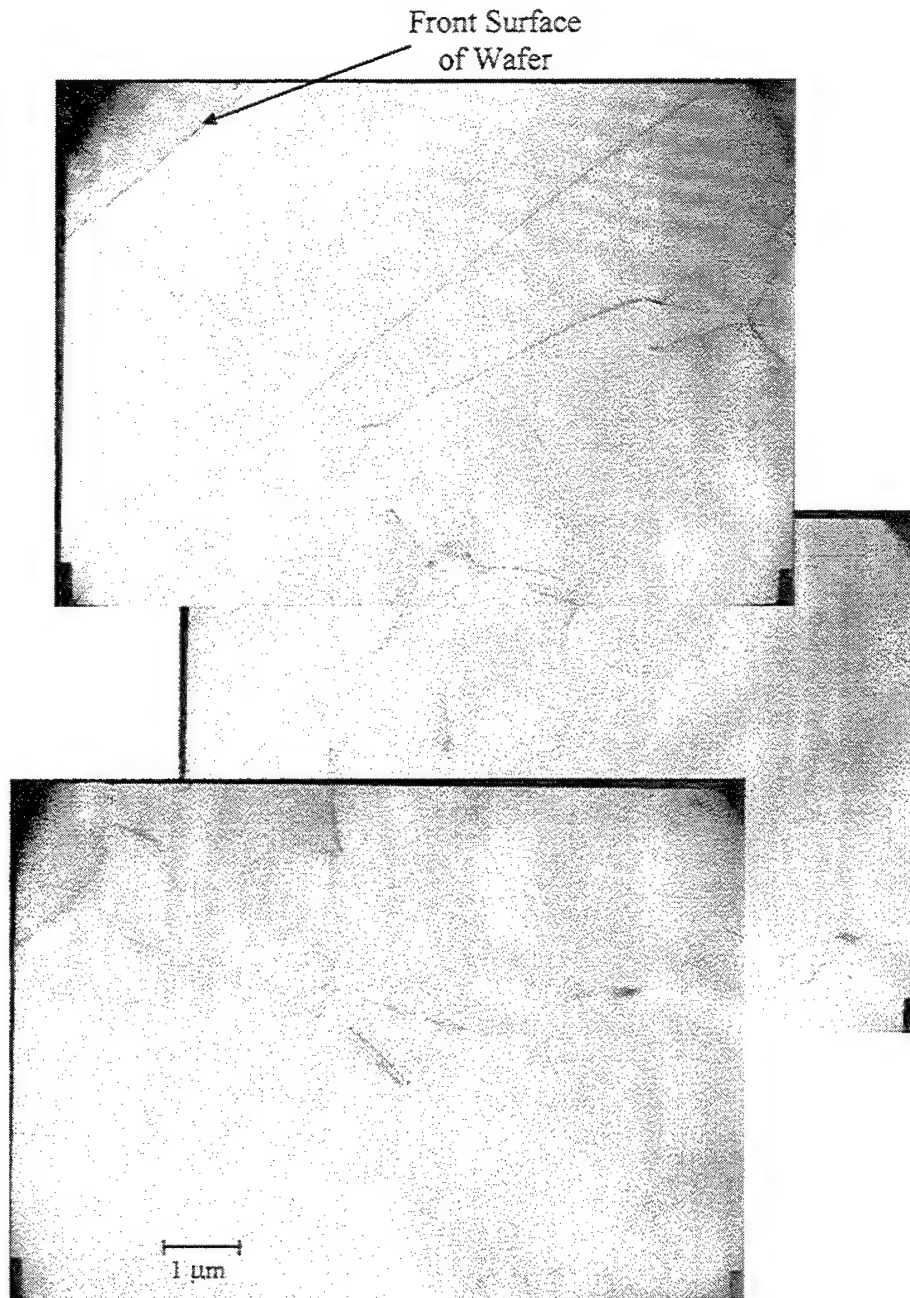


Figure 13: CS02-A Cross-Section Sample Dislocations

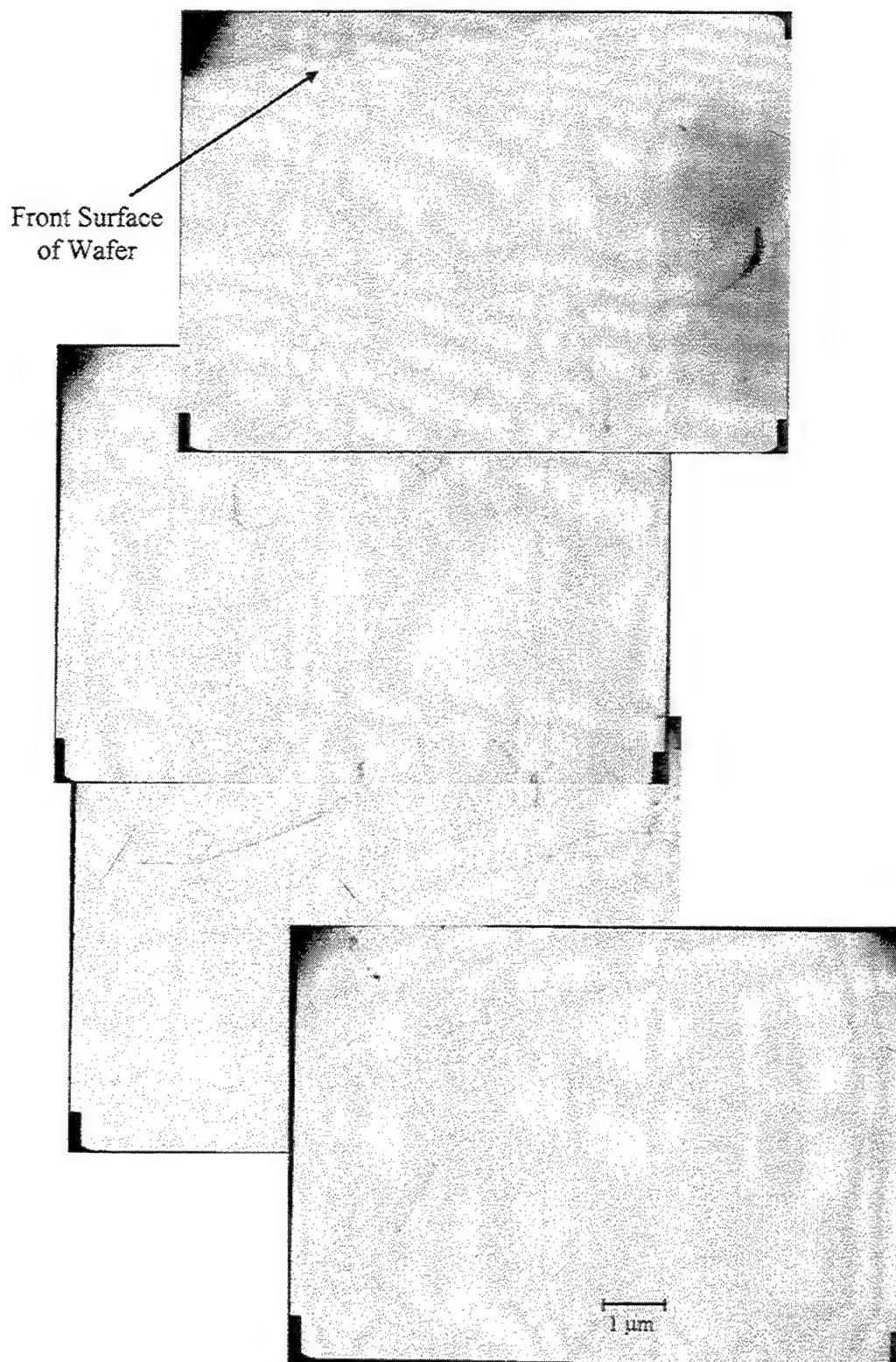


Figure 14: CS02-F Cross-Section Sample Dislocations

Plan-View TEM Photographs

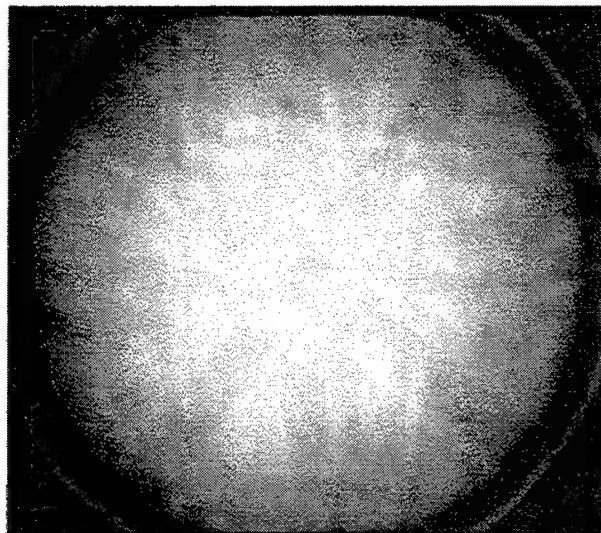


Figure 15: CS02-A Plan-View Sample Kikuchi Pattern

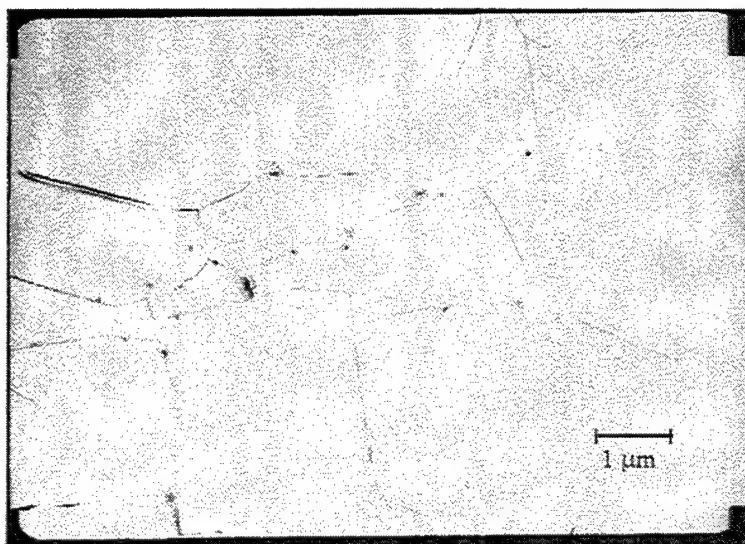


Figure 16: CS02-A Plan-View Sample Dislocations and Precipitates

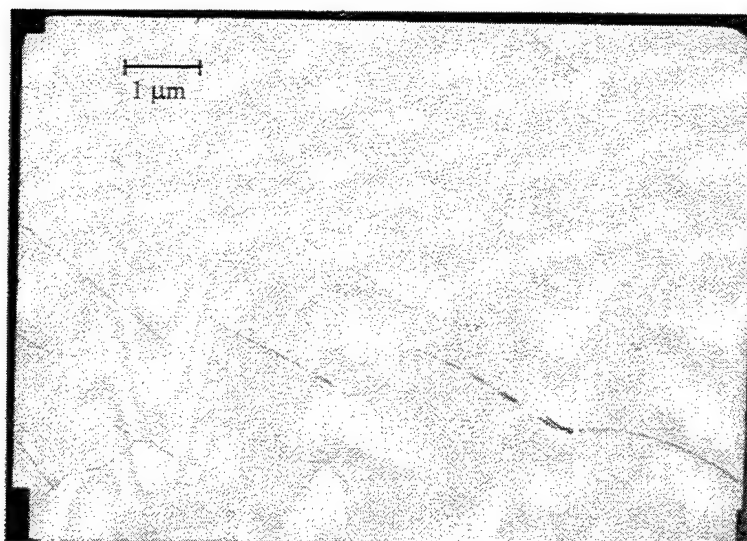


Figure 17: Plan-View Sample Precipitate-Free Region
(CS01-1175°C Test Wafer)

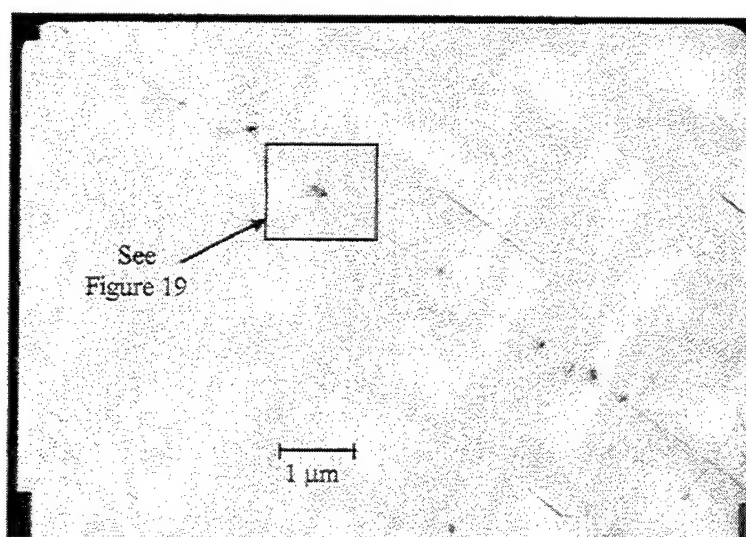


Figure 18: Plan-View Sample Dislocations and Precipitates
(CS01-1175°C Test Wafer)

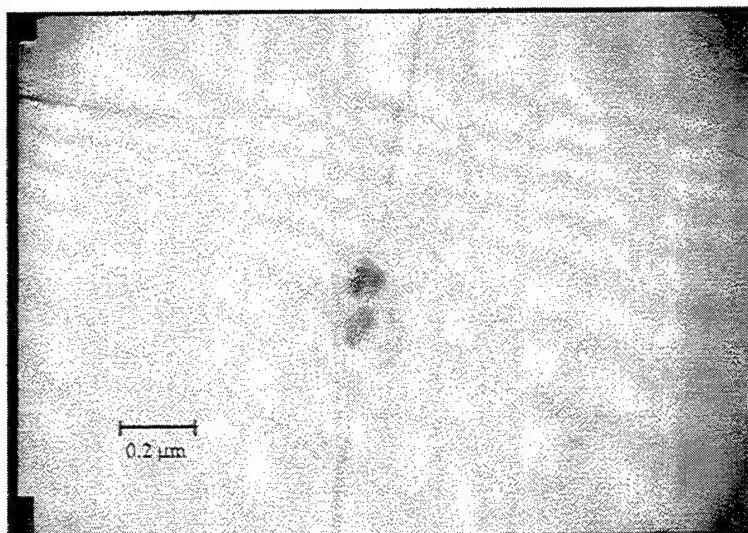


Figure 19: Plan-View Sample Precipitates – Boxed Region of Figure 18
(CS01-1175°C Test Wafer)

APPENDIX E: SIMS DATA

CS02 - A: No Anneal

Sputter Time (seconds)	Si Signal Amplitude	B Signal Amplitude	B/Si Amplitude Ratio	Sputter Time (seconds)	Si Signal Amplitude	B Signal Amplitude	B/Si Amplitude Ratio
22.47	222,447	12,274	0.0551772	628.94	224,267	51,615	0.2301498
37.26	219,183	12,839	0.0585766	643.73	223,105	50,766	0.2275431
52.04	211,433	13,383	0.0632966	658.52	220,879	51,912	0.2350246
66.83	182,997	19,931	0.1089144	673.30	225,189	51,103	0.2269338
81.62	221,001	26,201	0.1185560	688.09	225,199	51,488	0.2286333
96.41	218,245	28,221	0.1293088	702.88	226,367	51,540	0.2276834
111.20	219,259	32,633	0.1488331	717.67	222,587	51,384	0.2308491
125.99	218,567	34,405	0.1574117	732.46	222,657	50,538	0.2269769
140.78	212,463	36,378	0.1712204	747.25	226,251	51,041	0.2255946
155.57	214,493	38,559	0.1797681	762.05	226,049	51,068	0.2259156
170.35	213,561	40,230	0.1883771	776.84	225,589	50,986	0.2260128
185.14	217,037	41,511	0.1912623	791.63	225,449	50,719	0.2249688
199.93	214,183	42,726	0.1994836	806.42	227,401	50,978	0.2241767
214.72	214,443	43,738	0.2039610	821.21	223,507	50,725	0.2269504
229.51	214,621	45,454	0.2117873	836.00	225,981	51,259	0.2268288
244.30	217,155	46,113	0.2123506	850.79	226,225	50,808	0.2245906
259.09	213,673	46,810	0.2190731	865.58	223,867	50,423	0.2252364
273.88	216,009	48,206	0.2231666	880.36	224,391	50,651	0.2257265
288.66	215,147	48,259	0.2243071	895.15	223,625	51,178	0.2288563
303.45	218,071	48,219	0.2211161	909.94	225,621	50,385	0.2233170
318.24	219,321	49,170	0.2241919	924.73	230,047	51,211	0.2226110
333.03	219,197	48,989	0.2234930	939.52	227,589	50,046	0.2198964
347.82	218,125	50,623	0.2320825	954.31	224,269	50,539	0.2253499
362.61	217,805	50,409	0.2314410	969.10	226,389	50,196	0.2217246
377.40	221,587	50,674	0.2286867	983.88	223,977	49,336	0.2202726
392.18	217,439	50,566	0.2325526	998.67	226,119	49,435	0.2186238
406.97	218,187	50,458	0.2312603	1013.46	227,073	49,508	0.2180268
421.76	220,619	50,945	0.2309185	1028.42	227,787	49,601	0.2177517
436.55	218,561	51,322	0.2348177	1043.21	225,781	50,289	0.2227335
451.34	220,369	50,883	0.2308991	1058.00	224,159	49,866	0.2224582
466.13	219,763	51,183	0.2329009	1072.79	225,159	49,240	0.2186899
480.92	221,981	50,927	0.2294205	1087.58	224,903	49,514	0.2201571
495.71	222,259	51,964	0.2337993	1102.36	225,231	49,605	0.2202406
510.49	219,249	50,963	0.2324435	1117.15	221,141	49,234	0.2226362
525.42	223,705	51,659	0.2309247	1131.94	223,473	49,877	0.2231903
540.21	218,909	51,221	0.2339831	1146.73	227,813	49,532	0.2174239
554.99	222,897	51,121	0.2293481	1161.52	224,011	50,071	0.2235203
569.78	222,099	51,670	0.2326440	1176.31	223,867	48,901	0.2184377
584.57	222,605	51,040	0.2292851	1191.10	224,203	49,308	0.2199257
599.36	224,073	51,982	0.2319869	1205.89	226,831	48,993	0.2159890
614.15	221,149	51,624	0.2334354	1220.67	227,543	48,166	0.2116787

CS02 - A: No Anneal (continued)

Sputter Time (seconds)	Si Signal Amplitude	B Signal Amplitude	B/Si Amplitude Ratio	Sputter Time (seconds)	Si Signal Amplitude	B Signal Amplitude	B/Si Amplitude Ratio
1235.46	227,857	48,742	0.2139149	1871.62	228,953	44,865	0.1959573
1250.25	227,745	48,056	0.2110079	1886.41	229,049	45,138	0.1970670
1265.04	224,449	48,051	0.2140843	1901.20	229,661	44,979	0.1958495
1279.83	226,303	48,970	0.2163913	1915.99	229,667	45,575	0.1984395
1294.62	228,157	47,774	0.2093909	1930.77	228,497	45,062	0.1972105
1309.41	225,761	48,397	0.2143727	1945.56	228,203	44,547	0.1952078
1324.20	226,887	48,036	0.2117177	1960.35	230,465	44,609	0.1935608
1338.98	228,023	47,622	0.2088474	1975.14	228,597	44,763	0.1958162
1353.77	227,765	47,235	0.2073848	1989.93	229,439	44,346	0.1932801
1368.56	227,199	48,086	0.2116471	2004.72	227,929	44,399	0.1947931
1383.35	225,705	47,738	0.2115062	2019.79	230,859	44,458	0.1925764
1398.14	225,993	47,582	0.2105463	2034.58	228,829	44,371	0.1939046
1412.93	227,505	47,465	0.2086328	2049.37	228,315	43,938	0.1924447
1427.72	224,303	47,770	0.2129709	2064.15	229,535	44,352	0.1932254
1442.51	229,507	47,191	0.2056190	2078.94	226,605	44,075	0.1945015
1457.29	228,819	47,130	0.2059707	2093.73	231,389	43,739	0.1890280
1472.08	229,373	48,004	0.2092836	2108.52	229,005	43,358	0.1893321
1486.87	225,915	47,457	0.2100657	2123.31	227,477	43,746	0.1923096
1501.68	227,307	47,882	0.2106490	2138.10	228,295	43,755	0.1916599
1516.69	227,743	47,132	0.2069526	2152.89	231,231	43,376	0.1875873
1531.48	227,067	46,780	0.2060185	2167.68	232,569	43,262	0.1860179
1546.27	225,283	47,161	0.2093411	2182.46	231,149	42,850	0.1853783
1561.06	223,735	47,402	0.2118667	2197.25	231,011	42,543	0.1841601
1575.85	226,281	46,736	0.2065397	2212.04	228,047	43,091	0.1889567
1590.63	225,883	47,316	0.2094713	2226.83	231,121	42,713	0.1848080
1605.42	225,849	47,122	0.2086438	2241.64	232,259	42,341	0.1823008
1620.21	225,629	46,440	0.2058246	2256.43	229,139	42,751	0.1865723
1635.00	228,455	46,236	0.2023856	2271.22	231,891	42,130	0.1816802
1649.79	226,791	46,277	0.2040513	2286.00	230,515	41,838	0.1814980
1664.58	227,431	46,747	0.2055437	2300.79	227,367	41,959	0.1845431
1679.37	227,129	46,947	0.2066975	2315.58	231,453	41,375	0.1787620
1694.16	230,513	46,350	0.2010733	2330.37	232,091	41,429	0.1785033
1708.94	229,617	46,152	0.2009956	2345.16	227,695	41,692	0.1831046
1723.73	227,405	46,442	0.2042259	2359.95	230,961	41,461	0.1795152
1738.52	228,627	46,375	0.2028413	2374.74	230,553	40,930	0.1775297
1753.31	228,399	46,002	0.2014107	2389.53	229,525	41,484	0.1807385
1768.10	227,453	46,190	0.2030749	2404.31	229,835	40,768	0.1773794
1782.89	227,585	45,881	0.2015994	2419.10	231,453	40,402	0.1745581
1797.68	228,247	46,215	0.2024780	2433.89	225,859	40,411	0.1789214
1812.46	229,171	45,683	0.1993402	2448.68	231,533	41,289	0.1783288
1827.25	224,277	45,464	0.2027136	2463.47	230,293	40,599	0.1762928
1842.04	228,803	45,295	0.1979651	2478.26	232,635	40,572	0.1744020
1856.83	228,763	44,617	0.1950359	2493.05	231,457	40,645	0.1756050

CS02 - A: No Anneal (continued)

Sputter Time (seconds)	Si Signal Amplitude	B Signal Amplitude	B/Si Amplitude Ratio	Sputter Time (seconds)	Si Signal Amplitude	B Signal Amplitude	B/Si Amplitude Ratio
2507.84	229,797	40,461	0.1760728	3144.50	232,185	35,624	0.1534294
2522.96	232,347	40,177	0.1729181	3159.29	231,787	35,704	0.1540380
2537.75	227,713	40,382	0.1773373	3174.08	233,045	35,498	0.1523225
2552.54	231,335	39,293	0.1698532	3188.87	232,103	34,860	0.1501919
2567.33	230,305	40,025	0.1737913	3203.66	226,611	34,922	0.1541055
2582.12	230,135	40,130	0.1743759	3218.45	230,313	35,444	0.1538949
2596.91	229,785	39,222	0.1706900	3233.24	232,795	35,174	0.1510943
2611.69	231,919	39,395	0.1698653	3248.02	231,921	35,005	0.1509350
2626.48	233,917	39,460	0.1686923	3262.81	234,189	34,508	0.1473511
2641.27	231,537	39,505	0.1706207	3277.60	231,111	34,716	0.1502135
2656.06	231,057	38,700	0.1674911	3292.39	230,615	34,417	0.1492401
2670.85	231,383	38,964	0.1683961	3307.18	232,293	34,640	0.1491220
2685.64	231,291	39,370	0.1702185	3321.97	230,081	34,511	0.1499950
2700.43	237,083	38,788	0.1636052	3336.76	235,787	34,088	0.1445712
2715.22	229,107	38,825	0.1694623	3351.55	233,775	33,876	0.1449086
2730.00	231,191	38,196	0.1652140	3366.33	233,535	34,407	0.1473312
2744.79	231,391	38,362	0.1657886	3381.12	233,455	33,882	0.1451329
2759.58	231,451	38,643	0.1669598	3395.91	236,331	33,956	0.1436798
2774.37	232,549	37,909	0.1630151	3410.70	232,443	33,627	0.1446677
2789.16	233,845	38,361	0.1640446	3425.49	231,789	33,390	0.1440534
2803.95	233,017	38,203	0.1639494	3440.28	233,435	32,953	0.1411656
2818.74	233,495	38,075	0.1630656	3455.07	233,661	33,345	0.1427067
2833.53	230,869	37,927	0.1642793	3469.86	238,499	33,120	0.1388685
2848.31	236,235	38,035	0.1610049	3484.64	235,556	33,516	0.1422846
2863.10	232,229	37,586	0.1618489	3499.43	234,859	33,303	0.1418000
2877.89	232,455	37,302	0.1604698	3514.22	233,479	32,955	0.1411476
2892.68	231,007	37,818	0.1637093	3529.46	235,285	33,401	0.1419598
2907.47	232,409	37,457	0.1611685	3544.25	231,357	33,187	0.1434450
2922.26	235,483	37,326	0.1585083	3559.04	235,871	33,188	0.1407040
2937.05	231,751	36,841	0.1589680	3573.83	234,891	32,532	0.1384983
2951.84	231,605	37,002	0.1597634	3588.62	231,263	32,453	0.1403294
2966.62	233,645	36,684	0.1570074	3603.41	237,307	32,792	0.1381839
2981.43	229,947	36,940	0.1606457	3618.20	236,621	32,073	0.1355459
2996.22	229,873	37,077	0.1612934	3632.98	230,993	32,168	0.1392596
3011.01	231,971	36,495	0.1573257	3647.77	236,641	32,558	0.1375839
3026.19	231,829	36,381	0.1569303	3662.56	234,051	31,985	0.1366583
3040.98	232,415	35,686	0.1535443	3677.35	233,901	32,404	0.1385372
3055.77	231,143	36,289	0.1569981	3692.14	234,973	31,698	0.1349006
3070.56	231,635	36,060	0.1556760	3706.93	232,867	31,677	0.1360304
3085.35	231,035	35,343	0.1529768	3721.74	235,503	31,431	0.1334633
3100.14	233,095	35,634	0.1528733	3736.53	233,243	31,542	0.1352324
3114.93	230,735	35,932	0.1557284	3751.32	232,281	30,801	0.1326023
3129.71	235,443	35,206	0.1495309	3766.10	234,243	30,852	0.1317094

CS02 - A: No Anneal (continued)

Sputter Time (seconds)	Si Signal Amplitude	B Signal Amplitude	B/Si Amplitude Ratio	Sputter Time (seconds)	Si Signal Amplitude	B Signal Amplitude	B/Si Amplitude Ratio
3780.89	232,357	31,201	0.1342804	4417.32	236,861	26,016	0.1098366
3795.68	233,865	30,795	0.1316785	4432.11	237,173	26,198	0.1104595
3810.47	233,403	31,291	0.1340643	4446.90	235,865	26,167	0.1109406
3825.26	233,703	30,666	0.1312178	4461.70	235,189	26,019	0.1106302
3840.05	230,797	31,068	0.1346118	4476.49	237,149	25,969	0.1095050
3854.84	235,583	30,542	0.1296443	4491.28	236,211	25,608	0.1084116
3869.63	231,548	30,922	0.1335447	4506.07	236,477	25,439	0.1075749
3884.41	235,799	30,191	0.1280370	4521.42	237,235	25,484	0.1074209
3899.20	236,007	30,066	0.1273945	4536.21	242,235	25,488	0.1052201
3913.99	231,989	30,768	0.1326270	4551.00	237,985	25,476	0.1070488
3928.78	236,119	30,103	0.1274908	4565.79	237,177	25,163	0.1060938
3943.57	235,199	30,086	0.1279172	4580.58	239,425	25,237	0.1054067
3958.36	235,139	29,769	0.1266017	4595.36	236,963	24,958	0.1053245
3973.15	232,645	29,659	0.1274861	4610.15	234,878	25,006	0.1064638
3987.94	232,365	29,337	0.1262540	4624.94	237,153	24,381	0.1028071
4002.72	234,121	29,328	0.1252686	4639.73	236,795	24,264	0.1024684
4018.02	236,745	28,780	0.1215654	4654.52	236,889	23,714	0.1001060
4032.81	232,645	29,074	0.1249715	4669.31	237,904	23,893	0.1004313
4047.60	236,419	29,644	0.1253876	4684.10	238,625	24,174	0.1013054
4062.39	234,463	28,809	0.1228723	4698.89	232,719	23,717	0.1019126
4077.17	234,063	28,583	0.1221167	4713.68	236,355	23,987	0.1014872
4091.96	233,259	28,588	0.1225590	4728.46	234,231	23,576	0.1006528
4106.75	234,683	28,807	0.1227486	4743.25	237,165	23,842	0.1005292
4121.54	237,579	28,723	0.1208987	4758.04	236,569	23,480	0.0992522
4136.33	232,239	28,535	0.1228691	4772.83	233,295	23,169	0.0993120
4151.12	236,407	28,648	0.1211808	4787.62	235,255	23,322	0.0991350
4165.91	232,939	28,485	0.1222852	4802.41	239,614	22,831	0.0952824
4180.70	234,791	27,640	0.1177217	4817.20	235,611	22,528	0.0956152
4195.48	235,396	28,008	0.1189825	4831.99	238,807	22,875	0.0957886
4210.27	234,575	27,548	0.1174379	4846.78	233,767	23,035	0.0985383
4225.06	234,935	27,314	0.1162619	4861.56	238,725	22,610	0.0947115
4239.85	235,259	27,557	0.1171347	4876.35	236,215	22,422	0.0949220
4254.64	233,589	27,425	0.1174071	4891.14	239,185	22,126	0.0925058
4269.43	233,923	27,450	0.1173463	4905.93	236,437	21,789	0.0921556
4284.22	234,191	27,416	0.1170668	4920.72	234,285	22,269	0.0950509
4299.01	237,069	27,381	0.1154980	4935.51	236,625	21,602	0.0912921
4313.80	235,453	26,963	0.1145154	4950.30	236,457	21,872	0.0924988
4328.58	233,017	26,839	0.1151804	4965.09	235,910	21,709	0.0920224
4343.37	235,555	26,858	0.1140201	4979.88	236,983	21,597	0.0911331
4358.16	237,491	27,375	0.1152675	4994.66	235,925	21,535	0.0912790
4372.95	236,705	26,352	0.1113285	5009.45	237,579	21,419	0.0901553
4387.74	236,871	26,347	0.1112293	5024.86	236,815	21,162	0.0893609
4402.53	235,755	26,352	0.1117771	5039.65	237,553	20,769	0.0874289

CS02 - A: No Anneal (continued)

Sputter Time (seconds)	Si Signal Amplitude	B Signal Amplitude	B/Si Amplitude Ratio	Sputter Time (seconds)	Si Signal Amplitude	B Signal Amplitude	B/Si Amplitude Ratio
5054.44	237,225	20,585	0.0867742	5691.05	230,807	14,523	0.0629227
5069.23	239,569	20,922	0.0873318	5705.84	228,330	14,947	0.0654623
5084.02	234,429	20,463	0.0872887	5720.63	228,255	14,665	0.0642483
5098.81	237,051	20,593	0.0868716	5735.42	227,959	14,314	0.0627920
5113.59	237,329	20,882	0.0879876	5750.21	227,041	14,404	0.0634423
5128.38	234,227	20,022	0.0854812	5765.00	229,243	13,917	0.0607085
5143.17	234,466	20,328	0.0866991	5779.79	229,023	14,239	0.0621728
5157.96	233,551	20,065	0.0859127	5794.58	228,121	13,553	0.0594115
5172.75	232,413	19,916	0.0856923	5809.37	226,395	13,788	0.0609024
5187.54	234,563	19,419	0.0827880	5824.15	226,463	13,672	0.0603719
5202.35	236,311	19,278	0.0815789	5838.94	228,763	13,048	0.0570372
5217.14	235,671	19,421	0.0824073	5853.73	226,885	12,830	0.0565485
5231.92	236,363	19,240	0.0814002	5868.52	229,007	12,321	0.0538018
5246.71	234,417	18,819	0.0802800	5883.31	228,667	12,251	0.0535757
5261.50	233,975	18,639	0.0796624	5898.10	229,131	11,782	0.0514204
5276.29	233,063	18,825	0.0807722	5912.89	227,433	11,830	0.0520153
5291.08	231,939	18,539	0.0799305	5927.68	226,877	11,309	0.0498464
5305.87	233,340	18,380	0.0787692	5942.48	229,311	10,985	0.0479044
5320.66	232,169	18,297	0.0788090	5957.27	226,737	10,831	0.0477690
5335.45	232,343	18,366	0.0790469	5972.06	227,737	10,253	0.0450212
5350.23	233,475	18,033	0.0772374	5986.85	225,915	10,660	0.0471859
5365.02	233,417	17,747	0.0760313	6001.64	226,863	10,149	0.0447363
5379.81	229,961	18,025	0.0783829	6017.16	231,525	9,936	0.0429155
5394.60	233,473	17,590	0.0753406	6031.95	232,397	9,571	0.0411838
5409.39	234,707	17,408	0.0741691	6046.73	228,369	9,008	0.0394449
5424.18	232,817	17,377	0.0746380	6061.52	227,827	11,022	0.0483788
5438.97	232,127	17,331	0.0746617	6076.31	228,725	15,517	0.0678413
5453.76	231,985	16,783	0.0723452	6091.10	227,483	15,637	0.0687392
5468.55	226,409	16,883	0.0745686	6105.89	229,299	15,053	0.0656479
5483.33	230,091	17,055	0.0741228	6120.68	227,705	14,916	0.0655058
5498.12	229,449	16,736	0.0729400	6135.47	229,355	14,870	0.0648340
5512.91	230,399	16,529	0.0717408	6150.26	230,441	13,414	0.0582101
5528.38	229,749	16,794	0.0730972	6165.04	228,486	8,188	0.0358359
5543.17	229,225	16,034	0.0699487	6179.83	225,481	8,304	0.0368279
5557.95	227,997	16,219	0.0711369	6194.62	229,701	8,166	0.0355506
5572.74	230,571	15,902	0.0689679	6209.41	230,313	7,919	0.0343836
5587.53	228,949	15,782	0.0689324	6224.20	227,313	7,741	0.0340544
5602.32	231,695	15,567	0.0671875	6238.99	231,333	7,870	0.0340202
5617.11	230,113	15,650	0.0680101	6253.78	230,251	7,565	0.0328554
5631.90	231,141	15,525	0.0671668	6268.57	226,257	7,479	0.0330553
5646.69	226,041	15,365	0.0679744	6283.36	231,077	7,390	0.0319807
5661.48	228,001	15,098	0.0662190	6298.15	227,539	7,446	0.0327241
5676.27	231,461	14,589	0.0630301	6312.93	231,273	7,370	0.0318671

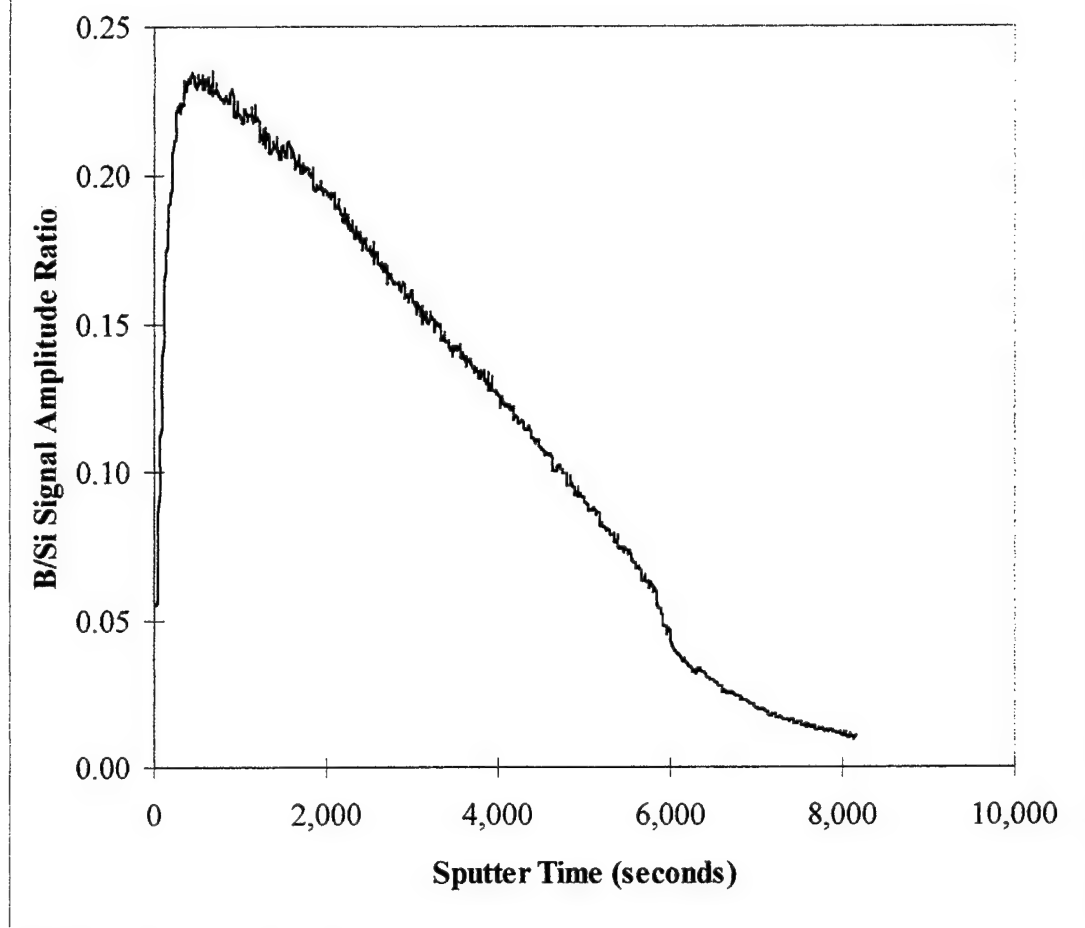
CS02 - A: No Anneal (continued)

Sputter Time (seconds)	Si Signal Amplitude	B Signal Amplitude	B/Si Amplitude Ratio	Sputter Time (seconds)	Si Signal Amplitude	B Signal Amplitude	B/Si Amplitude Ratio
6327.72	225,733	7,511	0.0332738	6964.45	226,107	4,768	0.0210874
6342.51	230,981	7,553	0.0326997	6979.24	226,757	4,749	0.0209431
6357.30	229,191	7,576	0.0330554	6994.03	228,271	4,553	0.0199456
6372.09	227,031	7,322	0.0322511	7008.82	224,933	4,492	0.0199704
6386.88	228,435	7,327	0.0320748	7024.45	224,705	4,389	0.0195323
6401.67	228,855	7,347	0.0321033	7039.24	225,755	4,360	0.0193130
6416.46	228,833	7,232	0.0316038	7054.03	226,395	4,380	0.0193467
6431.25	227,833	7,036	0.0308823	7068.82	228,841	4,601	0.0201057
6446.03	228,147	6,897	0.0302305	7083.61	226,167	4,396	0.0194370
6460.82	230,161	6,906	0.0300051	7098.39	225,327	4,319	0.0191677
6475.61	226,773	6,774	0.0298713	7113.18	223,705	4,270	0.0190876
6490.40	230,225	6,882	0.0298925	7127.97	228,353	4,307	0.0188611
6505.19	230,141	6,629	0.0288041	7142.76	224,929	4,197	0.0186592
6520.76	229,433	6,583	0.0286925	7157.55	224,389	3,996	0.0178084
6535.55	226,923	6,618	0.0291641	7172.34	228,995	4,074	0.0177908
6550.34	228,655	6,529	0.0285539	7187.13	225,313	4,061	0.0180238
6565.13	230,817	6,289	0.0272467	7201.92	224,403	4,052	0.0180568
6579.92	229,709	6,299	0.0274217	7216.71	227,557	3,902	0.0171474
6594.71	228,232	6,358	0.0278576	7231.49	225,031	3,962	0.0176065
6609.50	231,207	5,978	0.0258556	7246.28	226,061	3,856	0.0170573
6624.29	228,003	5,972	0.0261926	7261.07	223,913	3,873	0.0172969
6639.07	228,209	6,028	0.0264144	7275.86	226,870	3,955	0.0174329
6653.86	229,021	5,848	0.0255348	7290.65	226,713	3,805	0.0167833
6668.65	227,045	5,715	0.0251712	7305.44	227,767	3,731	0.0163808
6683.46	230,297	5,933	0.0257624	7320.23	225,208	3,676	0.0163227
6698.25	228,301	5,832	0.0255452	7335.02	224,693	3,651	0.0162488
6713.04	227,725	5,635	0.0247448	7349.81	222,409	3,595	0.0161639
6727.83	227,583	5,883	0.0258499	7364.60	223,977	3,589	0.0160240
6742.62	227,771	5,685	0.0249593	7379.39	221,457	3,430	0.0154883
6757.40	226,833	5,496	0.0242293	7394.17	222,903	3,434	0.0154058
6772.19	223,827	5,352	0.0239113	7408.96	224,029	3,541	0.0158060
6786.98	226,693	5,453	0.0240546	7423.77	225,115	3,513	0.0156054
6801.77	230,579	5,532	0.0239918	7438.56	225,455	3,467	0.0153778
6816.56	229,236	5,167	0.0225401	7453.35	224,633	3,373	0.0150156
6831.35	226,004	5,360	0.0237164	7468.14	225,095	3,424	0.0152114
6846.14	227,229	5,167	0.0227392	7482.93	224,207	3,335	0.0148746
6860.93	228,023	5,156	0.0226118	7497.72	218,768	3,356	0.0153405
6875.72	224,993	5,087	0.0226096	7512.51	226,121	3,398	0.0150274
6890.51	222,463	5,043	0.0226689	7528.20	226,647	3,327	0.0146792
6905.29	225,731	5,039	0.0223230	7542.98	224,379	3,211	0.0143106
6920.08	226,587	4,895	0.0216032	7557.77	220,171	3,201	0.0145387
6934.87	228,885	4,872	0.0212858	7572.56	223,113	3,277	0.0146876
6949.66	224,341	4,832	0.0215386	7587.35	224,595	3,052	0.0135889

CS02 - A: No Anneal (continued)

Sputter Time (seconds)	Si Signal Amplitude	B Signal Amplitude	B/Si Amplitude Ratio	Sputter Time (seconds)	Si Signal Amplitude	B Signal Amplitude	B/Si Amplitude Ratio
7602.14	222,023	3,212	0.0144670	7897.92	220,663	2,629	0.0119141
7616.93	218,787	3,117	0.0142467	7912.71	221,017	2,601	0.0117683
7631.72	221,743	3,026	0.0136464	7927.50	220,955	2,648	0.0119843
7646.51	224,271	3,150	0.0140455	7942.29	218,747	2,486	0.0113647
7661.30	222,395	3,058	0.0137503	7957.08	219,259	2,512	0.0114568
7676.09	220,427	3,069	0.0139230	7971.86	218,711	2,687	0.0122856
7690.87	222,003	2,998	0.0135043	7986.65	222,173	2,496	0.0112345
7705.66	220,575	2,869	0.0130069	8001.44	222,481	2,452	0.0110212
7720.45	222,021	2,994	0.0134852	8017.18	221,021	2,411	0.0109085
7735.24	222,153	2,929	0.0131846	8031.97	219,775	2,452	0.0111569
7750.03	220,663	2,798	0.0126800	8046.76	218,481	2,596	0.0118820
7764.82	217,823	2,995	0.0137497	8061.55	219,863	2,496	0.0113525
7779.61	220,431	2,874	0.0130381	8076.34	220,655	2,293	0.0103918
7794.40	221,283	2,786	0.0125902	8091.13	217,463	2,496	0.0114778
7809.19	221,057	2,729	0.0123452	8105.92	221,511	2,418	0.0109159
7823.97	220,701	2,749	0.0124558	8120.71	221,541	2,389	0.0107836
7838.76	223,765	2,675	0.0119545	8135.50	222,285	2,078	0.0093484
7853.55	221,097	2,726	0.0123294	8150.28	223,549	2,172	0.0097160
7868.34	223,103	2,808	0.0125861	8165.09	222,507	2,454	0.0110289
7883.13	219,771	2,767	0.0125904				

CS02 - A SIMS Analysis



CS02 - F: 1100°C Anneal Temperature

Sputter Time (seconds)	Si Signal Amplitude	B Signal Amplitude	B/Si Amplitude Ratio	Sputter Time (seconds)	Si Signal Amplitude	B Signal Amplitude	B/Si Amplitude Ratio
7.46	229,053	6,282	0.0274260	614.12	514,325	30,778	0.0598415
22.46	400,827	14,763	0.0368314	628.91	513,735	30,929	0.0602042
37.25	448,005	17,825	0.0397875	643.7	517,475	30,837	0.0595913
52.04	459,143	19,358	0.0421612	658.49	516,095	30,890	0.0598533
66.83	468,551	20,613	0.0439931	673.27	520,801	31,603	0.0606815
81.62	475,075	21,405	0.0450560	688.06	518,659	31,884	0.0614739
96.4	475,043	21,579	0.0454254	702.85	522,569	32,314	0.0618368
111.19	472,105	22,047	0.0466994	717.64	524,215	33,040	0.0630276
125.98	502,971	22,921	0.0455712	732.43	520,181	32,234	0.0619669
140.77	505,353	23,544	0.0465892	747.21	529,193	33,451	0.0632113
155.56	505,781	23,594	0.0466486	762.02	531,991	33,624	0.0632041
170.34	505,781	23,817	0.0470896	776.81	530,469	33,967	0.0640320
185.13	499,671	24,271	0.0485740	791.6	529,515	34,332	0.0648367
199.92	492,843	24,182	0.0490663	806.38	528,075	34,637	0.0655911
214.71	502,093	24,629	0.0490527	821.17	536,787	34,785	0.0648022
229.5	498,981	24,902	0.0499057	835.96	539,223	35,536	0.0659022
244.28	500,417	24,948	0.0498544	850.75	542,347	35,704	0.0658324
259.07	497,977	25,204	0.0506128	865.54	546,905	36,017	0.0658560
273.86	496,475	25,633	0.0516300	880.32	544,371	36,011	0.0661516
288.65	496,233	25,721	0.0518325	895.11	543,769	37,051	0.0681374
303.44	501,435	26,560	0.0529680	909.9	548,033	36,682	0.0669339
318.23	497,801	26,797	0.0538307	924.69	548,355	38,109	0.0694970
333.01	497,111	27,233	0.0547825	939.48	545,575	38,143	0.0699134
347.8	500,413	27,081	0.0541173	954.26	551,075	38,378	0.0696421
362.59	494,985	27,296	0.0551451	969.05	549,393	38,639	0.0703303
377.38	497,319	27,439	0.0551738	983.84	560,584	38,678	0.0689959
392.17	504,725	27,605	0.0546932	998.63	569,013	40,060	0.0704026
406.95	504,431	28,033	0.0555735	1013.42	569,689	39,919	0.0700716
421.74	506,631	28,342	0.0559421	1028.37	576,775	40,246	0.0697776
436.53	504,307	28,394	0.0563030	1043.16	576,377	40,014	0.0694233
451.32	504,949	29,032	0.0574949	1057.95	570,755	40,103	0.0702631
466.11	511,999	29,787	0.0581778	1072.73	578,933	40,159	0.0693673
480.89	507,825	29,285	0.0576675	1087.52	574,111	40,342	0.0702686
495.68	508,967	29,661	0.0582769	1102.31	573,095	40,716	0.0710458
510.47	512,463	29,116	0.0568158	1117.1	573,631	41,341	0.0720690
525.39	509,615	29,566	0.0580163	1131.89	579,869	41,701	0.0719145
540.18	511,865	30,047	0.0587010	1146.68	581,103	41,248	0.0709823
554.97	510,273	30,207	0.0591977	1161.46	574,963	42,505	0.0739265
569.76	508,543	30,502	0.0599792	1176.25	576,039	42,004	0.0729187
584.54	509,931	30,458	0.0597297	1191.04	582,747	42,740	0.0733423
599.33	513,889	30,725	0.0597892	1205.83	579,489	42,922	0.0740687

CS02 - F: 1100°C Anneal Temperature (continued)

Sputter Time (seconds)	Si Signal Amplitude	B Signal Amplitude	B/Si Amplitude Ratio	Sputter Time (seconds)	Si Signal Amplitude	B Signal Amplitude	B/Si Amplitude Ratio
1220.62	582,147	43,286	0.0743558	1856.74	600,309	47,692	0.0794458
1235.4	582,511	42,930	0.0736982	1871.53	599,511	47,352	0.0789844
1250.19	587,531	43,050	0.0732727	1886.32	603,985	47,858	0.0792371
1264.98	586,489	42,906	0.0731574	1901.11	603,845	47,674	0.0789507
1279.77	591,257	44,142	0.0746579	1915.89	602,589	47,506	0.0788365
1294.56	591,729	44,378	0.0749972	1930.68	598,028	47,928	0.0801434
1309.34	594,355	43,969	0.0739777	1945.47	597,623	48,042	0.0803885
1324.13	598,757	43,694	0.0729745	1960.26	597,865	47,935	0.0801770
1338.92	600,009	44,182	0.0736356	1975.05	600,437	47,637	0.0793372
1353.71	599,157	44,691	0.0745898	1989.83	598,063	48,322	0.0807975
1368.5	602,287	44,822	0.0744197	2004.62	599,849	47,736	0.0795800
1383.29	604,465	44,447	0.0735311	2019.69	600,783	48,030	0.0799457
1398.07	605,685	45,015	0.0743208	2034.47	597,457	47,519	0.0795354
1412.86	608,039	45,261	0.0744377	2049.26	596,537	48,363	0.0810729
1427.65	605,461	45,427	0.0750288	2064.05	590,909	48,347	0.0818180
1442.44	600,117	45,609	0.0760002	2078.84	592,739	48,016	0.0810070
1457.22	602,453	46,171	0.0766383	2093.63	598,651	48,620	0.0812159
1472.01	597,137	46,429	0.0777527	2108.41	596,429	48,875	0.0819460
1486.8	593,193	45,221	0.0762332	2123.2	600,633	48,279	0.0803802
1501.61	599,623	46,140	0.0769483	2137.99	592,707	47,929	0.0808646
1516.62	600,579	45,748	0.0761732	2152.78	594,665	47,618	0.0800753
1531.4	599,087	46,816	0.0781456	2167.57	596,951	47,470	0.0795208
1546.19	605,101	46,641	0.0770797	2182.36	603,413	48,009	0.0795624
1560.98	602,137	46,713	0.0775787	2197.14	594,701	47,168	0.0793138
1575.77	600,685	47,024	0.0782840	2211.93	598,599	48,093	0.0803426
1590.56	602,179	45,987	0.0763677	2226.72	591,303	47,645	0.0805763
1605.34	600,095	46,781	0.0779560	2241.53	588,389	47,118	0.0800797
1620.13	602,304	46,565	0.0773115	2256.31	597,003	47,225	0.0791035
1634.92	606,531	47,215	0.0778443	2271.1	594,781	47,058	0.0791182
1649.71	606,177	47,041	0.0776027	2285.89	597,307	46,778	0.0783148
1664.5	604,739	47,438	0.0784438	2300.68	597,523	47,050	0.0787417
1679.28	602,069	46,676	0.0775260	2315.47	598,253	46,394	0.0775491
1694.07	598,607	47,418	0.0792139	2330.26	602,523	46,965	0.0779472
1708.86	604,775	47,569	0.0786557	2345.04	602,443	46,810	0.0777003
1723.65	596,103	47,714	0.0800432	2359.83	605,311	47,020	0.0776791
1738.44	596,687	47,235	0.0791621	2374.62	599,233	46,186	0.0770752
1753.22	604,579	46,884	0.0775482	2389.41	599,547	46,871	0.0781774
1768.01	597,549	46,952	0.0785743	2404.2	602,459	47,194	0.0783356
1782.8	607,699	47,023	0.0773788	2418.98	596,961	47,285	0.0792095
1797.59	606,855	47,486	0.0782493	2433.77	597,781	46,294	0.0774431
1812.38	596,933	47,156	0.0789971	2448.56	596,159	46,778	0.0784656
1827.17	599,375	47,143	0.0786536	2463.35	600,414	46,260	0.0770468
1841.95	601,045	47,585	0.0791704	2478.14	596,155	46,540	0.0780669

CS02 - F: 1100°C Anneal Temperature (continued)

Sputter Time (seconds)	Si Signal Amplitude	B Signal Amplitude	B/Si Amplitude Ratio	Sputter Time (seconds)	Si Signal Amplitude	B Signal Amplitude	B/Si Amplitude Ratio
2492.93	596,931	45,441	0.0761244	3129.55	589,045	42,460	0.0720828
2507.71	595,043	46,193	0.0776297	3144.34	589,785	41,826	0.0709174
2522.83	597,699	45,591	0.0762775	3159.13	591,677	41,829	0.0706957
2537.62	598,741	45,386	0.0758024	3173.92	592,429	42,272	0.0713537
2552.41	601,081	45,792	0.0761827	3188.71	587,997	41,516	0.0706058
2567.2	598,499	46,016	0.0768857	3203.5	586,134	42,130	0.0718778
2581.99	597,871	45,202	0.0756049	3218.28	586,862	42,159	0.0718380
2596.77	595,489	45,232	0.0759577	3233.07	583,789	41,113	0.0704244
2611.56	596,729	45,305	0.0759222	3247.86	587,015	41,536	0.0707580
2626.35	598,233	45,138	0.0754522	3262.65	589,943	40,847	0.0692389
2641.14	593,449	45,488	0.0766502	3277.44	589,299	41,217	0.0699424
2655.93	595,151	44,252	0.0743542	3292.22	585,547	41,426	0.0707475
2670.72	594,679	45,435	0.0764026	3307.01	587,295	41,136	0.0700432
2685.5	592,205	44,832	0.0757035	3321.8	582,245	40,650	0.0698160
2700.29	591,702	44,405	0.0750462	3336.59	591,825	41,020	0.0693110
2715.08	597,697	44,481	0.0744207	3351.38	589,569	40,712	0.0690538
2729.87	593,283	44,400	0.0748378	3366.17	586,945	40,058	0.0682483
2744.66	595,731	44,439	0.0745957	3380.95	586,215	40,072	0.0683572
2759.44	589,929	44,091	0.0747395	3395.74	586,983	40,044	0.0682200
2774.23	586,411	43,579	0.0743148	3410.53	589,473	40,582	0.0688445
2789.02	586,113	43,941	0.0749702	3425.32	583,641	40,276	0.0690082
2803.81	586,415	43,625	0.0743927	3440.11	589,431	39,851	0.0676093
2818.6	588,605	43,690	0.0742263	3454.89	588,789	39,479	0.0670512
2833.39	586,719	43,413	0.0739928	3469.68	583,467	39,150	0.0670989
2848.17	582,109	43,244	0.0742885	3484.47	583,439	39,421	0.0675666
2862.96	582,077	42,950	0.0737875	3499.26	585,985	39,689	0.0677304
2877.75	587,685	42,867	0.0729421	3514.05	585,111	39,474	0.0674641
2892.54	587,427	42,759	0.0727903	3529.28	587,575	39,321	0.0669208
2907.33	591,025	42,444	0.0718142	3544.07	582,007	39,380	0.0676624
2922.11	590,099	43,246	0.0732860	3558.85	587,995	39,351	0.0669240
2936.9	583,945	42,917	0.0734949	3573.64	584,527	39,004	0.0667275
2951.69	587,479	42,946	0.0731022	3588.43	582,045	38,963	0.0669416
2966.48	589,505	43,131	0.0731648	3603.22	587,229	39,143	0.0666571
2981.28	594,167	42,883	0.0721733	3618.01	576,727	38,683	0.0670733
2996.07	592,125	42,958	0.0725489	3632.8	587,135	38,779	0.0660478
3010.86	584,143	42,592	0.0729137	3647.58	581,323	38,274	0.0658395
3026.04	588,463	42,053	0.0714624	3662.37	579,585	38,687	0.0667495
3040.83	589,371	42,080	0.0713982	3677.16	585,901	39,232	0.0669601
3055.61	586,143	42,196	0.0719893	3691.95	588,175	38,753	0.0658869
3070.4	589,963	42,329	0.0717486	3706.74	590,623	39,166	0.0663130
3085.19	593,731	42,851	0.0721724	3721.54	587,157	38,459	0.0655004
3099.98	589,331	42,512	0.0721360	3736.33	586,713	38,240	0.0651767
3114.77	592,649	41,983	0.0708396	3751.12	579,599	38,473	0.0663787

CS02 - F: 1100°C Anneal Temperature (continued)

Sputter Time (seconds)	Si Signal Amplitude	B Signal Amplitude	B/Si Amplitude Ratio	Sputter Time (seconds)	Si Signal Amplitude	B Signal Amplitude	B/Si Amplitude Ratio
3765.91	583,841	38,245	0.0655058	4400.65	580,799	33,510	0.0576964
3780.7	588,713	38,125	0.0647599	4415.44	585,293	34,358	0.0587022
3795.48	589,455	37,590	0.0637708	4430.23	579,713	33,867	0.0584203
3810.27	580,405	37,821	0.0651631	4445.02	582,909	33,392	0.0572851
3825.06	587,359	37,227	0.0633803	4459.82	581,715	33,623	0.0577998
3839.85	580,511	37,984	0.0654320	4474.61	584,181	33,580	0.0574822
3854.64	582,016	37,263	0.0640240	4489.4	578,381	33,440	0.0578166
3869.42	582,133	36,813	0.0632381	4504.19	581,847	33,748	0.0580015
3884.21	583,045	36,732	0.0630003	4519.53	578,947	33,099	0.0571710
3899	583,993	36,580	0.0626377	4534.32	582,517	33,026	0.0566953
3913.79	582,621	36,492	0.0626342	4549.11	580,743	33,453	0.0576038
3928.58	581,773	36,409	0.0625828	4563.89	581,993	32,744	0.0562618
3943.37	587,595	36,431	0.0620002	4578.68	586,927	32,486	0.0553493
3958.15	582,309	35,879	0.0616151	4593.47	582,899	32,728	0.0561469
3972.94	578,627	36,279	0.0626984	4608.26	575,639	32,454	0.0563791
3987.73	583,197	35,864	0.0614955	4623.05	577,119	32,993	0.0571685
4002.52	584,039	35,581	0.0609223	4637.83	579,327	32,529	0.0561496
4017.8	575,185	35,147	0.0611056	4652.62	583,587	32,095	0.0549961
4032.59	583,461	35,174	0.0602851	4667.41	585,701	32,178	0.0549393
4047.38	584,571	35,827	0.0612877	4682.2	580,937	32,035	0.0551437
4062.17	582,109	35,441	0.0608838	4696.99	577,981	31,995	0.0553565
4076.96	577,201	35,419	0.0613634	4711.78	581,455	32,087	0.0551840
4091.74	583,384	35,281	0.0604765	4726.56	586,561	32,072	0.0546780
4106.53	576,611	35,966	0.0623748	4741.35	586,177	31,400	0.0535674
4121.32	579,267	35,432	0.0611670	4756.14	583,919	31,907	0.0546429
4136.11	580,635	35,370	0.0609161	4770.93	584,963	31,383	0.0536495
4150.9	579,850	35,337	0.0609416	4785.72	573,317	31,310	0.0546120
4165.69	576,041	35,052	0.0608498	4800.51	581,159	31,128	0.0535619
4180.47	580,679	35,442	0.0610354	4815.29	584,493	30,965	0.0529775
4195.26	585,443	35,167	0.0600690	4830.08	579,389	31,116	0.0537049
4210.05	581,819	34,586	0.0594446	4844.87	578,277	31,095	0.0537718
4224.84	585,167	34,253	0.0585354	4859.66	581,443	31,462	0.0541102
4239.63	582,195	34,870	0.0598940	4874.45	580,889	30,812	0.0530428
4254.42	585,835	34,820	0.0594365	4889.24	578,561	31,726	0.0548361
4269.2	585,375	34,308	0.0586086	4904.02	578,041	30,635	0.0529980
4283.99	586,635	34,901	0.0594936	4918.81	581,973	30,722	0.0527894
4298.78	579,621	34,260	0.0591076	4933.6	577,187	30,918	0.0535667
4313.57	586,029	33,937	0.0579101	4948.39	574,109	30,325	0.0528210
4328.36	590,509	33,982	0.0575470	4963.18	579,827	30,943	0.0533659
4343.14	586,716	35,145	0.0599012	4977.96	580,099	30,634	0.0528082
4357.93	587,966	34,152	0.0580850	4992.75	577,973	30,219	0.0522844
4371.9	470,054	27,373	0.0582337	5007.54	581,277	30,256	0.0520509
4385.86	583,311	34,116	0.0584868	5022.94	585,929	29,931	0.0510830

CS02 - F: 1100°C Anneal Temperature (continued)

Sputter Time (seconds)	Si Signal Amplitude	B Signal Amplitude	B/Si Amplitude Ratio	Sputter Time (seconds)	Si Signal Amplitude	B Signal Amplitude	B/Si Amplitude Ratio
5037.73	580,439	29,806	0.0513508	5674.3	581,865	24,969	0.0429120
5052.51	574,029	29,552	0.0514817	5689.09	581,627	25,187	0.0433044
5067.3	580,713	29,670	0.0510924	5703.88	577,665	24,957	0.0432032
5082.09	578,719	29,319	0.0506619	5718.67	579,077	24,929	0.0430495
5096.88	577,127	29,026	0.0502940	5733.46	580,223	24,971	0.0430369
5111.67	577,003	29,438	0.0510188	5748.24	579,237	25,159	0.0434347
5126.45	577,715	29,279	0.0506807	5763.03	580,057	24,572	0.0423614
5141.24	573,035	29,049	0.0506932	5777.82	575,159	24,801	0.0431203
5156.03	576,092	29,457	0.0511325	5792.61	575,773	24,560	0.0426557
5170.82	577,081	29,320	0.0508074	5807.4	572,361	24,560	0.0429100
5185.61	578,003	29,179	0.0504824	5822.19	579,405	24,542	0.0423572
5200.41	577,055	28,811	0.0499277	5836.97	580,365	24,217	0.0417272
5215.2	579,853	29,158	0.0502852	5851.76	577,025	24,471	0.0424089
5229.99	576,279	28,754	0.0498960	5866.55	575,559	23,934	0.0415839
5244.78	578,472	28,463	0.0492038	5881.34	576,549	23,907	0.0414657
5259.57	575,163	28,104	0.0488627	5896.13	576,699	23,479	0.0407127
5274.36	578,903	28,260	0.0488165	5910.92	584,997	23,956	0.0409506
5289.14	574,139	28,393	0.0494532	5925.7	589,373	23,231	0.0394165
5303.93	577,583	28,199	0.0488224	5940.51	581,431	23,225	0.0399446
5318.72	573,165	28,165	0.0491394	5955.3	587,181	22,995	0.0391617
5333.51	578,351	28,155	0.0486815	5970.09	588,385	22,950	0.0390051
5348.3	574,617	27,760	0.0483104	5984.88	583,199	22,841	0.0391650
5363.09	574,733	27,541	0.0479196	5999.66	587,451	22,668	0.0385870
5377.87	576,288	27,373	0.0474988	6014.45	586,159	22,757	0.0388239
5392.66	574,359	27,808	0.0484157	6029.96	587,409	22,267	0.0379071
5407.45	572,353	27,244	0.0476000	6044.75	585,943	22,096	0.0377102
5422.24	574,599	27,336	0.0475740	6059.54	588,212	22,254	0.0378333
5437.03	577,857	27,430	0.0474685	6074.33	581,393	22,027	0.0378866
5451.81	579,141	26,886	0.0464239	6089.11	580,273	21,951	0.0378287
5466.6	576,683	26,895	0.0466374	6103.9	586,809	21,957	0.0374176
5481.39	581,241	26,956	0.0463766	6118.69	587,539	21,720	0.0369678
5496.18	578,565	26,833	0.0463785	6133.48	588,961	21,547	0.0365848
5510.97	572,293	25,806	0.0450923	6148.27	577,563	21,695	0.0375630
5526.42	572,067	26,568	0.0464421	6163.06	582,929	21,234	0.0364264
5541.21	573,895	26,332	0.0458830	6177.84	591,557	20,526	0.0346983
5556	570,681	26,394	0.0462500	6192.63	586,465	21,140	0.0360465
5570.79	574,721	26,473	0.0460624	6207.42	587,131	20,803	0.0354316
5585.57	569,689	26,016	0.0456670	6222.21	581,579	20,715	0.0356185
5600.36	576,539	25,781	0.0447168	6237	576,483	20,672	0.0358588
5615.15	568,579	26,259	0.0461836	6251.78	581,175	20,324	0.0349705
5629.94	571,081	25,781	0.0451442	6266.57	588,517	19,948	0.0338954
5644.73	571,639	25,774	0.0450879	6281.36	586,851	19,736	0.0336303
5659.51	571,193	25,476	0.0446014	6296.15	587,895	19,706	0.0335196

CS02 - F: 1100°C Anneal Temperature (continued)

Sputter Time (seconds)	Si Signal Amplitude	B Signal Amplitude	B/Si Amplitude Ratio	Sputter Time (seconds)	Si Signal Amplitude	B Signal Amplitude	B/Si Amplitude Ratio
6310.94	590,299	20,058	0.0339794	6947.63	567,033	13,699	0.0241591
6325.73	579,927	19,691	0.0339543	6962.42	561,465	14,091	0.0250968
6340.52	583,359	19,784	0.0339139	6977.21	572,635	13,965	0.0243873
6355.3	582,643	19,620	0.0336741	6992	573,187	13,640	0.0237968
6370.09	584,998	19,396	0.0331557	7006.78	573,571	13,563	0.0236466
6384.88	577,771	19,445	0.0336552	7022.4	575,235	13,214	0.0229715
6399.67	580,005	18,928	0.0326342	7037.19	571,967	13,483	0.0235730
6414.46	579,239	19,208	0.0331608	7051.98	572,425	13,202	0.0230633
6429.24	582,035	19,216	0.0330152	7066.77	570,067	13,475	0.0236376
6444.03	586,049	18,834	0.0321372	7081.55	570,427	13,144	0.0230424
6458.82	578,557	18,488	0.0319554	7096.34	568,417	12,610	0.0221844
6473.61	585,385	18,505	0.0316117	7111.13	565,923	12,182	0.0215259
6488.4	582,755	18,469	0.0316926	7125.92	563,400	12,452	0.0221015
6503.19	577,963	18,338	0.0317287	7140.71	567,635	12,251	0.0215825
6518.75	577,803	17,896	0.0309725	7155.5	569,553	12,210	0.0214379
6533.54	582,399	18,017	0.0309358	7170.28	570,449	12,086	0.0211868
6548.33	580,257	18,107	0.0312051	7185.07	563,843	12,034	0.0213428
6563.11	577,751	17,810	0.0308264	7199.86	562,003	11,587	0.0206173
6577.9	576,091	17,442	0.0302765	7214.65	564,315	11,866	0.0210273
6592.69	576,747	17,418	0.0302004	7229.44	563,907	11,438	0.0202835
6607.48	578,155	17,209	0.0297654	7244.23	564,798	11,674	0.0206693
6622.27	575,011	17,221	0.0299490	7259.01	565,785	11,222	0.0198344
6637.06	575,337	17,031	0.0296018	7273.8	568,173	11,542	0.0203142
6651.84	574,439	16,720	0.0291067	7288.59	566,661	11,408	0.0201320
6666.63	573,644	16,666	0.0290529	7303.38	566,777	10,976	0.0193656
6681.44	577,299	16,393	0.0283960	7318.17	563,367	10,855	0.0192681
6696.23	584,241	16,098	0.0275537	7332.95	564,827	10,433	0.0184711
6711.02	574,757	16,425	0.0285773	7347.74	565,469	10,570	0.0186924
6725.81	578,587	15,944	0.0275568	7362.53	562,587	10,419	0.0185198
6740.59	572,624	15,974	0.0278961	7377.32	564,581	10,678	0.0189131
6755.38	576,873	16,084	0.0278814	7392.11	566,057	10,206	0.0180300
6770.17	574,397	15,753	0.0274253	7406.9	560,405	10,561	0.0188453
6784.96	573,455	15,682	0.0273465	7421.7	560,959	10,071	0.0179532
6799.75	570,953	15,583	0.0272930	7436.49	561,431	9,930	0.0176869
6814.54	577,641	15,654	0.0270999	7451.28	559,303	10,077	0.0180171
6829.32	573,517	15,177	0.0264630	7466.07	562,323	9,707	0.0172623
6844.11	581,131	15,289	0.0263090	7480.86	565,815	9,514	0.0168147
6858.9	577,703	14,945	0.0258697	7495.65	560,965	9,850	0.0175590
6873.69	582,151	14,989	0.0257476	7510.43	558,066	9,630	0.0172560
6888.48	572,013	14,820	0.0259085	7526.11	561,999	9,517	0.0169342
6903.27	577,261	14,321	0.0248085	7540.9	559,407	9,166	0.0163852
6918.05	569,971	14,694	0.0257803	7555.68	562,465	9,061	0.0161094
6932.84	571,547	14,162	0.0247784	7570.47	558,275	9,134	0.0163611

CS02 - F: 1100°C Anneal Temperature (continued)

Sputter Time (seconds)	Si Signal Amplitude	B Signal Amplitude	B/Si Amplitude Ratio	Sputter Time (seconds)	Si Signal Amplitude	B Signal Amplitude	B/Si Amplitude Ratio
7585.26	557,688	8,974	0.0160914	8222.12	540,003	6,094	0.0112851
7600.05	563,603	8,967	0.0159101	8236.91	534,343	6,047	0.0113167
7614.84	559,547	9,230	0.0164955	8251.7	536,513	5,978	0.0111423
7629.63	561,219	8,656	0.0154236	8266.48	536,203	5,989	0.0111693
7644.41	557,075	8,655	0.0155365	8281.27	539,911	5,691	0.0105406
7659.2	556,119	8,461	0.0152144	8296.06	538,300	5,863	0.0108917
7673.99	560,051	8,285	0.0147933	8310.85	541,417	5,734	0.0105907
7688.78	564,569	8,425	0.0149229	8325.64	537,751	5,811	0.0108061
7703.57	559,803	8,267	0.0147677	8340.43	537,867	5,719	0.0106327
7718.36	559,711	8,245	0.0147308	8355.22	542,159	5,652	0.0104250
7733.15	562,249	8,207	0.0145967	8370	539,903	5,686	0.0105315
7747.93	555,527	7,869	0.0141649	8384.79	541,261	5,557	0.0102668
7762.72	553,037	8,082	0.0146139	8399.58	537,532	5,465	0.0101668
7777.51	551,059	7,814	0.0141800	8414.37	532,343	5,557	0.0104388
7792.3	552,630	8,016	0.0145052	8429.16	539,379	5,334	0.0098892
7807.09	556,271	7,954	0.0142988	8443.95	536,067	5,375	0.0100267
7821.87	557,327	7,593	0.0136240	8458.73	533,161	5,171	0.0096988
7836.66	555,923	7,737	0.0139174	8473.52	531,735	5,381	0.0101197
7851.45	558,875	7,730	0.0138314	8488.31	531,423	5,339	0.0100466
7866.24	549,047	7,327	0.0133449	8503.1	532,067	5,090	0.0095665
7881.03	553,727	7,470	0.0134904	8518.88	519,770	5,054	0.0097235
7895.82	553,867	7,276	0.0131367	8533.67	514,957	5,098	0.0098999
7910.6	546,361	7,049	0.0129017	8548.46	511,569	5,090	0.0099498
7925.39	547,205	7,341	0.0134154	8563.25	519,549	5,177	0.0099644
7940.18	547,257	7,266	0.0132771	8578.03	521,809	5,213	0.0099902
7954.97	548,687	7,000	0.0127577	8592.82	517,345	4,969	0.0096048
7969.76	550,379	7,041	0.0127930	8607.61	521,535	4,875	0.0093474
7984.55	551,765	7,135	0.0129312	8622.4	518,757	4,866	0.0093801
7999.33	546,179	6,856	0.0125527	8637.19	511,262	4,905	0.0095939
8014.12	547,127	6,852	0.0125236	8651.97	524,215	4,918	0.0093816
8029.85	545,055	6,904	0.0126666	8666.76	519,721	4,756	0.0091511
8044.64	546,933	6,950	0.0127072	8681.55	518,333	4,625	0.0089228
8059.43	544,847	6,642	0.0121906	8696.34	516,611	4,692	0.0090823
8074.22	544,761	6,789	0.0124623	8711.13	508,559	4,576	0.0089980
8089.01	540,465	6,712	0.0124189	8725.92	508,265	4,439	0.0087336
8103.79	546,742	6,584	0.0120422	8740.71	505,083	4,438	0.0087867
8118.58	542,565	6,495	0.0119709	8755.49	509,337	4,242	0.0083285
8133.37	540,389	6,463	0.0119599	8770.28	512,953	4,285	0.0083536
8148.16	543,625	6,270	0.0115337	8785.07	509,502	4,318	0.0084749
8162.97	539,263	6,335	0.0117475	8799.86	506,309	4,260	0.0084138
8177.75	541,907	6,260	0.0115518	8814.65	511,801	4,333	0.0084662
8192.54	541,577	6,188	0.0114259	8829.44	518,467	4,254	0.0082050
8207.33	542,039	6,340	0.0116966	8844.22	508,385	4,268	0.0083952

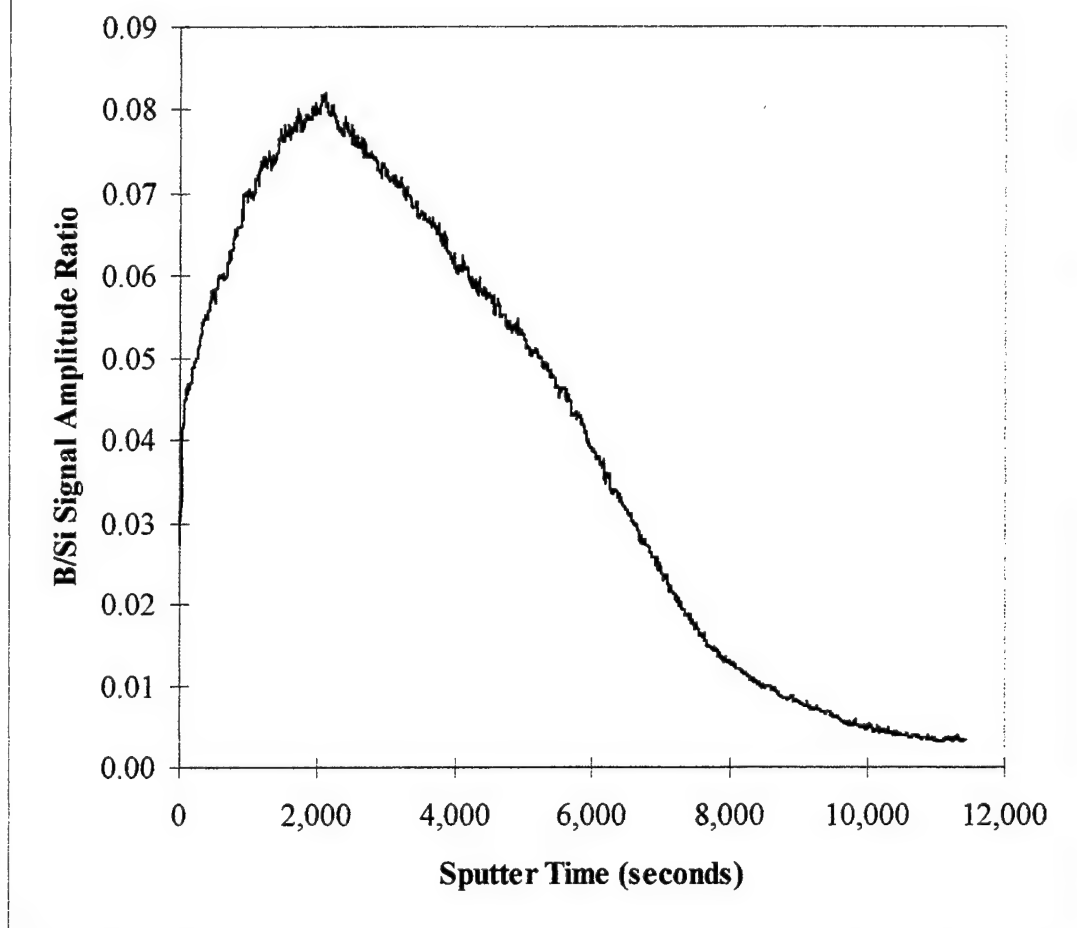
CS02 - F: 1100°C Anneal Temperature (continued)

Sputter Time (seconds)	Si Signal Amplitude	B Signal Amplitude	B/Si Amplitude Ratio	Sputter Time (seconds)	Si Signal Amplitude	B Signal Amplitude	B/Si Amplitude Ratio
8859.01	507,979	4,243	0.0083527	9495.99	480,148	2,914	0.0060690
8873.8	512,381	4,369	0.0085269	9510.77	475,661	2,985	0.0062755
8888.59	504,323	4,346	0.0086175	9526.68	481,607	2,903	0.0060277
8903.4	504,773	4,348	0.0086138	9541.47	474,055	3,007	0.0063431
8918.19	512,475	4,119	0.0080375	9556.26	478,991	2,894	0.0060419
8932.98	511,293	4,104	0.0080267	9571.05	484,697	3,055	0.0063029
8947.76	508,979	4,236	0.0083225	9585.84	513,821	2,928	0.0056985
8962.55	512,315	4,102	0.0080068	9600.63	510,681	2,926	0.0057296
8977.34	505,023	4,132	0.0081818	9615.41	512,491	2,836	0.0055338
8992.13	502,453	3,975	0.0079112	9630.2	508,839	2,830	0.0055617
9006.92	505,419	3,990	0.0078944	9645.01	509,729	2,875	0.0056403
9022.76	498,727	3,810	0.0076395	9659.8	512,097	2,888	0.0056396
9037.54	500,761	3,846	0.0076803	9674.59	508,157	2,649	0.0052130
9052.33	512,171	3,940	0.0076927	9689.38	517,075	2,839	0.0054905
9067.12	507,047	3,772	0.0074392	9704.17	512,879	2,765	0.0053911
9081.91	509,939	3,811	0.0074734	9718.95	513,141	2,780	0.0054176
9096.7	511,029	3,804	0.0074438	9733.74	510,561	2,610	0.0051120
9111.49	502,361	4,003	0.0079684	9748.53	498,707	2,730	0.0054742
9126.27	514,385	3,738	0.0072669	9763.32	512,667	2,632	0.0051339
9141.06	508,845	3,798	0.0074640	9778.11	506,197	2,640	0.0052154
9155.85	505,931	3,827	0.0075643	9792.9	507,549	2,577	0.0050773
9170.64	500,707	3,553	0.0070960	9807.68	504,619	2,636	0.0052237
9185.43	490,139	3,496	0.0071327	9822.47	506,049	2,879	0.0056892
9200.22	484,557	3,408	0.0070332	9837.26	496,205	2,606	0.0052519
9215.01	494,321	3,448	0.0069752	9852.05	496,835	2,468	0.0049674
9229.79	496,287	3,632	0.0073183	9866.84	502,029	2,511	0.0050017
9244.58	488,711	3,584	0.0073336	9881.63	502,143	2,482	0.0049428
9259.37	483,053	3,557	0.0073636	9896.42	502,221	2,409	0.0047967
9274.16	485,519	3,434	0.0070728	9911.2	499,437	2,509	0.0050237
9288.95	482,629	3,330	0.0068997	9925.99	498,233	2,461	0.0049395
9303.74	488,409	3,436	0.0070351	9940.78	500,761	2,475	0.0049425
9318.52	487,329	3,284	0.0067388	9955.57	504,511	2,546	0.0050465
9333.31	482,195	3,307	0.0068582	9970.36	508,521	2,405	0.0047294
9348.1	489,341	3,265	0.0066722	9985.15	503,793	2,360	0.0046845
9362.89	479,211	3,289	0.0068634	9999.93	499,111	2,334	0.0046763
9377.68	482,579	3,183	0.0065958	10014.72	490,019	2,605	0.0053161
9392.47	483,185	3,322	0.0068752	10030.66	494,525	2,337	0.0047257
9407.26	484,527	3,125	0.0064496	10045.45	493,701	2,345	0.0047498
9422.04	477,959	3,181	0.0066554	10060.24	486,639	2,435	0.0050037
9436.83	475,671	3,090	0.0064961	10075.03	493,909	2,320	0.0046972
9451.62	477,793	3,024	0.0063291	10089.82	492,093	2,253	0.0045784
9466.41	476,987	3,054	0.0064027	10104.61	499,676	2,146	0.0042948
9481.2	472,517	2,966	0.0062770	10119.4	501,649	2,291	0.0045669

CS02 - F: 1100°C Anneal Temperature (continued)

Sputter Time (seconds)	Si Signal Amplitude	B Signal Amplitude	B/Si Amplitude Ratio	Sputter Time (seconds)	Si Signal Amplitude	B Signal Amplitude	B/Si Amplitude Ratio
10134.18	496,217	2,331	0.0046975	10786.11	487,675	1,601	0.0032829
10148.97	494,973	2,466	0.0049821	10800.9	493,201	1,667	0.0033800
10163.76	496,165	2,095	0.0042224	10815.69	486,603	1,725	0.0035450
10178.55	491,610	2,365	0.0048107	10830.48	493,851	1,842	0.0037299
10193.34	495,221	2,291	0.0046262	10845.26	493,171	1,808	0.0036661
10208.13	503,783	2,238	0.0044424	10860.05	490,743	1,663	0.0033887
10222.92	485,743	2,277	0.0046877	10874.84	486,935	1,733	0.0035590
10237.7	489,627	2,167	0.0044258	10889.63	482,207	1,826	0.0037868
10252.49	491,053	2,259	0.0046003	10904.42	483,361	1,614	0.0033391
10267.28	495,351	2,299	0.0046412	10919.21	490,365	1,653	0.0033710
10282.07	492,017	2,044	0.0041543	10934	489,461	1,647	0.0033649
10296.86	502,065	2,390	0.0047603	10948.78	478,929	1,700	0.0035496
10311.65	488,937	2,173	0.0044443	10963.57	490,125	1,721	0.0035113
10326.43	492,985	2,059	0.0041766	10978.36	486,045	1,576	0.0032425
10341.22	491,033	2,078	0.0042319	10993.15	489,729	1,607	0.0032814
10356.01	490,858	2,055	0.0041865	11007.94	496,287	1,720	0.0034657
10370.8	496,029	2,073	0.0041792	11023.99	489,113	1,542	0.0031526
10385.61	500,559	1,991	0.0039776	11038.78	491,297	1,585	0.0032262
10400.4	489,109	2,100	0.0042935	11053.57	492,519	1,542	0.0031308
10415.19	486,565	1,924	0.0039543	11068.36	490,471	1,502	0.0030624
10429.97	490,077	2,073	0.0042299	11083.15	487,603	1,546	0.0031706
10444.76	494,949	2,012	0.0040651	11097.94	489,567	1,604	0.0032764
10459.55	501,433	1,904	0.0037971	11112.73	490,501	1,531	0.0031213
10474.34	495,751	2,028	0.0040908	11127.54	485,455	1,729	0.0035616
10489.13	488,344	1,907	0.0039050	11142.32	482,825	1,654	0.0034257
10503.92	500,886	1,934	0.0038612	11157.11	481,187	1,601	0.0033272
10519.92	497,309	1,897	0.0038145	11171.9	473,579	1,683	0.0035538
10534.71	499,481	1,876	0.0037559	11186.69	484,703	1,675	0.0034557
10549.49	494,981	1,873	0.0037840	11201.48	483,568	1,704	0.0035238
10564.28	497,995	1,924	0.0038635	11216.27	484,913	1,630	0.0033614
10579.07	501,333	2,091	0.0041709	11231.06	477,668	1,622	0.0033957
10593.86	497,705	1,884	0.0037854	11245.84	481,697	1,556	0.0032302
10608.65	487,077	1,788	0.0036709	11260.63	471,899	1,729	0.0036639
10623.44	493,736	1,799	0.0036436	11275.42	479,923	1,659	0.0034568
10638.22	491,533	1,814	0.0036905	11290.21	477,519	1,634	0.0034219
10653.01	489,343	1,777	0.0036314	11305	477,993	1,834	0.0038369
10667.8	487,427	1,812	0.0037175	11319.79	478,805	1,809	0.0037782
10682.59	490,045	1,844	0.0037629	11334.58	472,103	1,648	0.0034908
10697.38	483,167	1,713	0.0035454	11349.36	491,143	1,548	0.0031518
10712.17	485,195	1,873	0.0038603	11364.15	486,647	1,534	0.0031522
10726.96	492,849	1,845	0.0037435	11378.94	489,445	1,595	0.0032588
10741.74	487,381	1,785	0.0036624	11393.73	480,988	1,541	0.0032038
10756.53	486,907	1,766	0.0036270	11408.52	480,066	1,618	0.0033704
10771.32	490,017	1,771	0.0036142	11423.95	475,791	1,591	0.0033439

CS02 - F SIMS Analysis



BIBLIOGRAPHY

- J. M. Baribeau and S. J. Rolfe, "Characterization of Boron-Doped Silicon Epitaxial Layers by X-ray Diffraction," *Appl. Phys. Lett.*, vol. 58, pp. 2129-2131, 1991.
- C. Cabuz, K. Fukatsu, T. Kurabayashi, K. Minami and M. Esashi, "Microphysical Investigations on Mechanical Structures Realized in p+ Silicon," *Journal of Microelectromechanical Systems*, vol. 4, pp. 109-117, 1995.
- W. Chu and M. Mehregany, "A Study of Residual Stress Distribution Through the Thickness of p+ Silicon Films," *IEEE Transactions on Electron Devices*, vol. 40, pp. 1245-1250, 1993.
- X. Ding, W. H. Ko and J. M. Mansour, "Residual Stress and Mechanical Properties of Boron-Doped p+ Silicon Films," *Sensors and Actuators*, vol. A21-A23, pp. 866-871, 1990.
- J. W. Edington, Practical Electron Microscopy in Materials Science, N. V. Philips' Gloeilampenfabrieken, sections 2 and 3, 1976.
- V. N. Erofeev and V. I. Nikitenko, "Mobility of Dislocations in Silicon Containing Substitutional and Interstitial Impurities," *Sov. Phys. - Solid State*, vol. 13, pp. 116-120, 1971.
- R. B. Fair, "Boron Diffusion in Silicon - Concentration and Orientation Dependence, Background Effects, and Profile Estimation," *J. Electrochem. Soc.*, vol. 122, pp. 800-805, 1975.
- H. Holloway, "Curvature in Boron-Doped Silicon and Other Compositionally Graded Single Crystals," *J. Appl. Phys.*, vol. 75, pp. 2297-2299, 1994.
- H. Holloway and S. L. McCarthy, "Determination of the Lattice Contraction of Boron-Doped Silicon," *J. Appl. Phys.*, vol. 73, pp. 103-111, 1993.
- A. M. Lin, D. A. Antoniadis and R. W. Dutton, "The Oxidation Rate Dependence of Oxidation-Enhanced Diffusion of Boron and Phosphorus in Silicon," *J. Electrochem. Soc.: Solid-State Science and Technology*, vol. 128, pp. 1131-1137, 1981.
- S. Lippold and J. Podlesny, WYKO Surface Profilers Technical Reference Manual, WYKO Corporation, p. 1-3, 1995.
- X. J. Ning and P. Pirouz, "Dislocations in Heavily Boron-Doped Silicon," *Institute of Physics Conference Series*, vol. 117, pp. 205-210, 1991.

X. J. Ning, P. Pirouz, M. Mehregany and W. Chu, "Cross-Sectional TEM Studies of Heavily Boron Doped Silicon," TRANSDUCERS '91. 1991 International Conference on Solid-State Sensors and Actuators. Digest of Technical Papers, pp. 755-758, 1991.

K. E. Peterson, "Silicon as a Mechanical Material," Proc. IEEE, vol. 70, pp. 420-456, 1982.

S. Prussin, "Generation and Distribution of Dislocations by Solute Diffusion," J. Appl. Phys., vol. 32, pp. 1876-1881, 1961.

N. D. Thai, "Concentration-Dependent Diffusion of Boron and Phosphorus in Silicon," J. Appl. Phys., vol. 41, pp. 2859-2866, 1970.

J. Wang, Q. Xu, F. Lu, H. Sun and X. Wang, "Effects of Rapid Thermal Annealing on Heavily Boron Doped Silicon Epitaxial Layers," Mat. Res. Soc. Symp. Proc., vol. 355, pp. 637-642, 1995.

J. Wang, Q. Xu, J. Yuan, F. Lu and H. Sun, "Effect of Rapid Thermal Annealing on the Strain Relaxation in Heavily Boron Doped Silicon Epitaxial Layer," J. Appl. Phys., vol. 77, pp. 2974-2977, 1995.

J. Washburn, G. Thomas and H. J. Queisser, "Diffusion-Induced Dislocations in Silicon," J. Appl. Phys., vol. 35, pp. 1909-1914, 1964.

S. Wolf and R. N. Tauber, Silicon Processing for the VLSI Era, Volume 1: Process Technology, Lattice Press, p. 244, 1986.

REFERENCES

1. K. E. Peterson, "Silicon as a Mechanical Material," Proc. IEEE, vol. 70, pp. 420-456, 1982.
2. H. Holloway and S. L. McCarthy, "Determination of the Lattice Contraction of Boron-Doped Silicon," J. Appl. Phys., vol. 73, pp. 103-111, 1993.
3. S. Wolf and R. N. Tauber, Silicon Processing for the VLSI Era, Volume 1: Process Technology, Lattice Press, p. 244, 1986.
4. N. D. Thai, "Concentration-Dependent Diffusion of Boron and Phosphorus in Silicon," J. Appl. Phys., vol. 41, pp. 2859-2866, 1970.
5. R. B. Fair, "Boron Diffusion in Silicon - Concentration and Orientation Dependence, Background Effects, and Profile Estimation," J. Electrochem. Soc., vol. 122, pp. 800-805, 1975.
6. A. M. Lin, D. A. Antoniadis and R. W. Dutton, "The Oxidation Rate Dependence of Oxidation-Enhanced Diffusion of Boron and Phosphorus in Silicon," J. Electrochem. Soc.: Solid-State Science and Technology, vol. 128, pp. 1131-1137, 1981.
7. K. Wu, Unpublished Data - MIT Department of Materials Science and Engineering.
8. S. Prussin, "Generation and Distribution of Dislocations by Solute Diffusion," J. Appl. Phys., vol. 32, pp. 1876-1881, 1961.
9. J. Washburn, G. Thomas and H. J. Queisser, "Diffusion-Induced Dislocations in Silicon," J. Appl. Phys., vol. 35, pp. 1909-1914, 1964.
10. X. J. Ning and P. Pirouz, "Dislocations in Heavily Boron-Doped Silicon," Institute of Physics Conference Series, vol. 117, pp. 205-210, 1991.
11. X. J. Ning, P. Pirouz, M. Mehregany and W. Chu, "Cross-Sectional TEM Studies of Heavily Boron Doped Silicon," TRANSDUCERS '91. 1991 International Conference on Solid-State Sensors and Actuators. Digest of Technical Papers, pp. 755-758, 1991.
12. V. N. Erofeev and V. I. Nikitenko, "Mobility of Dislocations in Silicon Containing Substitutional and Interstitial Impurities," Sov. Phys. - Solid State, vol. 13, pp. 116-120, 1971.
13. J. M. Baribeau and S. J. Rolfe, "Characterization of Boron-Doped Silicon Epitaxial Layers by X-ray Diffraction," Appl. Phys. Lett., vol. 58, pp. 2129-2131, 1991.

14. X. Ding, W. H. Ko and J. M. Mansour, "Residual Stress and Mechanical Properties of Boron-Doped p⁺ Silicon Films," *Sensors and Actuators*, vol. A21-A23, pp. 866-871, 1990.
15. W. Chu and M. Mehregany, "A Study of Residual Stress Distribution Through the Thickness of p⁺ Silicon Films," *IEEE Transactions on Electron Devices*, vol. 40, pp. 1245-1250, 1993.
16. H. Holloway, "Curvature in Boron-Doped Silicon and Other Compositionally Graded Single Crystals," *J. Appl. Phys.*, vol. 75, pp. 2297-2299, 1994.
17. J. Wang, Q. Xu, F. Lu, H. Sun and X. Wang, "Effects of Rapid Thermal Annealing on Heavily Boron Doped Silicon Epitaxial Layers," *Mat. Res. Soc. Symp. Proc.*, vol. 355, pp. 637-642, 1995.
18. J. Wang, Q. Xu, J. Yuan, F. Lu and H. Sun, "Effect of Rapid Thermal Annealing on the Strain Relaxation in Heavily Boron Doped Silicon Epitaxial Layer," *J. Appl. Phys.*, vol. 77, pp. 2974-2977, 1995.
19. C. Cabuz, K. Fukatsu, T. Kurabayashi, K. Minami and M. Esashi, "Microphysical Investigations on Mechanical Structures Realized in p⁺ Silicon," *Journal of Microelectromechanical Systems*, vol. 4, pp. 109-117, 1995.
20. S. Lippold and J. Podlesny, WYKO Surface Profilers Technical Reference Manual, WYKO Coporation, p. 1-3, 1995.
21. J. W. Edington, Practical Electron Microscopy in Materials Science, N. V. Philips' Gloeilampenfabrieken, sections 2 and 3, 1976.